PNE-603F

D-1 PNE-603F
FINAL REPORT

Plowshare / peaceful uses for nuclear explosives

UNITED STATES ATOMIC ENERGY COMMISSION / PLOWSHARE PROGRAM

project DUGOUT

NEVADA TEST SITE — JUNE 24, 1964

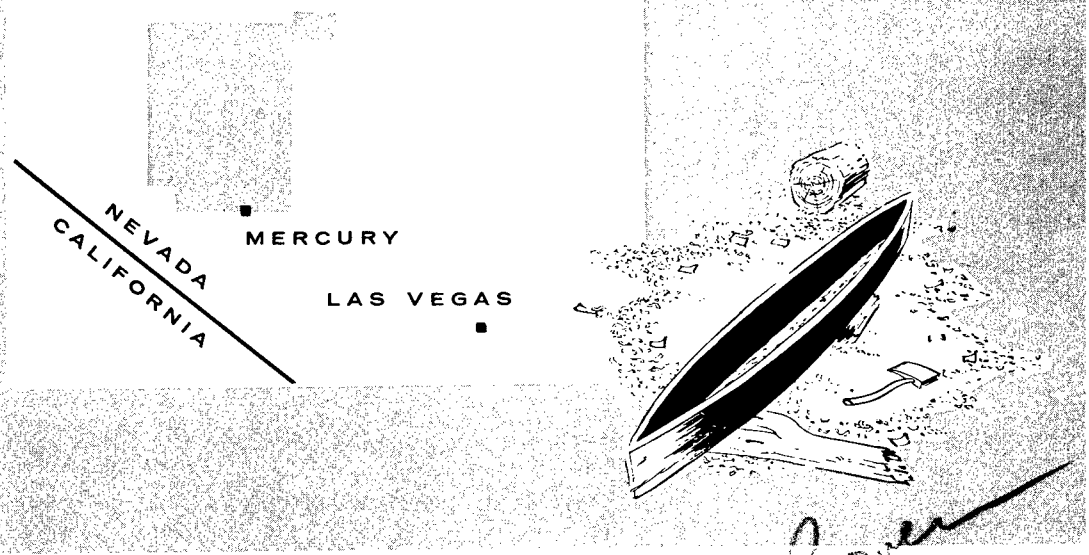

DISTRIBUTION STATEMENT A
Approved for Public Release
Distribution Unlimited

Surface Motion Measurements

R. W. Terhune

Lawrence Radiation Laboratory

Issuance Date: August 2, 1966

LEGAL NOTICE

Printed in USA. Price $2.00. Available from the Clearinghouse for Federal Scientific and Technical Information, National Bureau of Standards, U. S. Department of Commerce, Springfield, Virginia 22151.

USAEC Division of Technical Information Extension, Oak Ridge, Tennessee

PNE - 603F
NUCLEAR EXPLOSIONS – PEACEFUL
APPLICATIONS (TID - 4500)

PROJECT DUGOUT

SURFACE MOTION MEASUREMENTS

R. W. Terhune
University of California
Lawrence Radiation Laboratory
Livermore, California

December 1965

CONTENTS

CONTENTS (Continued)

CONTENTS (Continued)

ABSTRACT

Accelerometers and high-speed motion picture photography were used to measure the motion of the surface as it was thrown up by Dugout – a chemical row-charge cratering experiment in basalt, in which five 20-ton charges spaced 45 feet apart and at a depth of 59 feet were fired simultaneously. This report describes the experimental procedure for the surface motion measurements and gives the results obtained. Velocity profiles at various points on the rising "mound" of upthrown material from Dugout are presented and compared with those from another cratering experiment, Pre-Schooner Alpha, in which a single 20-ton chemical charge (equivalent to one of the five Dugout charges) was fired in the same basalt material as Dugout and at the same depth.

CHAPTER 1

INTRODUCTION

1.1 DESCRIPTION OF DUGOUT EVENT

Project Dugout was a chemical row-charge cratering experiment in hard rock executed as part of the Plowshare Program for development of nuclear excavation. The purpose of the experiment was to develop a more complete understanding of the fundamental processes involved in row charge cratering.

Dugout was fired June 24, 1964, at approximately 0806 Pacific Daylight Time or 1506 Greenwich Mean Time. Five separately placed (20 ± 1.5)-ton charges were fired simultaneously. The liquid nitromethane explosive was contained in five mined spherical cavities approximately 10.3 feet in diameter. The centers of the cavities were at a depth of 58.8 ± 0.2 feet, and they were spaced 45 feet apart horizontally.

Emplacement hole U18i, the center hole in the array, was located at geodetic coordinates:

Lat. 37° 5' 37.8381"
Long. 116° 20' 39.3410"

The collar elevations and coordinates of the holes in the array were as follows:

Hole	Collar elevation	Collar coordinates
U18g	5384.56	N 853,289.90 E 594,120.20
U18h	5385.45	N 853,290.00 E 594,075.00
U18i	5386.51	N 853,289.94 E 594,030.06
U18j	5386.90	N 853,290.00 E 593,985.12
U18k	5387.50	N 853,290.10 E 593,940.00

1.2 PURPOSE OF SURFACE MOTION MEASUREMENTS

Detailed description of the surface motion is desired in order to develop general diagnostic information concerning cratering physics for row charge events. Surface motion measurements for the Scooter event[1] led to the development of a simple, two-dimensional model of cratering for single-charge H. E. events in alluvium.[2,3] Project Dugout provided a key experiment which may contribute to an extension of this model work to a hard rock medium and to row charge events.

Examples of problems under study are: (1) the relative contributions to cratering of hard rock by spall and the gas acceleration phase, (2) the extent of coalescence of the cavities prior to vent, and (3) end effects on row charge cratering.

Evaluation of surface motion data of past events has been such a tedious and lengthy process that the published data has been restricted to a few targets measured at relatively large time intervals. Accuracy and completeness of data has been further restricted by poor fiducial markers and loss of targets from the initial shock. From experimentation on Pre-Buggy I, Pre-Buggy II,[4] and the Pre-Schooner series,[5] a program of targeting and data analysis has been developed to eliminate the majority of these problems.[6]

CHAPTER 2

EXPERIMENTAL PROCEDURES

Three separate experiments were developed to obtain surface motion information on Dugout: (1) accelerometers, (2) a falling mass experiment, and (3) surface motion targets. The accelerometers and falling mass experiment were designed to determine accurately the surface motion at very early times ($t < 50$ msec). The surface-motion target experiment was designed to give surface motion information over the entire mound of rock lifted by the explosion, up to the time it broke apart and vented.

2.1 ACCELEROMETER PROGRAM

The layout of the accelerometers over the cratering area is shown in Figure 2.1. The accelerometers were triaxial, piezoelectric

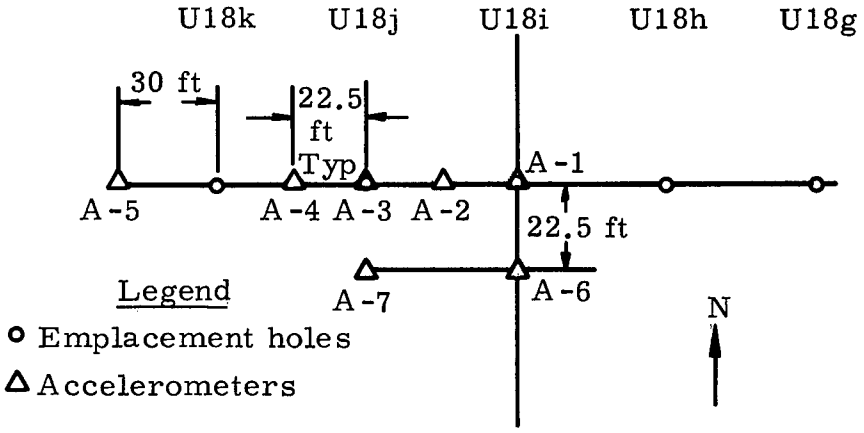

Fig. 2.1 Accelerometer layout.

Endevco Type 2223C. Each accelerometer was mounted on a wood block, which was in turn mounted on a concerte slab poured into the base of the respective target. This mounting scheme minimized ringing of the accelerometer. Each accelerometer was connected by a short length of coaxial cable to a cathode follower

The cathode followers used are of special design, incorporating negative feedback to provide stable, linear, near-unity gain and a very low output impedance, so that they maintain gain when driving standard low-impedance coaxial cable. The cathode followers and associated battery pack were shock-mounted and isolated from initial earth movement by suspending them from a cable stretched between two telephone poles.

The cathode follower outputs were fed, via coaxial cable, to an Ampex FR 1300 instrumentation tape recorder where shock information was recorded on magnetic tape. A zero-time fiducial pulse was summed with a precision 4-kc time reference and recorded. A voice channel containing the countdown was also recorded for convenience in data reduction.

A block diagram illustrating the overall system is shown in Figure 2.2. The accuracy of the system is given as follows:

Accelerometer to cathode follower:

Calibration ± 5% of peak acceleration

Temperature ± 5%

Cathode follower to tape:

Linearity ± 1%

Gain stability ± 1%

Voltage calibration ± 3%

Assuming normal error distribution, the 3 σ accuracy of information on tape is 7.8%.

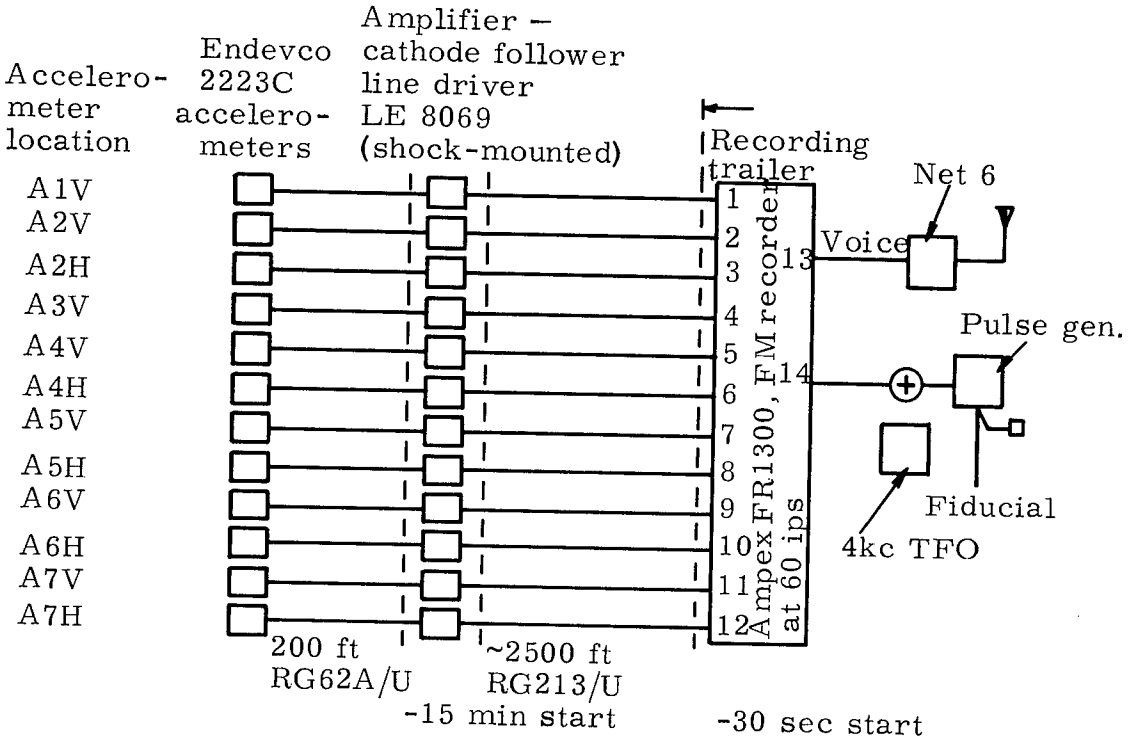

Fig. 2.2 Block diagram of accelerometer system.

The system specifications are as follows:

Measurement range	0-1000 g's
Band pass (±5%)	20-4000 cps
Linearity (±3%)	0-1000 g's
Resolution	7 g's
Cross-axis sensitivity	5% maximum
Number data channels	12

2.2 FALLING MASS EXPERIMENT

A 3.6- × 1-m graduated plywood target was mounted on a 7.6-m telephone pole, emplaced in concrete at a depth of 1.2 m, 1.5m east of hole U18i. A 7.3-kg ball, 0.3 m in diameter, was suspended 0.4 m in front of the graduated target by means of a supporting cable attached to the top of the telephone pole. The plywood target was graduated by alternating black and white lines, 0.1524 m apart. The ball was released at the same time the charges were detonated, by exploding a detonator inserted in the supporting cable. The relative displacement between the ball and the graduated target, which moved with the surface spall velocity, was obtained by photography from a close-in photosonic camera station.

2.3 SURFACE MOTION TARGETS

The target layout for Dugout is shown in Figure 2.3. All targets

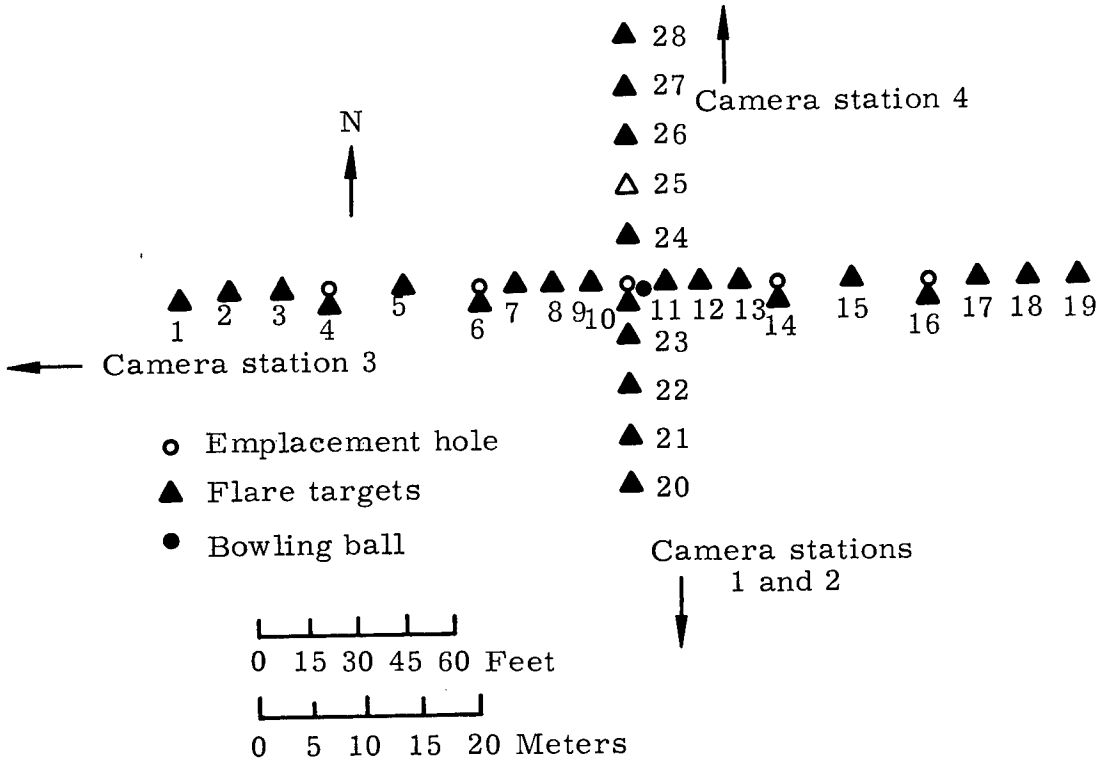

Fig. 2.3 Target array.

over the cratering area are MK III targets with 250,000-candlepower flares attached. Two independent fiducial systems were used for each array as shown in Figure 2.3. The target array along the charge line was photographed by camera station 2. The target array perpendicular to the charge line was photographed from camera station 3.

In order to obtain the detailed description of the surface motion over the entire mound, required to develop general diagnostic information concerning cratering physics, a large number of targets were required. Also, to avoid aliasing important frequencies in the data analysis, a sampling rate of 1 msec was desired. Computers handled the big data reduction job of analyzing the photographically recorded surface-motion information. The flares used as targets facilitated the reading and analysis of the film by computers. The film for the general surface motion was read by PDPI computer equipped with a visual CRT. The PDPI computes the center of each flare image and stores the target position-coordinate data (for each flare image) for each frame on tape. The tape is then used as input for a 7094 code which does a coordinate transformation, independently smooths the position data, and then computes velocity and acceleration components of each target as a function of time.

CHAPTER 3

SCIENTIFIC PHOTOGRAPHY DESCRIPTION

Table 3.1 shows the camera stations and contents for scientific photography on Dugout.

Cameras 1, 3, 9, 13, and 15 were mainly for documentary films.

Cameras 10, 14, and 16 were for base-surge and cloud development studies, and will be discussed in the base-surge report.

Cameras 4 and 5 photographed the falling ball experiment.

Cameras 2, 7, and 8 photographed the east-west row of targets to obtain surface motion data along the row charge, and to study mound development and venting.

Cameras 11 and 12 had the same purpose as cameras 2, 7, and 8, but photographed the north-south row of targets.

TABLE 3.1 DUGOUT CAMERA STATIONS

Camera No. and type	Frames per second	Lens focal length (mm)	Type of film
Station 1, 500 ft S of GZ			
1. Hulcher	20	80	Neg. color
2. Fastax	1000	25	Tri-X Reversible
3. Auricon	24	13	Color, K-II
4. Fastax	5000	255	Black and white
5. Photosonics	1000	300	MS color
Station 2, 1000 ft S of GZ			
6. Photosonics	1000	50	IR (infrared)
7. Photosonics	1000	50	Tri-X
8. Photosonics	200	100	Color
9. Hulcher	20	80	Neg. color
10. Bell and Howell	24	13	K-II
Station 3, 1650 ft W of GZ			
11. Photosonics	1000	50	IR
12. Photosonics	1000	50	Tri-X
13. Photosonics	100	25	K-II
14. Bell and Howell	24	13	K-II
Station 4, 3000 ft N of GZ			
15. Photosonics	100	50	K-II
16. Bell and Howell	24	13	K-II

CHAPTER 4

PRESHOT PREDICTIONS

Empirical equations for peak spall velocities and accelerations in basalt have been developed,[7] based primarily on Danny Boy and the Buckboard shots. These are:

$$a = 1.4 \times 10^{10} \Lambda^{-4.3} \text{ g's},$$

$$v = 1.6 \times 10^{5} \Lambda^{-2.1} \text{ m/sec},$$

where

$$\Lambda = R/W^{1/3},$$

R is the radial distance from the shot point to the free surface in meters, and W is the equivalent charge weight in kilotons.

By assuming superposition of velocity and acceleration components from each charge, estimates were made as to maximum surface motion over the crater area (the locations are numbered from the center charge out – 1, 2, and 3):

Location	Velocity (m/sec)	Acceleration (g's)
1	53.9	445
2	51.8	430
3	40.5	350

Time of vent is estimated at 1.0 sec.

Height of dome at vent is estimated at 14.9 m

CHAPTER 5

RESULTS

5.1 PHOTOGRAPHY

Table 5.1 gives pertinent remarks on observations made from a study of the film from Dugout. The description of the venting of Dugout

TABLE 5.1 OBSERVATIONS FROM DUGOUT FILMS

Time (msec)	Comments
0	Supporting cable on falling ball experiment detonated.
11.1-24.2	Targets illuminated by light from unknown source.
40.0	Small venting nitromethane gas from hole H. Magnitude of venting did not increase with time.
72.5-73.5	Zero-time flashbulbs ignited as they fell.
483.4	Primary vent occurred, approximately 5 m north of target over hole U18j.
523.6	Secondary venting along fault line in southeast quadrant. Also, simultaneous venting on north side at 45° from hole U18i.
543.8	Spotty venting along fault in southwest quadrant.
624.3	Vent along fault complete and main cloud beginning to form.

is fairly complete. The height of the dome at the time of primary vent was 20.4 m, and the width as measured from east to west was 104.8 m.

A major fault in the dome developed early about 7.6 m south of the charge row, extending over almost the entire dome, and continued to grow rapidly.

5.2 ACCELEROMETER EXPERIMENT

The magnetic tape from the Ampex FR 1300 tape recorder was read by a Pace 231 R analog computer, which plotted the information. The plots are presented in Appendix A. At first inspection the data seemed to contain a significant amount of information with frequency components below 20 cps. An attempt to recover this information – using an integral equation solvable on an analog computer – yielded entirely unrealistic results when the known capacitances, resistance, and time constants of the system were used.

Many of the accelerometers recorded results that exceeded the limits of the instruments.

Table 5.2 gives the time of arrival of the elastic wave, time and amount of peak acceleration, and elastic wave velocity for each

TABLE 5.2 ACCELEROMETER DATA

Tape channel	Accel. No.	Time of arrival (msec)	Time of peak g's (msec)	Peak g's[a]	Elastic wave velocity[b] (m/sec)
1	A-2N[c]	8.0	11.8	660	
2	A-2V	7.4		>1000	2525
3	A-6N	9.0	12.0	80	
4	A-6V	8.0		>1000	2006
5	A-3V	6.4		>1000	2313
6	A-4E	8.2		>1000	
7	A-4V	7.2		>1000	2525
8	A-7N	7.6	12.6	400	
9	A-1V	6.6	14.1	900	2243
10	A-7V	7.2	9.0	580	2204
11	A-5E	10.0	15.0	460	
12	A-5V	9.0		>1000	1846

[a] All accelerations >1000 g's exceeded the limits of the measuring instruments.

[b] Based on arrival times.

[c] Note: N, V, E are direction of positive voltage where N = north, V = vertical up, and E = east.

accelerometer. The elastic wave velocity was calculated by the time of arrival of the shock and the distance to the nearest shot point. All velocities seem to be in good agreement with each other.

5.3 FALLING MASS EXPERIMENT

The field of view of camera 4, station 1, encompassed target 10 (1 m south of center charge), the falling mass and graduated target (1.5 m east of center charge), and target 11 (3.4 m east of center charge). The zero-time reference frame was established as the frame on which the detonation of the supporting cable was observed. The framing rate of the film, determined by the timing marks, was 5225 ± 10 pps. The common reference coordinate system, used from frame to frame, was determined by a line parallel to the film edge and the top of the falling mass. The quantity $0.5\ gt^2$ was added to the vertical coordinate of the falling mass to account for its displacement due to gravitational forces.

The film was first read by means of the Oscar digitizer at a data interval of 0.385 msec. The ball disappeared into the mound 100 msec after zero time. Only the east and west edges of the graduated target were read. A second reading of the film was done on the microscope digitizer at a data interval of 0.1925 msec for a total of 40 msec after zero time.

Targets 10 and 11 were also read beside the edges of the graduated target. Target 10 was very difficult to read because of the distortions and obscuring effects caused by the flares along the north-south target array, and was consequently discarded. The horizontal and vertical displacement plots for both readings are given in Appendix B. Errors in the horizontal displacement were due entirely to errors in the measurement of the center of the top of the ball in both readings. Errors in the vertical displacement were ±0.005 m for the microscope digitizer and ±0.01 m for the Oscar digitizer. The vertical displacement data was smoothed with a normal smoothing operator[6] and differentiated.

Figures 5.1, 5.2, and 5.3 show the vertical velocities for the east and west edge of the graduated target and target 11, respectively.

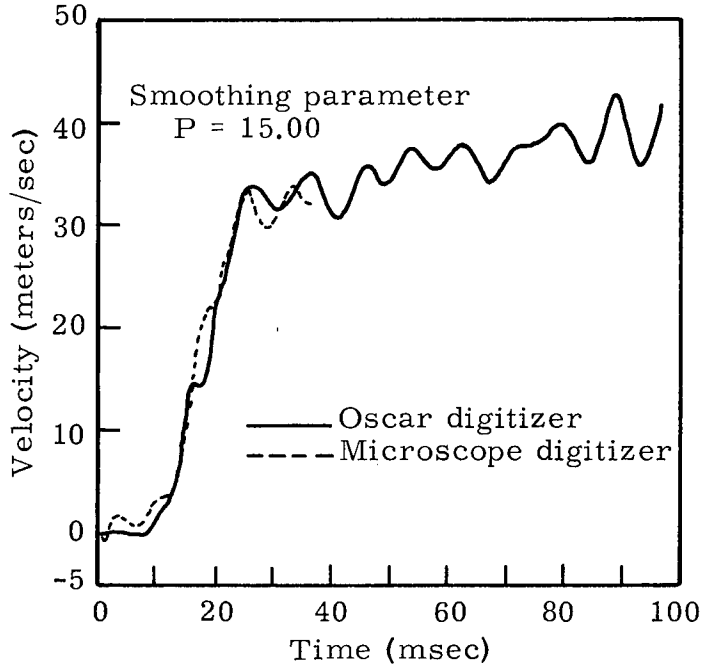

Fig. 5.1 Vertical velocity, east edge of graduated target.

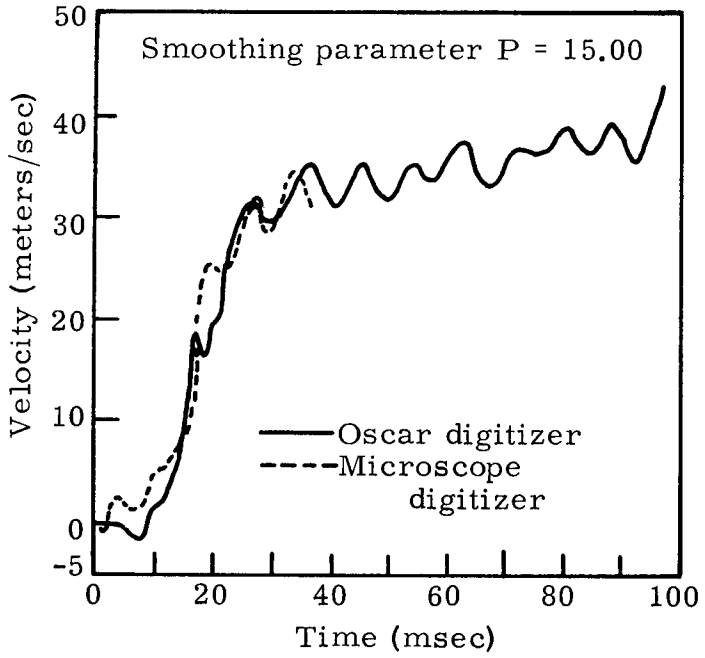

Fig. 5.2 Vertical velocity, west edge of graduated target.

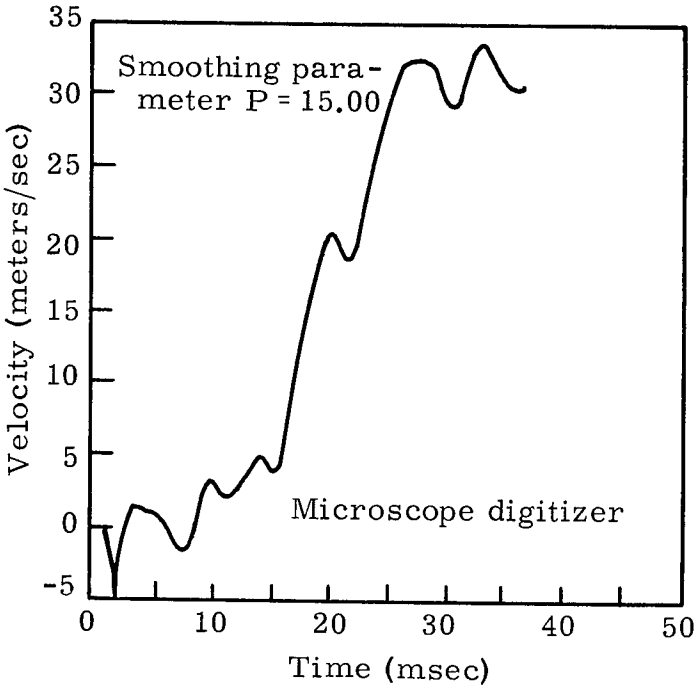

Fig. 5.3 Vertical velocity, target 11.

5.4 GENERAL SURFACE MOTION

Figure 2.3 shows the target distribution over the cratering area. Of the 19 targets running from east to west over the cratering area, all but 9 broke and dropped off early in the mound history.

The flare targets 20-28, running from north to south in Figure 2.3, were obscured by sun and smoke, and films of them were not processed.

The photographic film of the target displacement data was read by the PDPI computer and processed in the manner described in Reference 6. The framing rate of the film as determined by the timing marks was 995 pps, giving a data interval of 1.005 msec. Zero time was determined by correlating the time the targets were illuminated, as described in Table 5.1. The reading error is ±0.05 m. All targets were read except 9, 10, and 18, which did not register on the film. Displacement and velocity plots for each target are given in Appendix C. Comments as to the target and flare behavior at various times have been included

on the velocity plots. Vertical velocity plots for those flares that were representative of the mound motion are shown in Figures 5.4 and 5.5.

Figure 5.6 shows a hodograph of the flares with the cavity size at $t = 0$ and $t = 13$ msec, the time the rarefaction returned to the cavity, as calculated by the computer code SOC for a single charge.

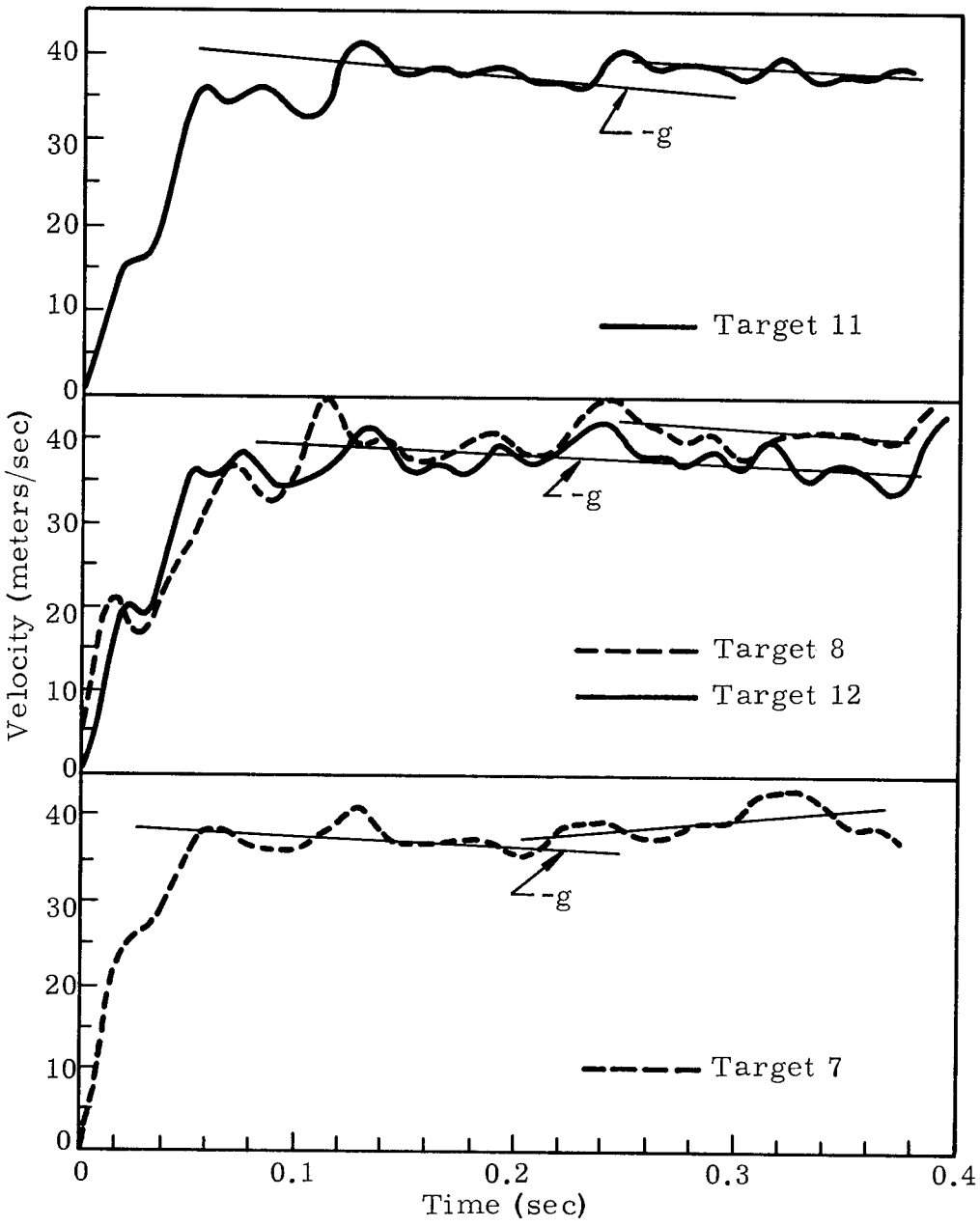

Fig. 5.4. Vertical velocity of targets 7, 8, 11, and 12.

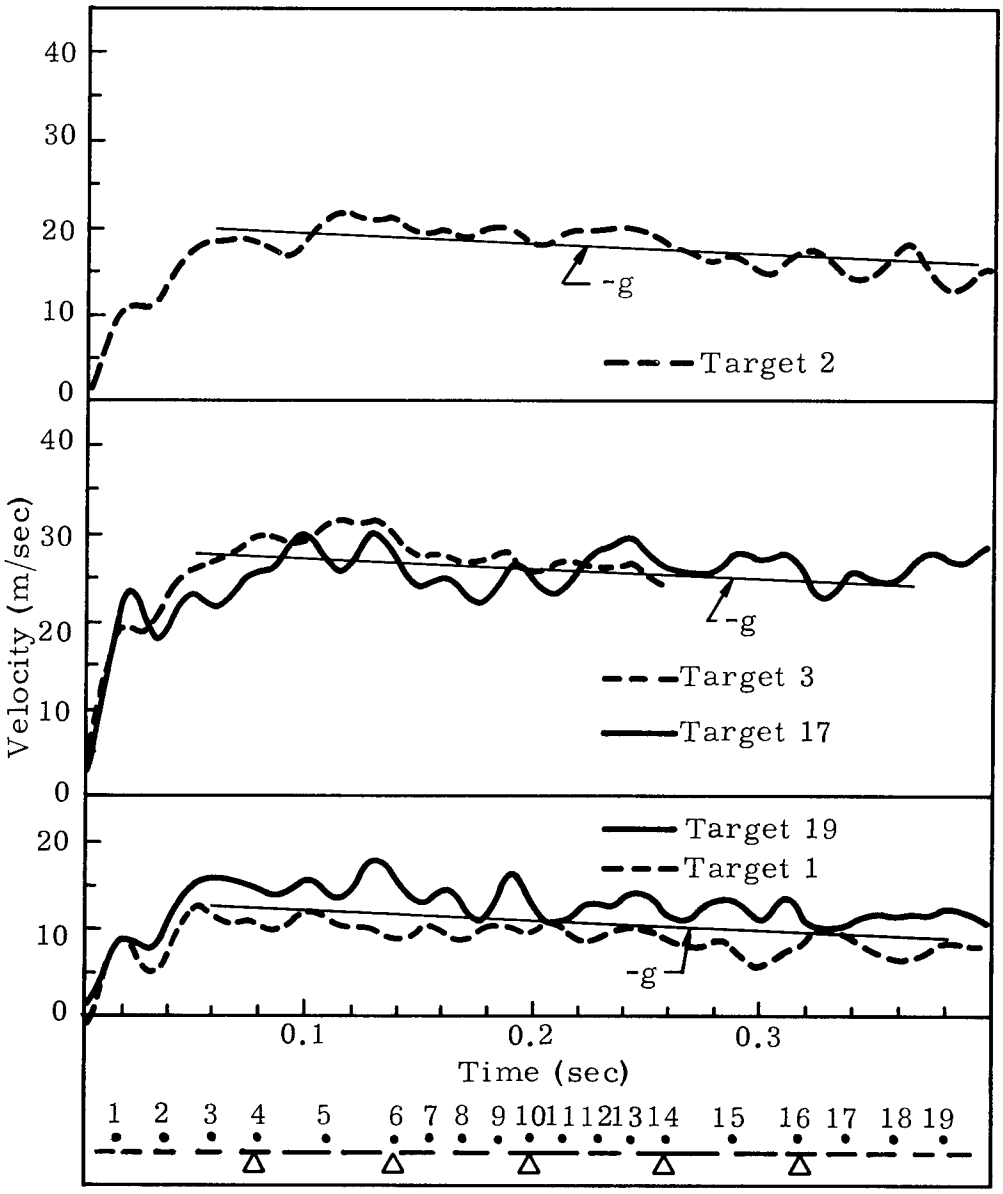

Fig. 5.5 Vertical velocity of targets 1, 2, 3, 17, and 19.

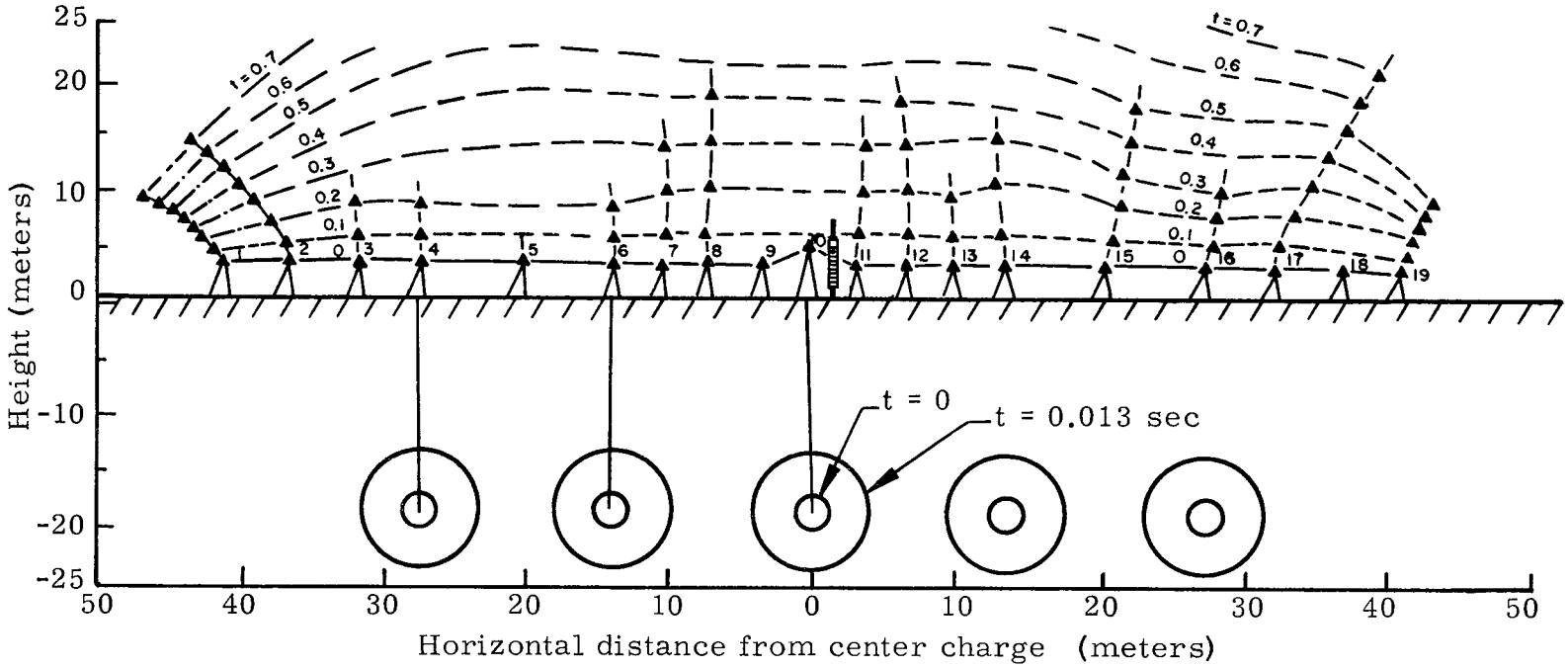

Fig. 5.6 Hodograph of flares.

CHAPTER 6

EVALUATION AND ERROR ANALYSIS

The purpose of this section is to provide the reader with additional information and comparisons that will aid in the interpretation of the surface motion data.

6.1 EARLY SURFACE MOTION ($t < 0.1$ sec)

The accelerometer data, as shown in Appendix A and summarized in Table 5.2, showed excellent agreement as to arrival time of the initial shock. Two accelerometers, A-3 and A-1 over a shot point, agreed within 1 msec for an average arrival time of 6.5 msec. The amplitude and wave form of the accelerometer traces do not show the same agreement with other data.

Figure 6.1 compares the integrated velocity from accelerometer A-1 with the velocity of the mound as determined from the falling mass experiment. The velocities from the accelerometer are considerably larger than those indicated by the falling mass experiment or surface motion targets.

The velocity profiles from the falling mass experiment (Figures 5.1, 5.2, and 5.3) require an investigation to determine the source of the pulses at 10, 14, and 20 msec. The displacement data for both readings (microscope and Oscar digitizers) were smoothed to severely dampen random noise frequencies above 175 cps. The noise frequencies remaining can be attributed to systematic errors introduced by (a) the instrument by which the film is read, (b) the operator who read the film,

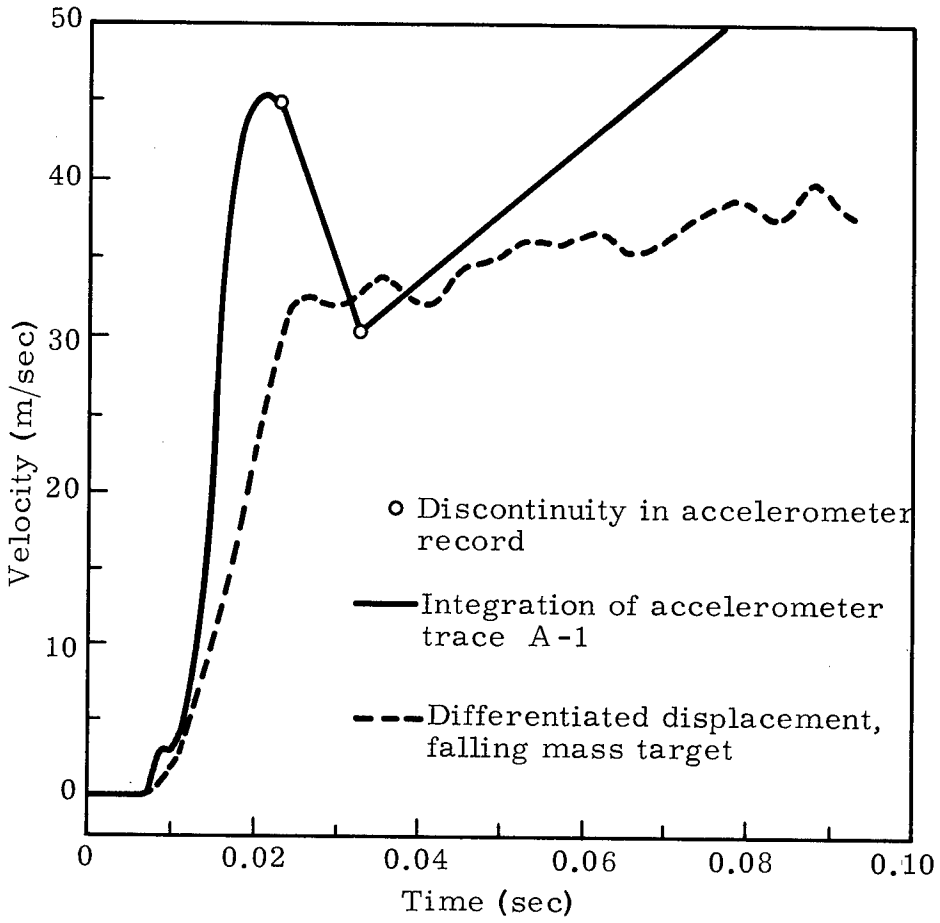

Fig. 6.1 Comparison of velocities from accelerometer A-1 and falling mass experiment.

or (c) errors in the framing rate of the camera. Errors due to (c) can be eliminated immediately, since they would be on the order of 2×10^{-3}%. Figures 5.1 and 5.2 show a comparison of the velocity profile determined from displacement data read on different types of instruments by different operators and at different frame intervals. While each data set contains errors, as indicated by (a) and (b), it is highly improbable that these errors would affect the data identically at the same time. It is therefore concluded that the pulses at 10, 14, and 20 msec, while containing some noise, signify real changes in the

velocity. It now remains to determine if these changes in velocity represent the mound motion or the air shock on the falling mass or a possible distortion effect caused by viewing through the air shock interface.

If a maximum shock velocity of 335 m/sec in air is assumed, the time for the shock to travel from the ground surface to the falling mass 2.75 m above would be 8.2 msec. Adding the time for the shock to reach the surface, 6.5 msec (from the accelerometer data), gives a time of 14.7 msec for the shock to reach the falling mass.

The graduated target of the falling mass experiment provided an excellent opportunity to measure the effects of any distortions of measurements taken through the air shock interface. Figure 6.2 is a plot of the width of the graduated target measured every frame from 0 to

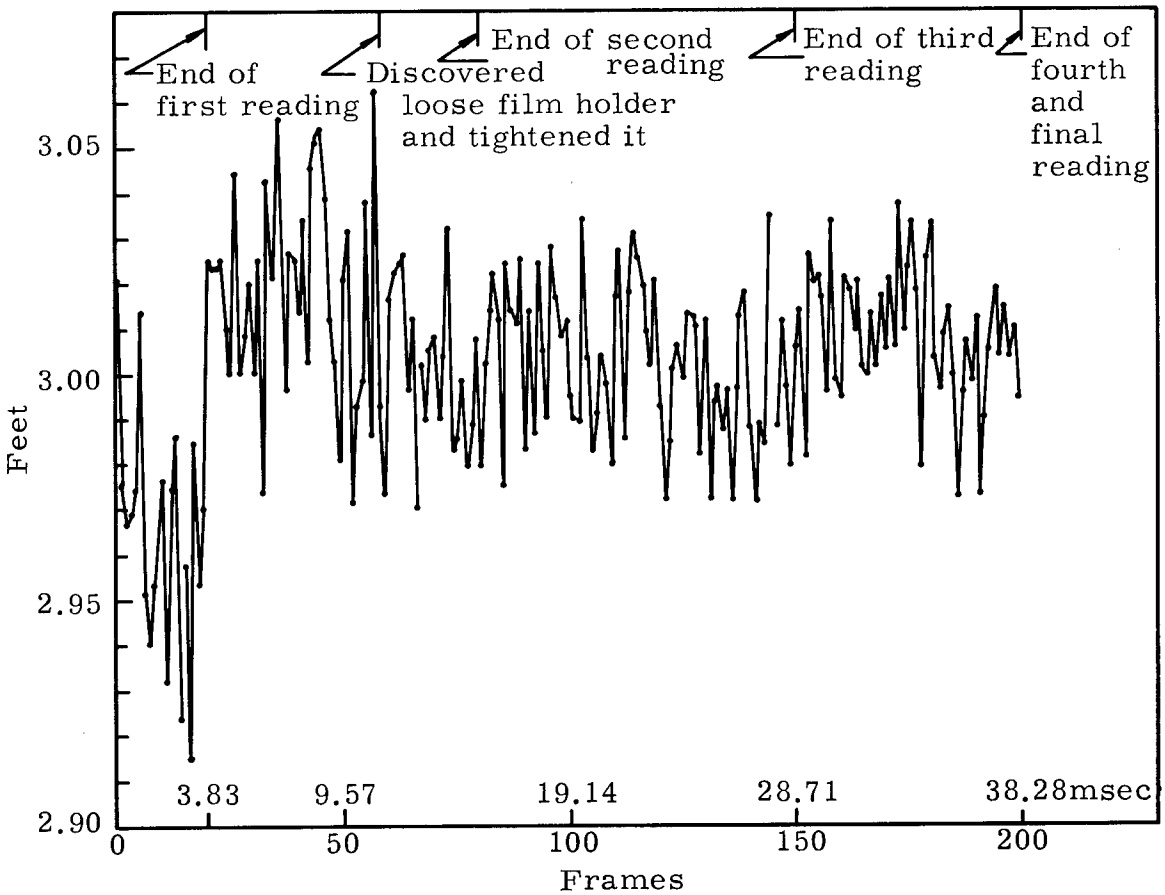

Fig. 6.2 Measured width of graduated target for every frame between 0 and 40 msec.

40 msec. The variation in the measurement for the first 10 msec was due to a loose film holder plate which resulted in a backlash effect as the vernier table was moved in reading each point on the film. When this is taken into account, the results show no distortion due to the air shock.

6.2 LATE SURFACE MOTION ($t > 0.1$ sec)

An examination of the vertical velocity plots shows a sudden velocity decrease then increase at $t \approx 30$ msec and $t \approx 80$ msec. The effect at $t \approx 30$ msec is due to the top of the target rotating toward the source of the incoming shock as it is accelerated by the shock. The second effect at $t \approx 80$ msec can be explained as the effect of the shock on the fiducials. The fiducials were 500 feet from the charge row; at this distance and with the shock velocities indicated by accelerometers A-6 and A-7 (Table 5.2), the fiducials would begin to rise at 70-80 msec. This would decrease the relative velocity between the fiducials and targets.

The targets over the center of the mound (Figure 5.4) show a peak velocity of 40 m/sec at 0.12 sec, then free fall till 0.2 sec, where an additional pulse is seen. Target 7 is especially interesting because the first vent occurred just 5 m NW of it.

CHAPTER 7

SUMMARY

In this section, data from the various experiments are combined to present a general picture of the surface motion of Dugout. Comparisons of surface motion between Dugout and Pre-Schooner Alpha are presented.

A general picture of the surface motion for the center 20 m of the mound is given by target 11. Figure 7.1 is a composite of the velocity

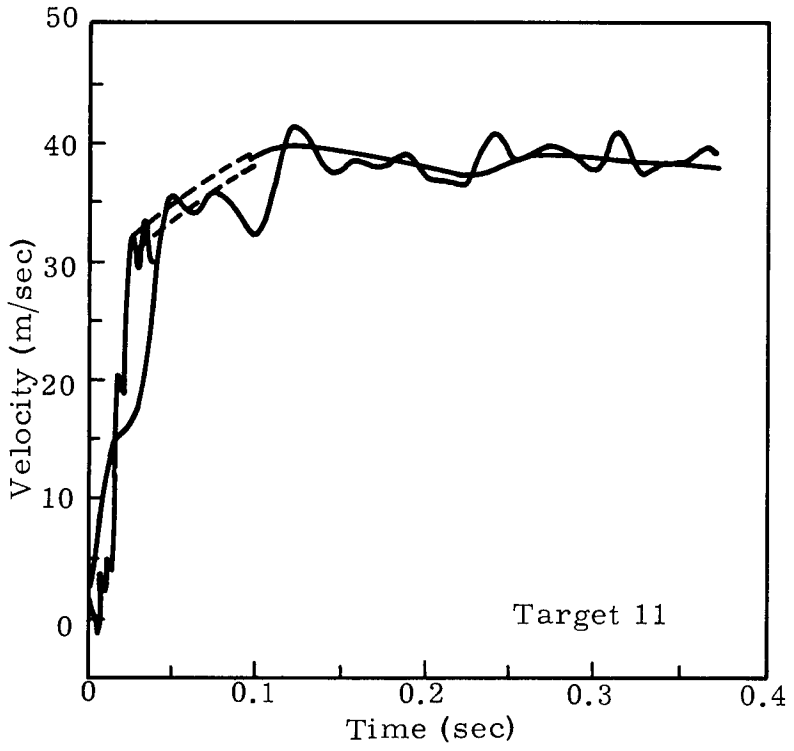

Fig. 7.1 Composite velocity profile, based on falling mass target and target 11.

profiles of the falling mass target and target 11. The initial shock arrived at target 11 at 7 msec, resulting in an elastic precursor velocity of 5 m/sec. At 16 msec the crush wave arrived, resulting in a spall velocity of 20-22 m/sec. At 22 msec, an additional pulse boosted the spall velocity to 32 m/sec.

At 30 msec, there is a change in accelerations that is not characteristic of spalling, but is characteristic of gas acceleration. This peaks out at 0.12 sec, where we have a period of apparent free fall till 0.20 to 0.22 sec. Here a small but definite increase in the velocity is observed which could be connected with cavity coalescence. Targets 7, 8, and 12 also show the same behavior from 0.12 sec on.

Pre-Schooner Alpha was a high-explosive cratering experiment in basalt, fired near the Dugout site. The explosive was 20 tons of nitromethane at a depth of burial of 58.5 feet. Thus it was equivalent to one of the five Dugout charges. The surface motion targets were spaced at 10-foot intervals with a center target over SGZ. The mound rose asymmetrically in the center 20 feet, but was fairly symmetrical outside this region.

Velocities in two areas of the Dugout mound — between the center charge and its neighbors, and beyond the end charge — were compared with Pre-Alpha Schooner velocities. Velocities 10 and 20 feet out from the Dugout center charge were compared respectively with velocities 11 and 22 feet from Pre-Schooner Alpha (Figure 7.2). Then velocities 15, 30, and 45 feet beyond the Dugout end charge were compared respectively with velocities 10 and 20, 30, and 40 and 50 feet out from Pre-Schooner Alpha (Figure 7.3).

Figure 7.2 compares the target velocities over the center of the Dugout mound with corresponding targets on Pre-Schooner Alpha. The velocities over the center of the Dugout mound were considerably higher than those on Pre-Schooner Alpha.

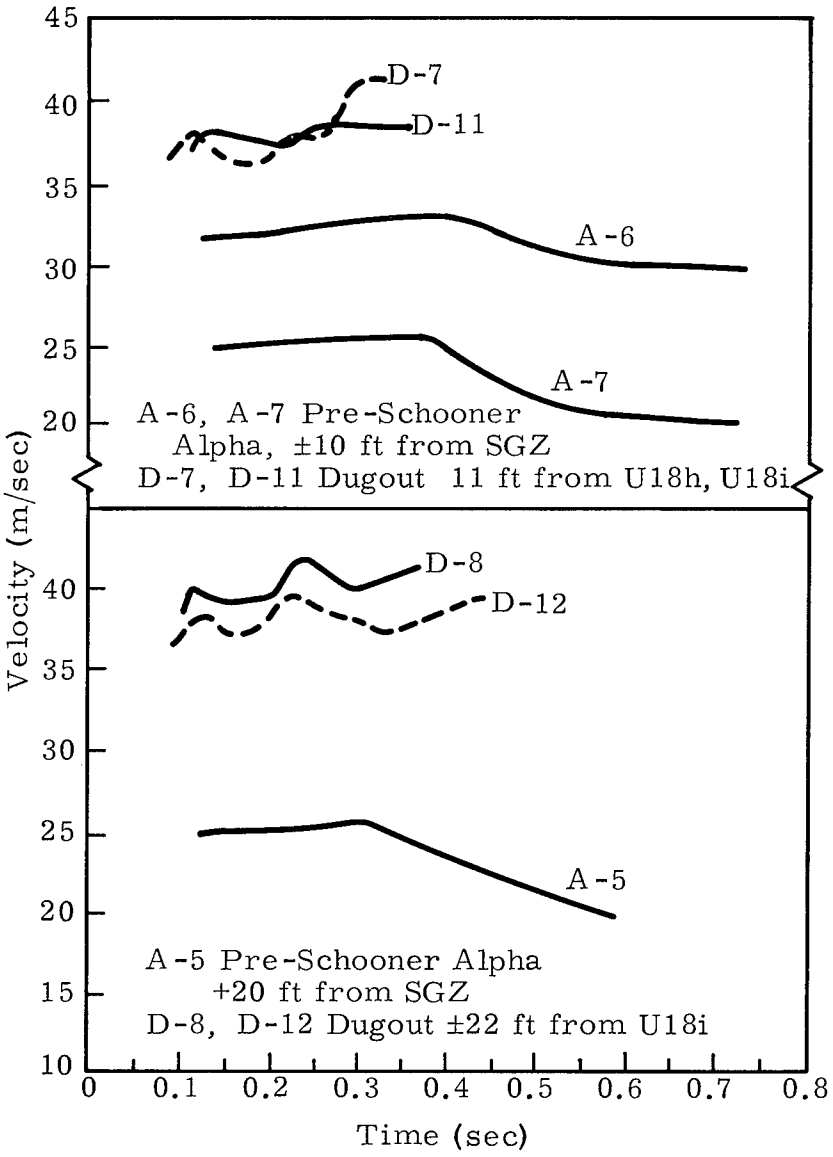

Fig. 7.2 Comparison of velocities of Pre-Schooner Alpha targets with Dugout targets near center charge.

Figure 7.3 shows a comparison between the targets on the end of the array for Dugout and the corresponding targets on Pre-Schooner Alpha. Comparison here yielded a completely unexpected results: i. e. while agreement is within reason near the shot hole, Dugout velocities were higher away from the shot point at 30 to 45 feet.

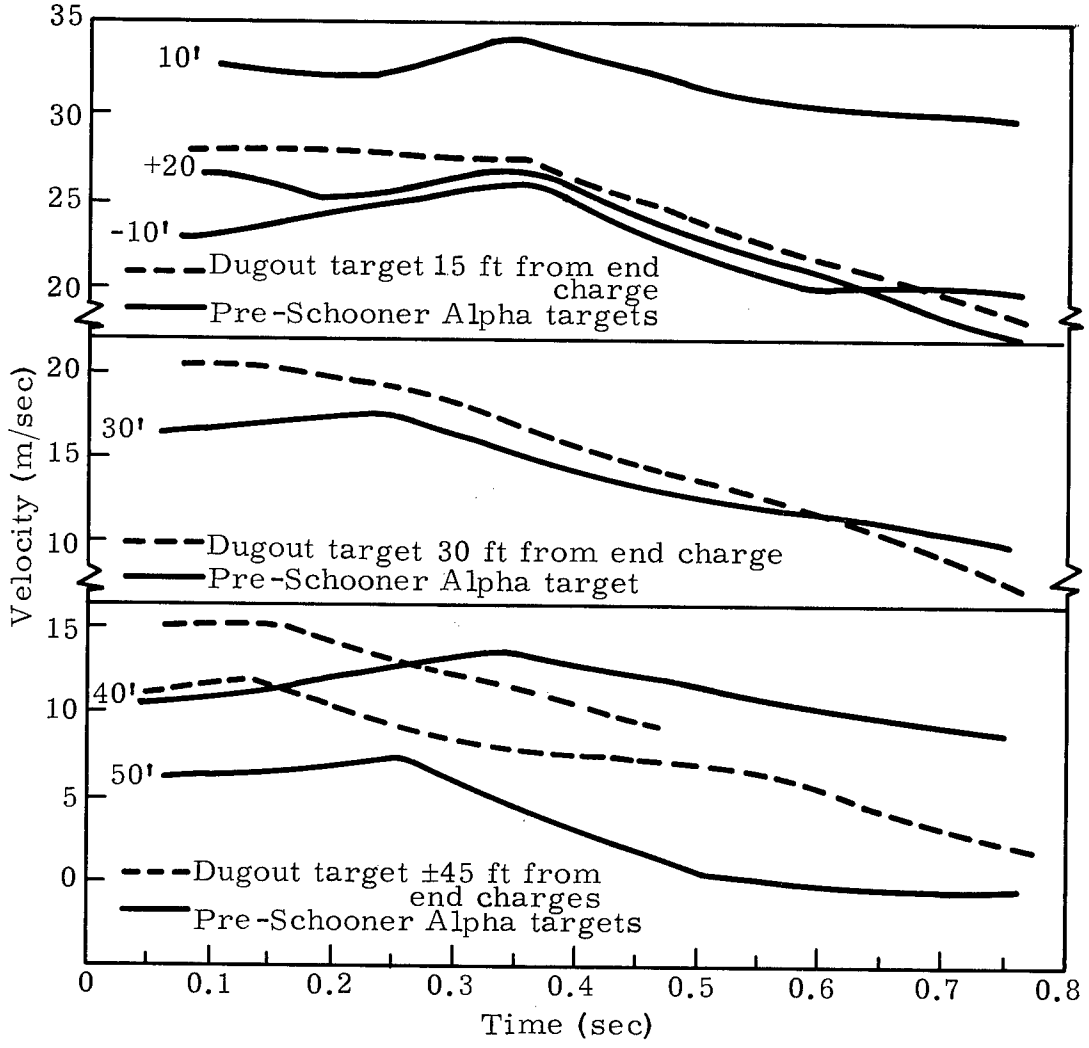

Fig. 7.3 Comparison of velocities of Pre-Schooner Alpha targets with Dugout targets near end charges.

REFERENCES

1. Feegenbaum, S. A., and P. L. Wegkamp, Final Report, "Photographic Earth Motion Study, Scooter Event," Edgerton, Germeshausen & Grier, Inc., Rept L-510, 1961.
2. Knox, J. B., and R. W. Terhune, "Cratering Physics Concepts Derived From an Analysis of Ground Surface Motion" Lawrence Radiation Laboratory, Livermore, Rept. UCID-4664, 1963.
3. Knox, J. B., and R. W. Terhune; "Calculation of Explosion-Produced Craters – H. E. Sources," J. Geophys. Res. 70(10), 2377-2393 (1965).
4. Graves, E., W. R. Wray, and R. B. Pierce, "Project Pre-Buggy, Scope of Chemical Explosive Cratering Experiment," USA Engineering Nuclear Cratering Group, Lawrence Radiation Laboratory, Livermore, Rept. PNE-300, 1963.
5. Spruill, J., USA Engineering Nuclear Cratering Group, private communication, 1965.
6. Terhune, R. W., R. L. Fulton, and J. B. Knox, "Surface Motion Photography Data Reduction by Digital Computers," Lawrence Radiation Laboratory, Livermore, Rept. UCRL-14155, 1965.
7. Vortman, L. et al., "Project Buckboard," Sandia Corporation, Albuquerque, N. Mexico Rept. SC-4486 (RR) 1960.

APPENDIX A

ACCELEROMETER TRACES

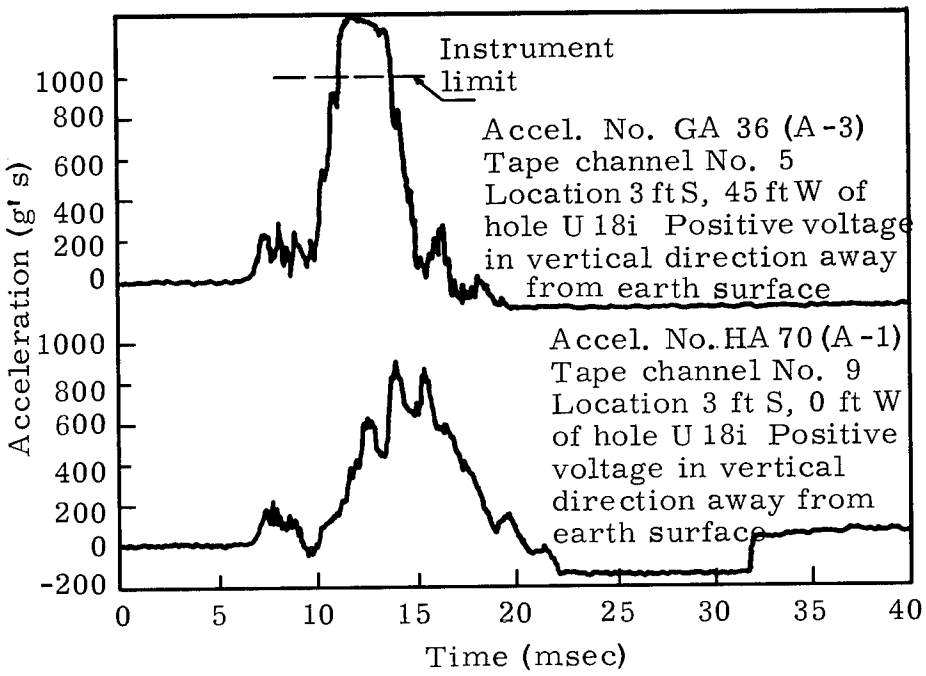

Fig. A-1 Traces from accelerometers at A-1 and A-3.

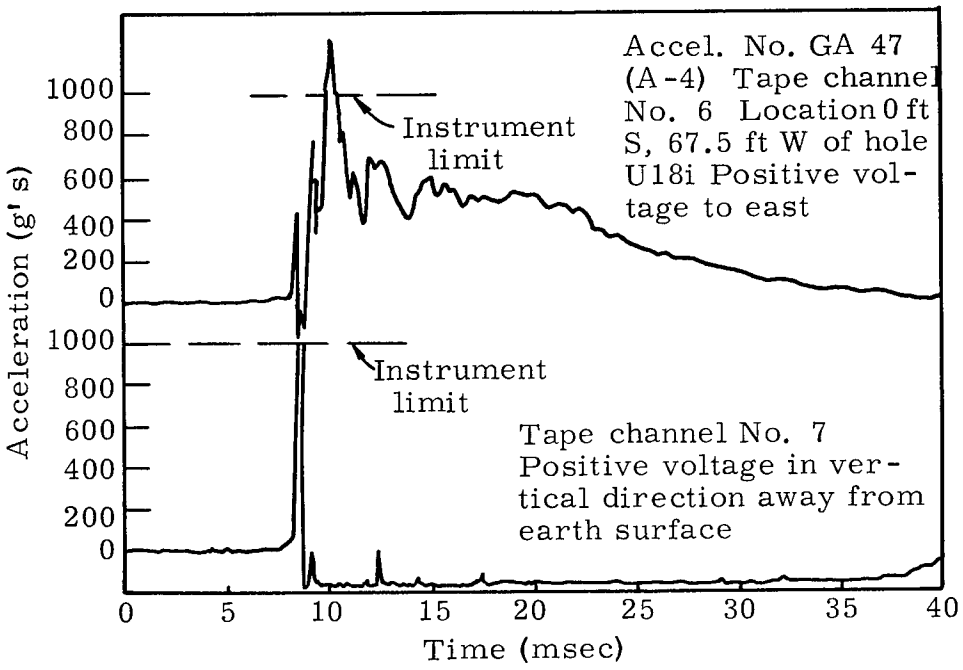

Fig. A-2 Traces from accelerometer at A-4.

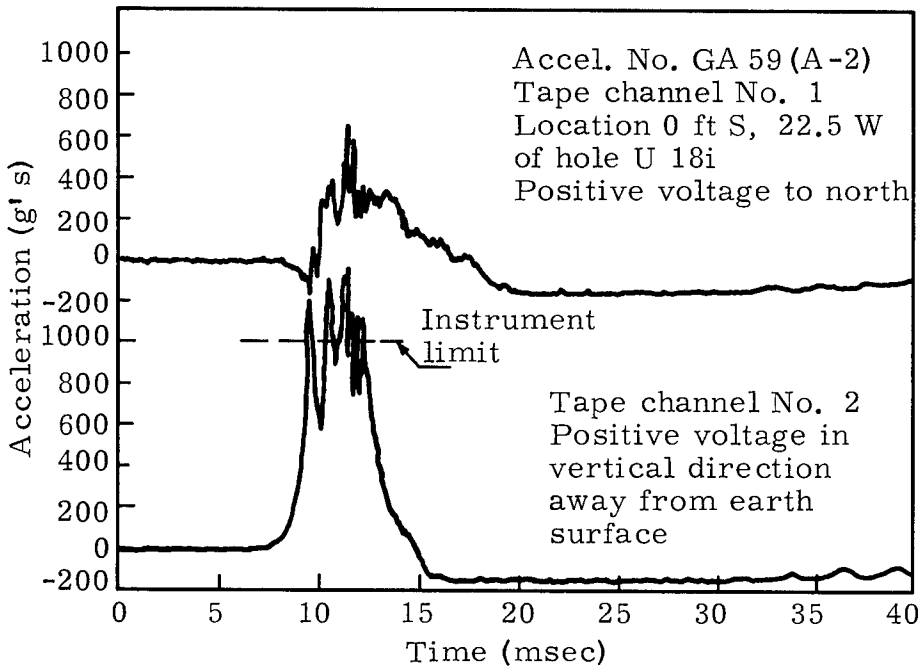

Fig. A-3 Traces from accelerometer at A-2.

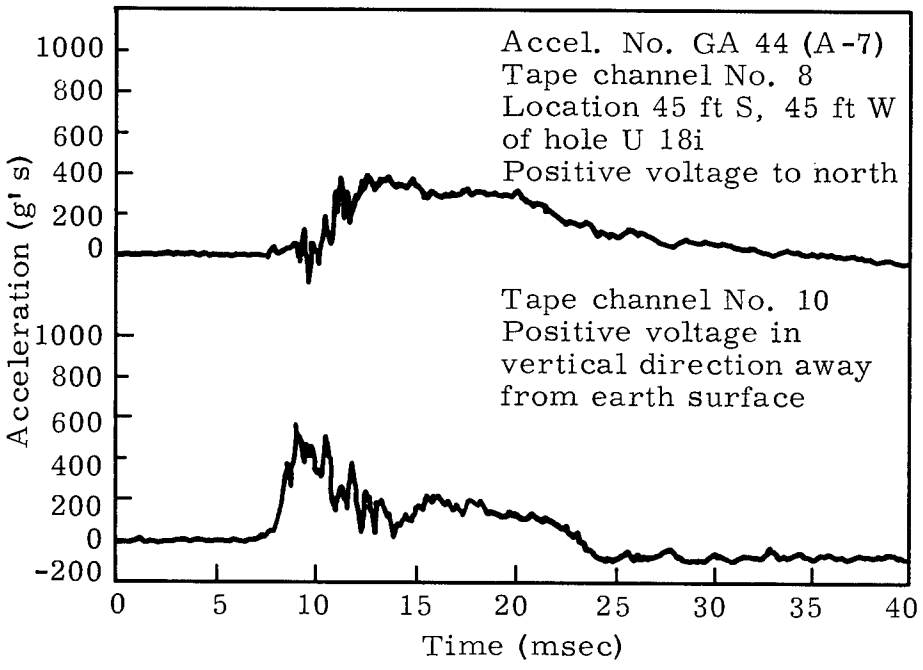

Fig. A-4 Traces from accelerometer at A-7.

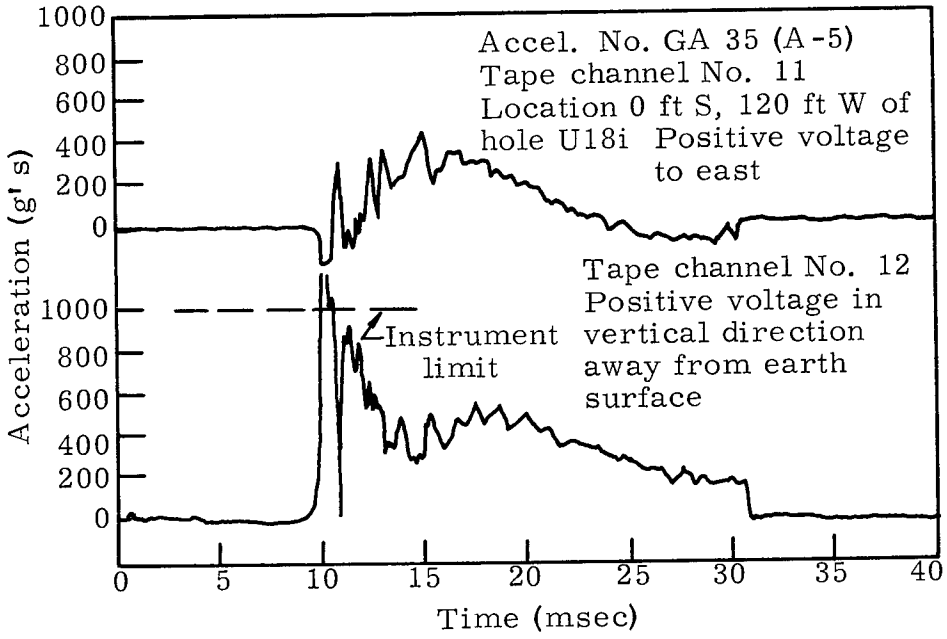

Fig. A-5 Traces from accelerometer at A-5.

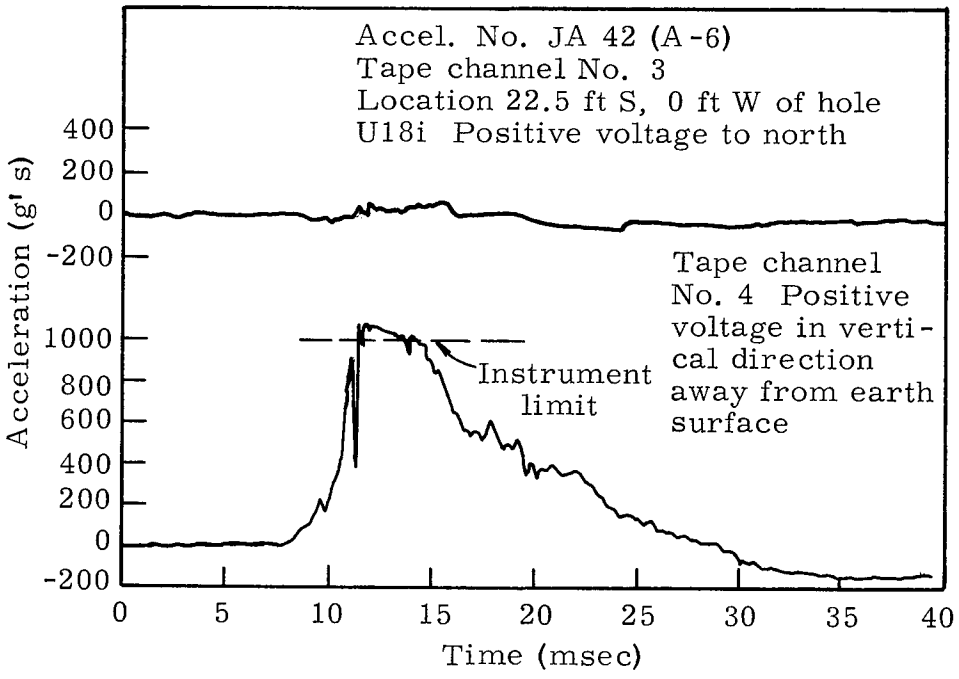

Fig. A-6 Traces from accelerometer at A-6.

APPENDIX B

BOWLING BALL TARGET DISPLACEMENT PLOTS

B-1 Series: Microscope Digitizer Readings

B-2 Series: Oscar Digitizer Readings

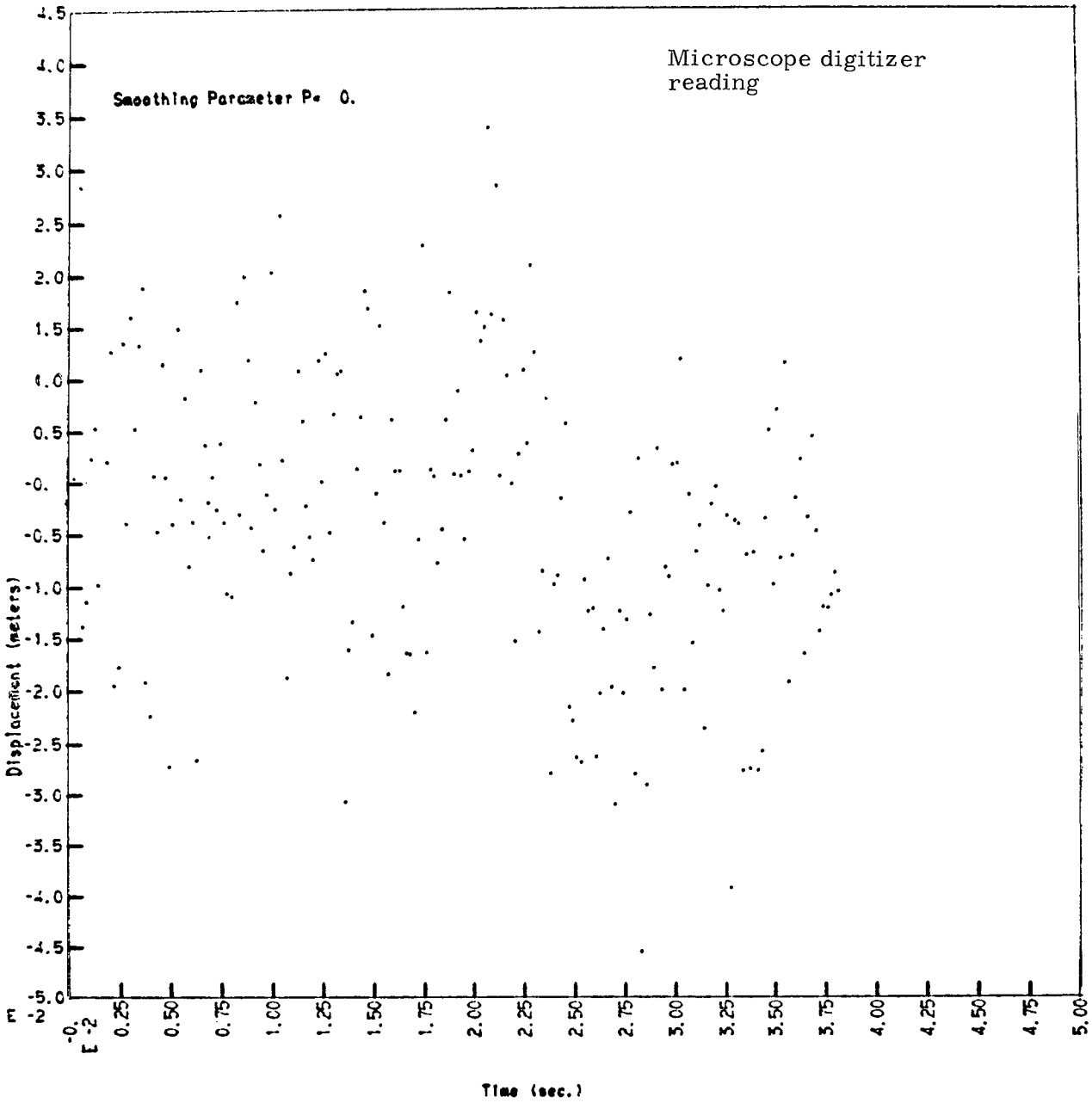

Figure B-1-1

Horizontal Displacement Target 11

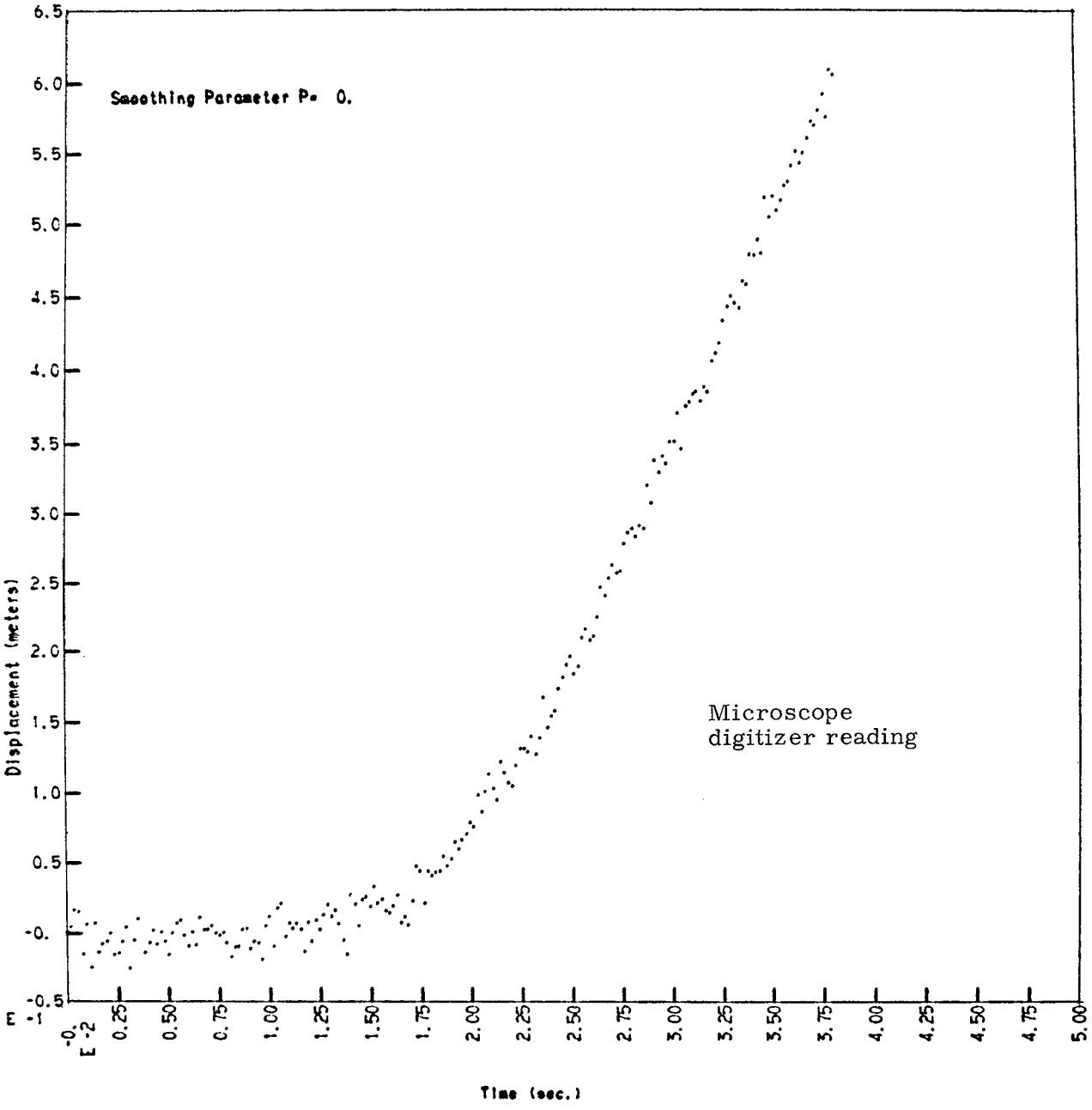

Figure B-1-2

Vertical Displacement Target 11

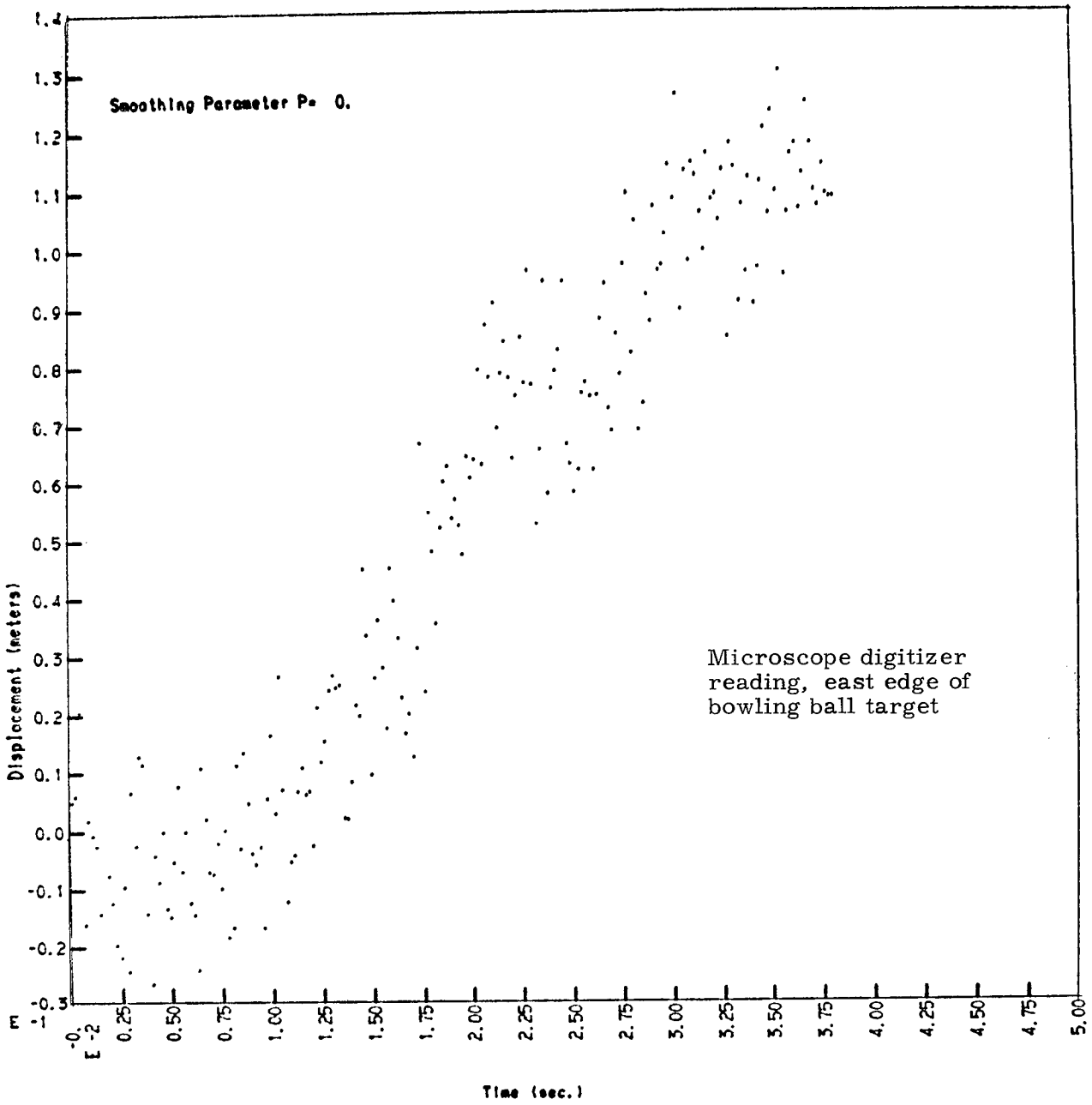

Figure B-1-3
Horizontal Displacement

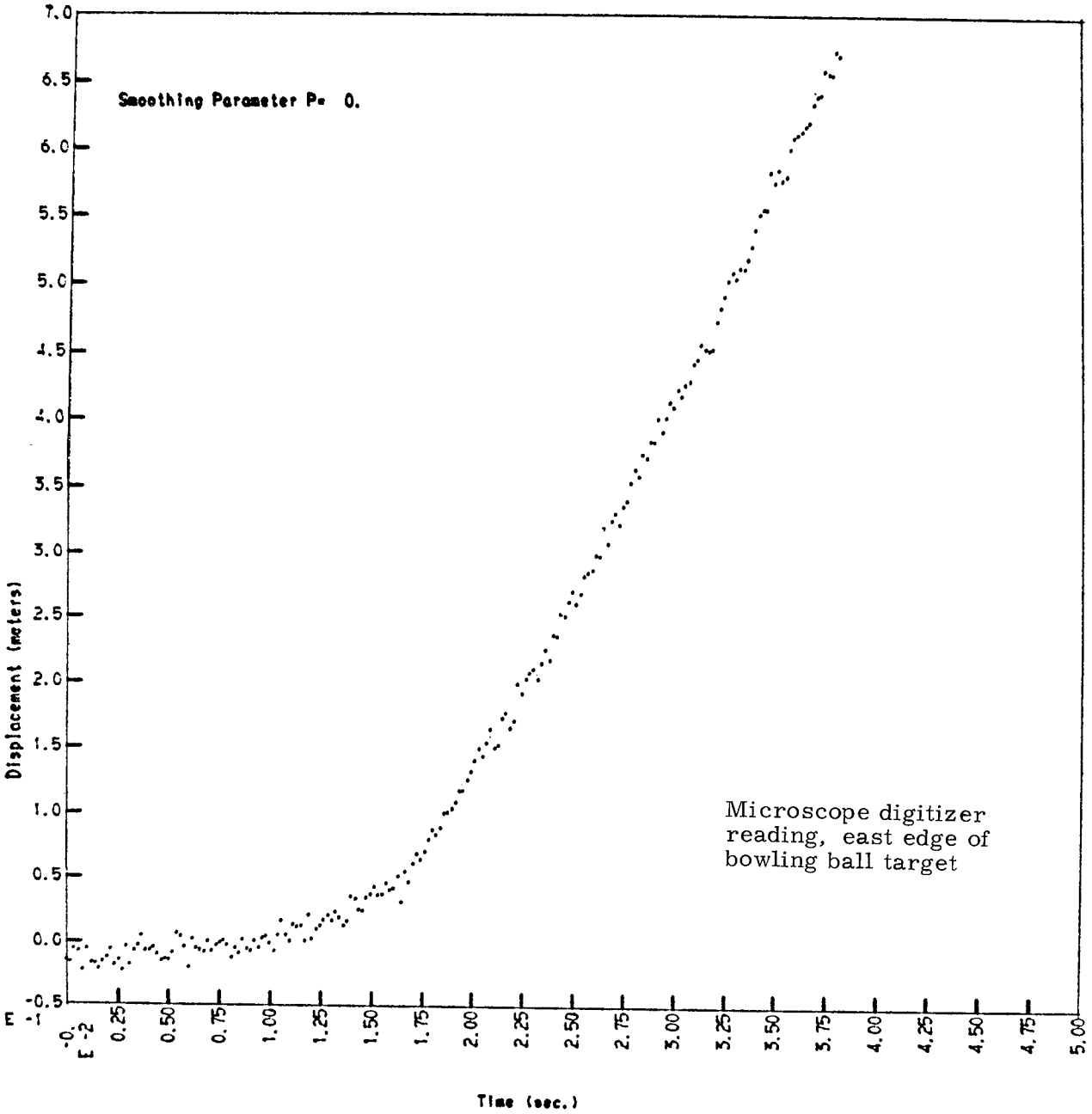

Figure B-1-4
Vertical Displacement

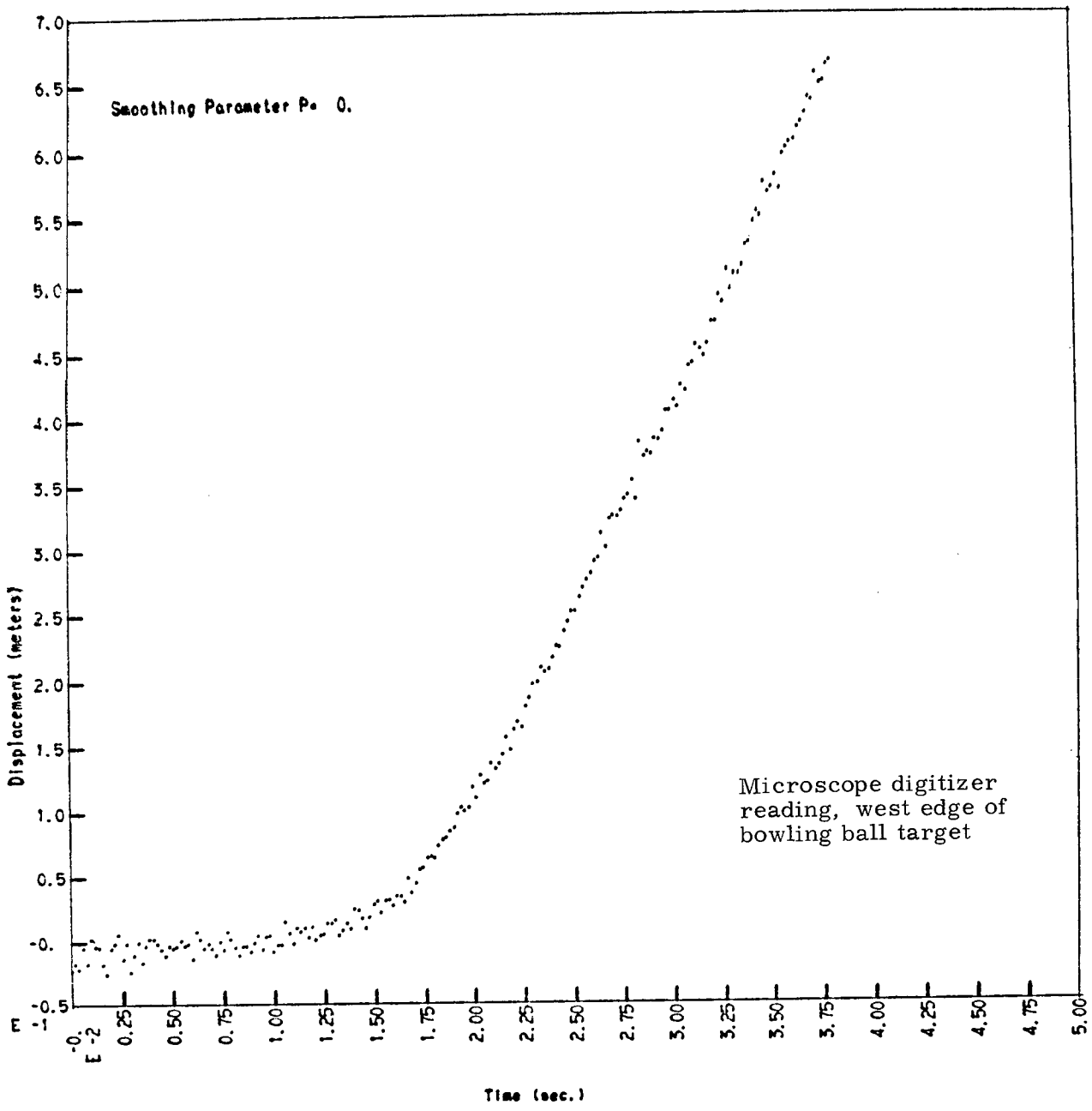

Figure B-1-5
Vertical Displacement

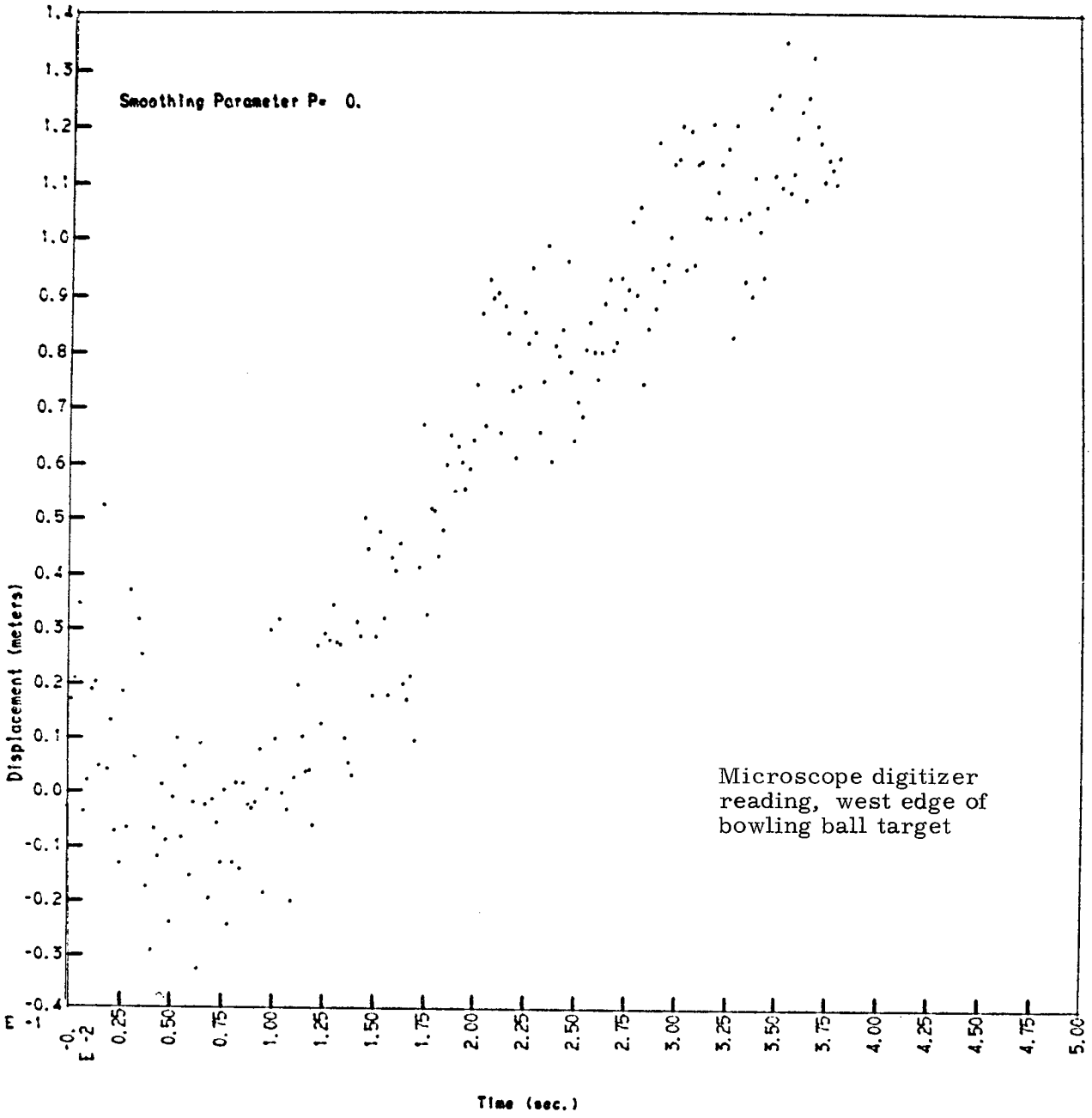

Figure B-1-6
Horizontal Displacement

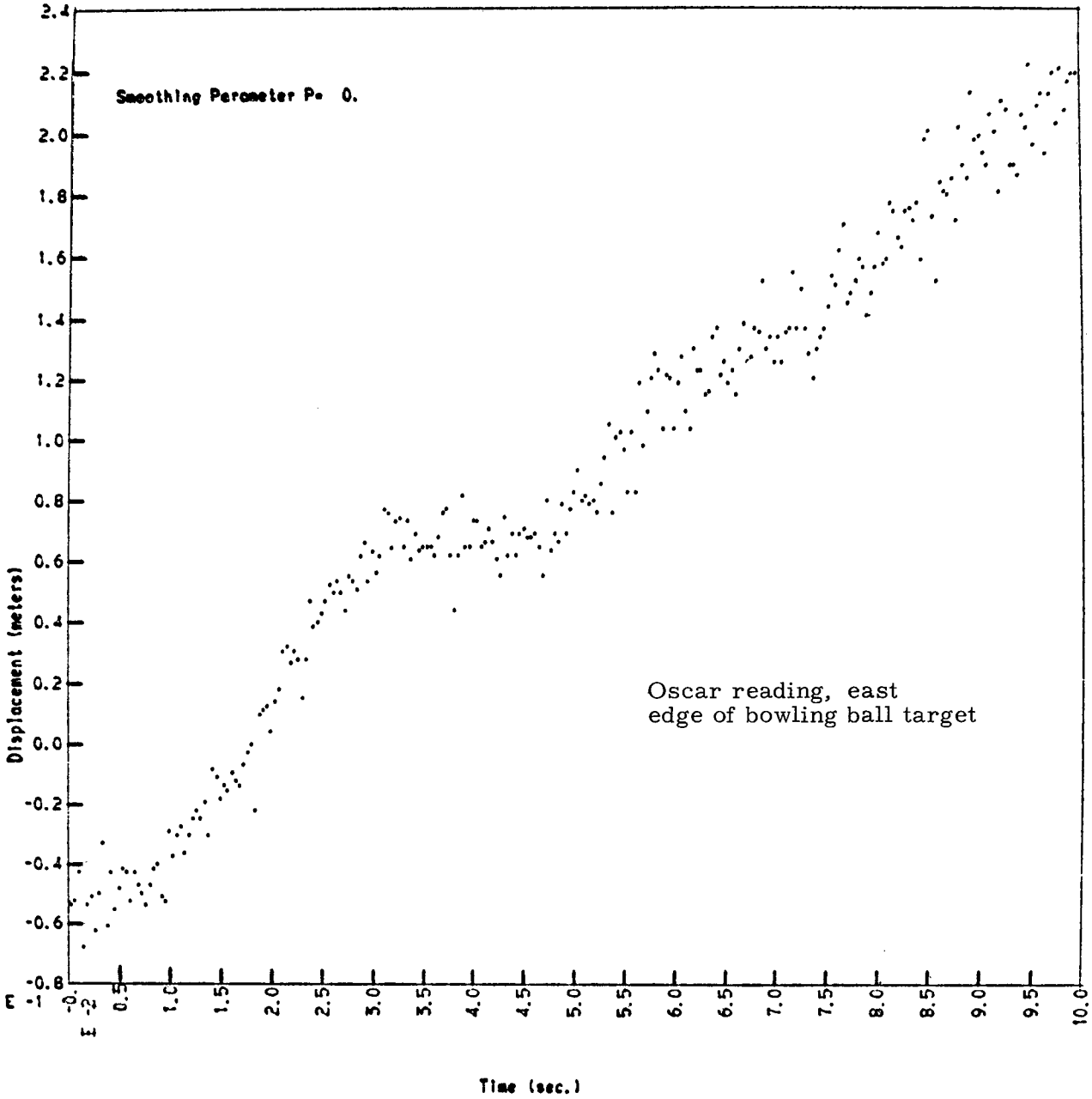

Figure B-2-1
Horizontal Displacement

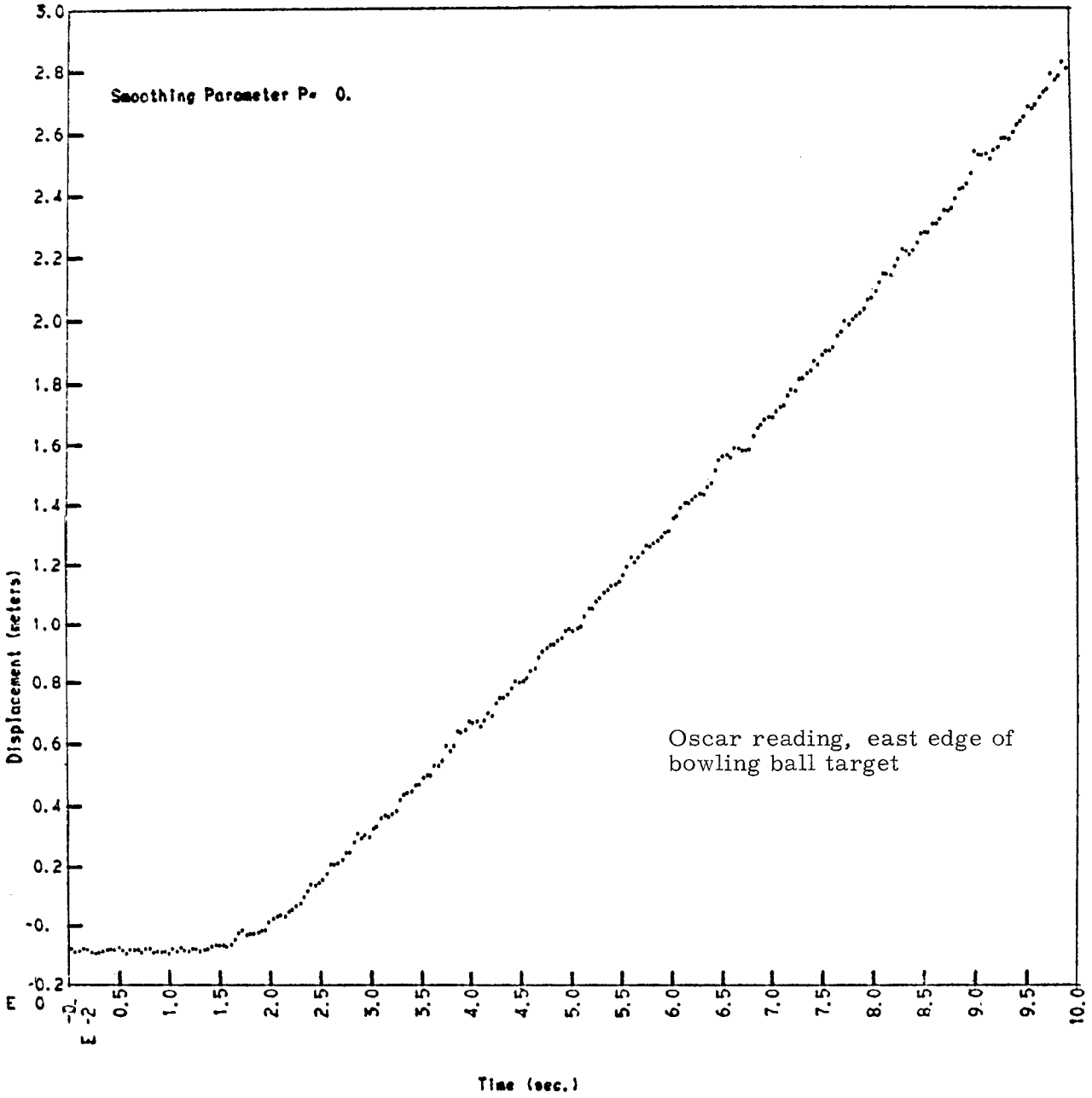

Figure B-2-2
Vertical Displacement

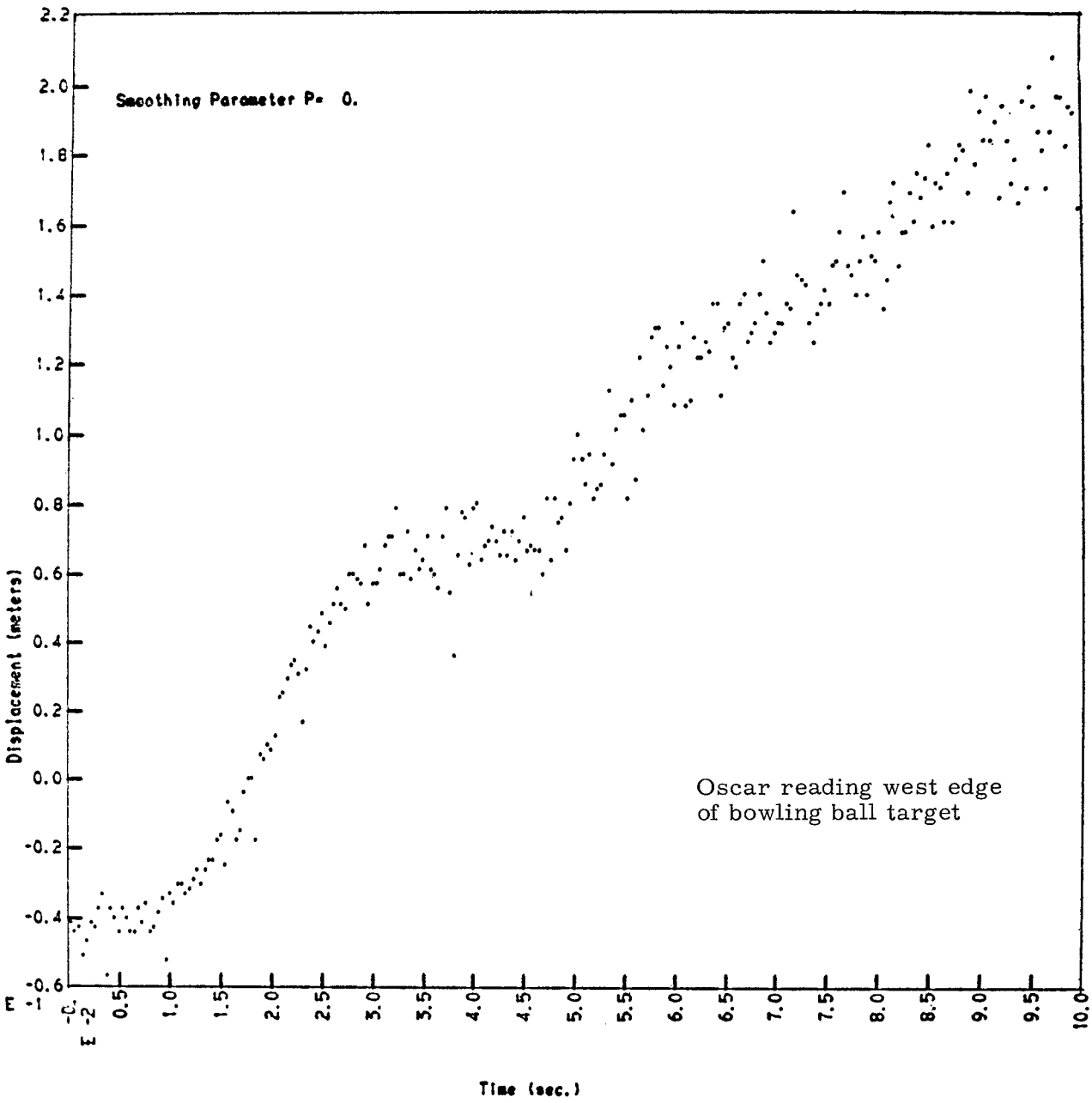

Figure B-2-3
Horizontal Displacement Target 2

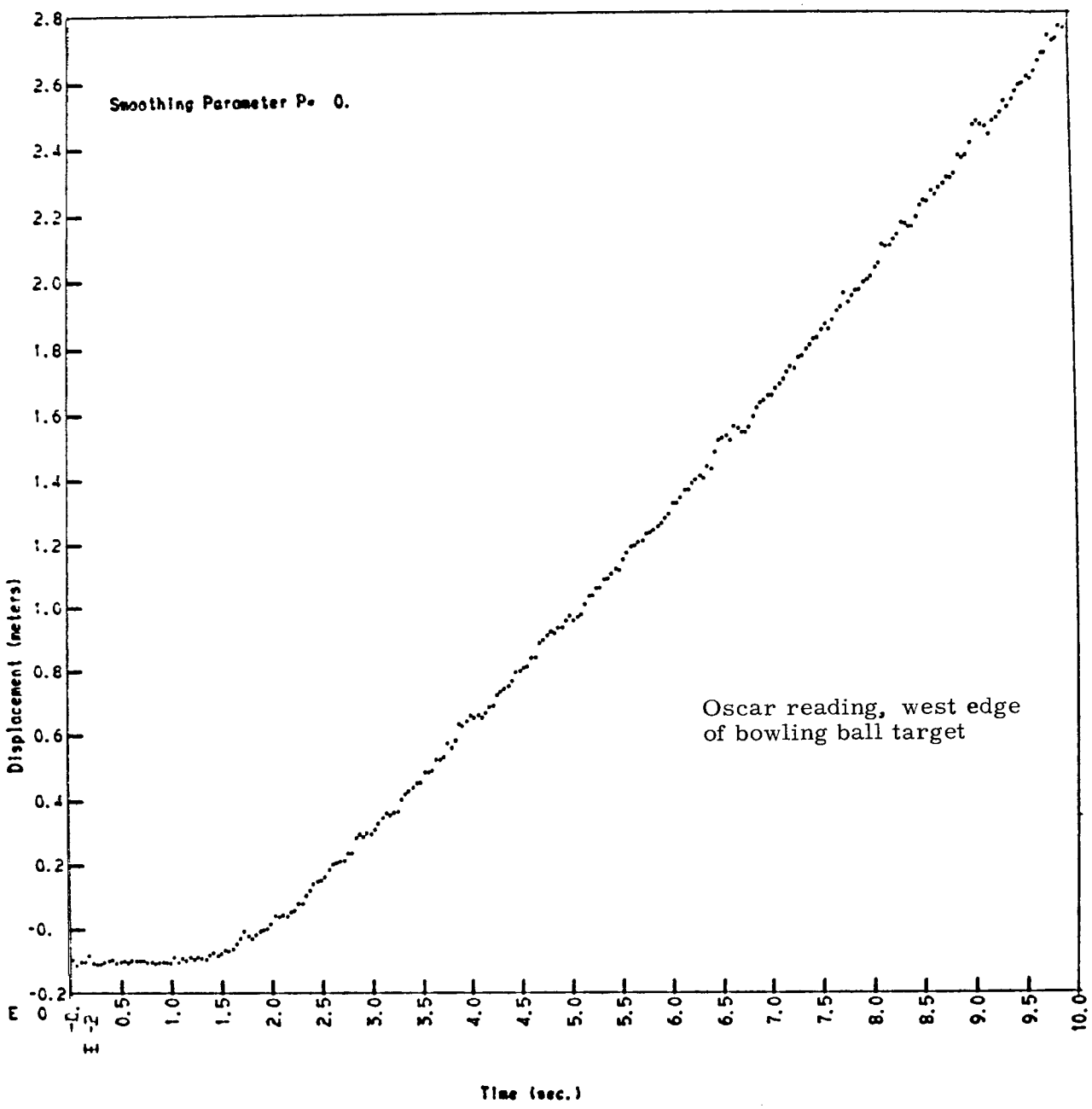

Figure B-2-4

Vertical Displacement Target 2

APPENDIX C

SURFACE MOTION TARGETS, HORIZONTAL AND VERTICAL DISPLACEMENT DATA

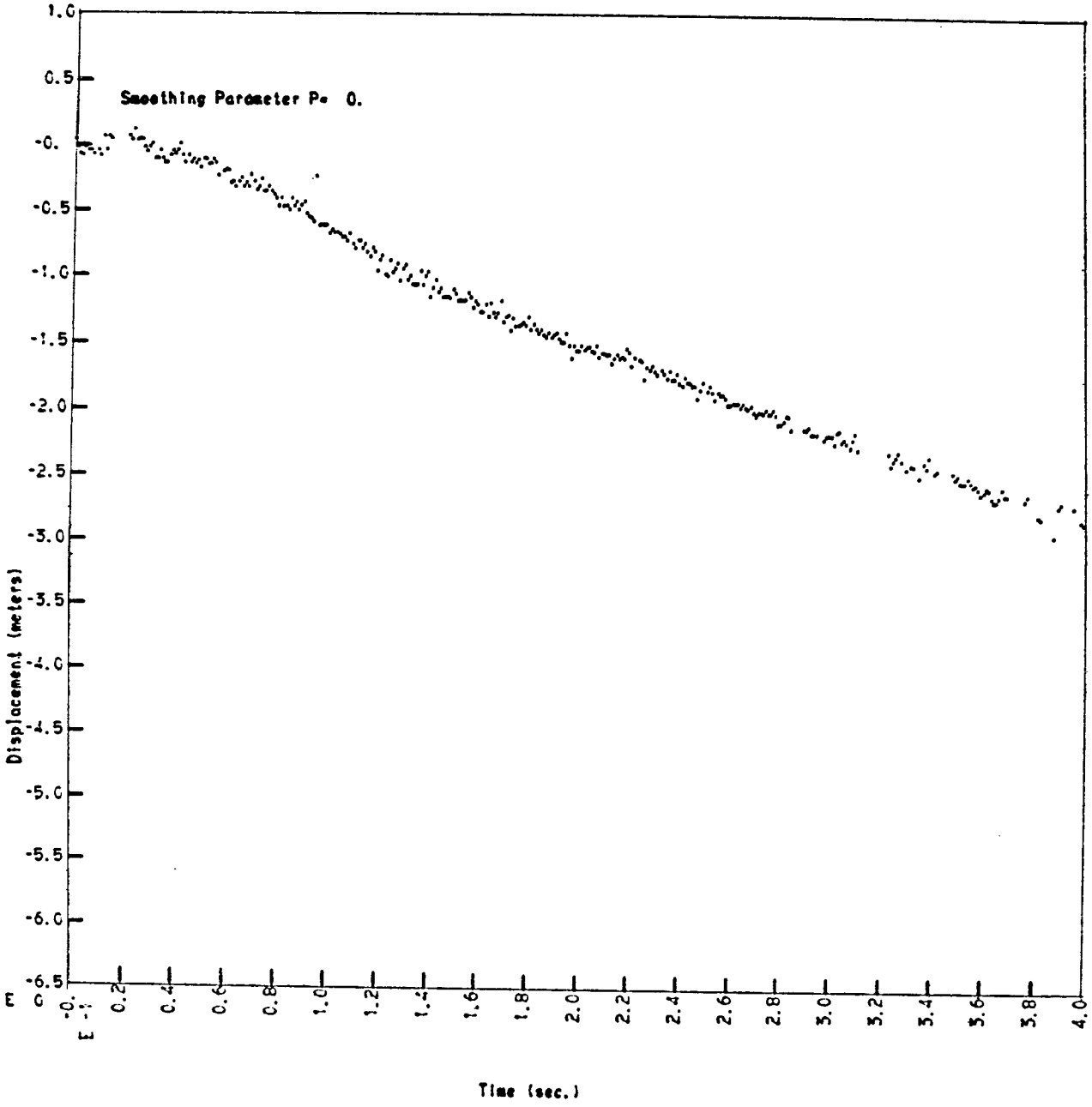

FIGURE C-1
Horizontal Displacement Target 1

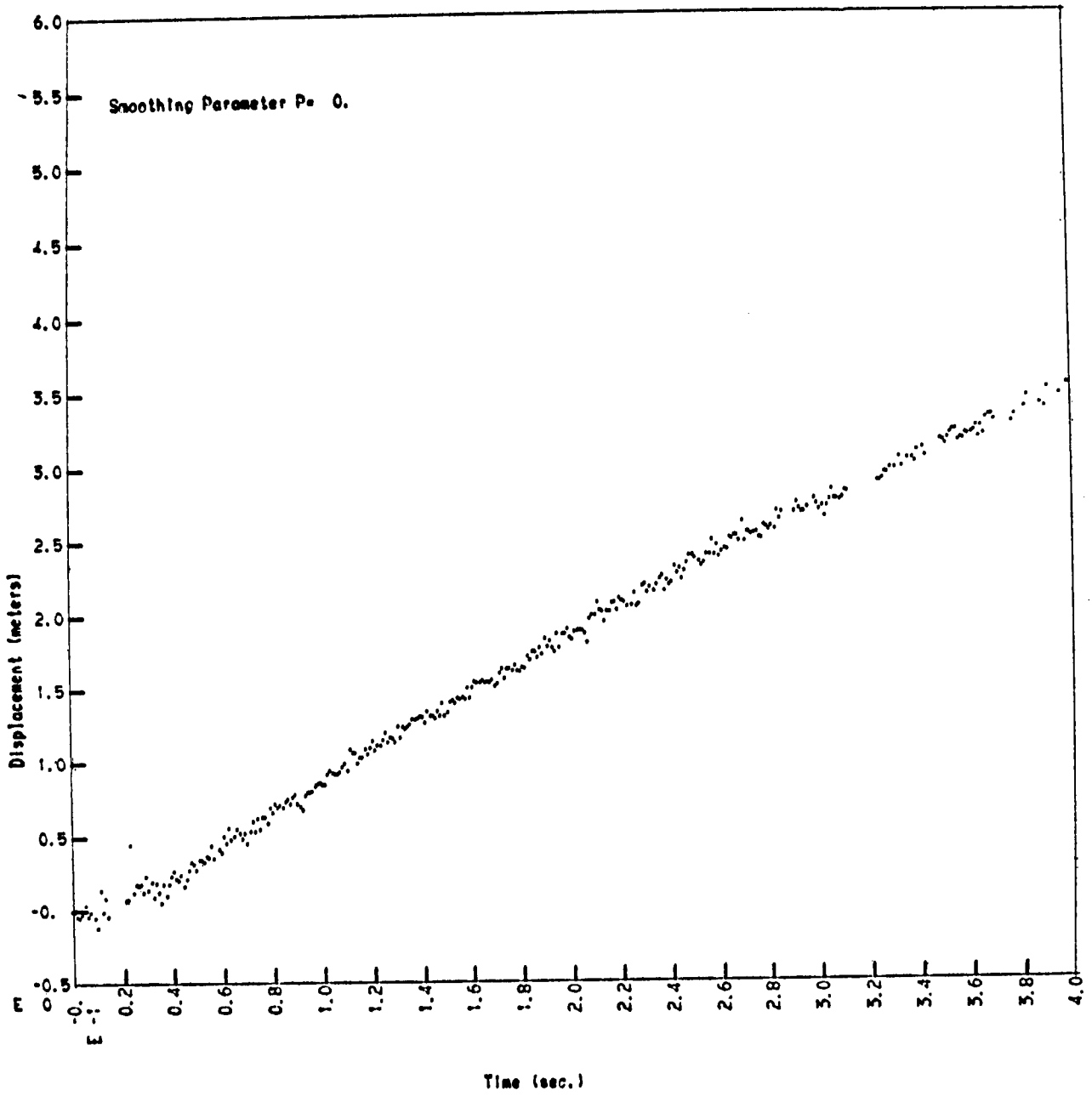

FIGURE C-2
Vertical Displacement Target 1

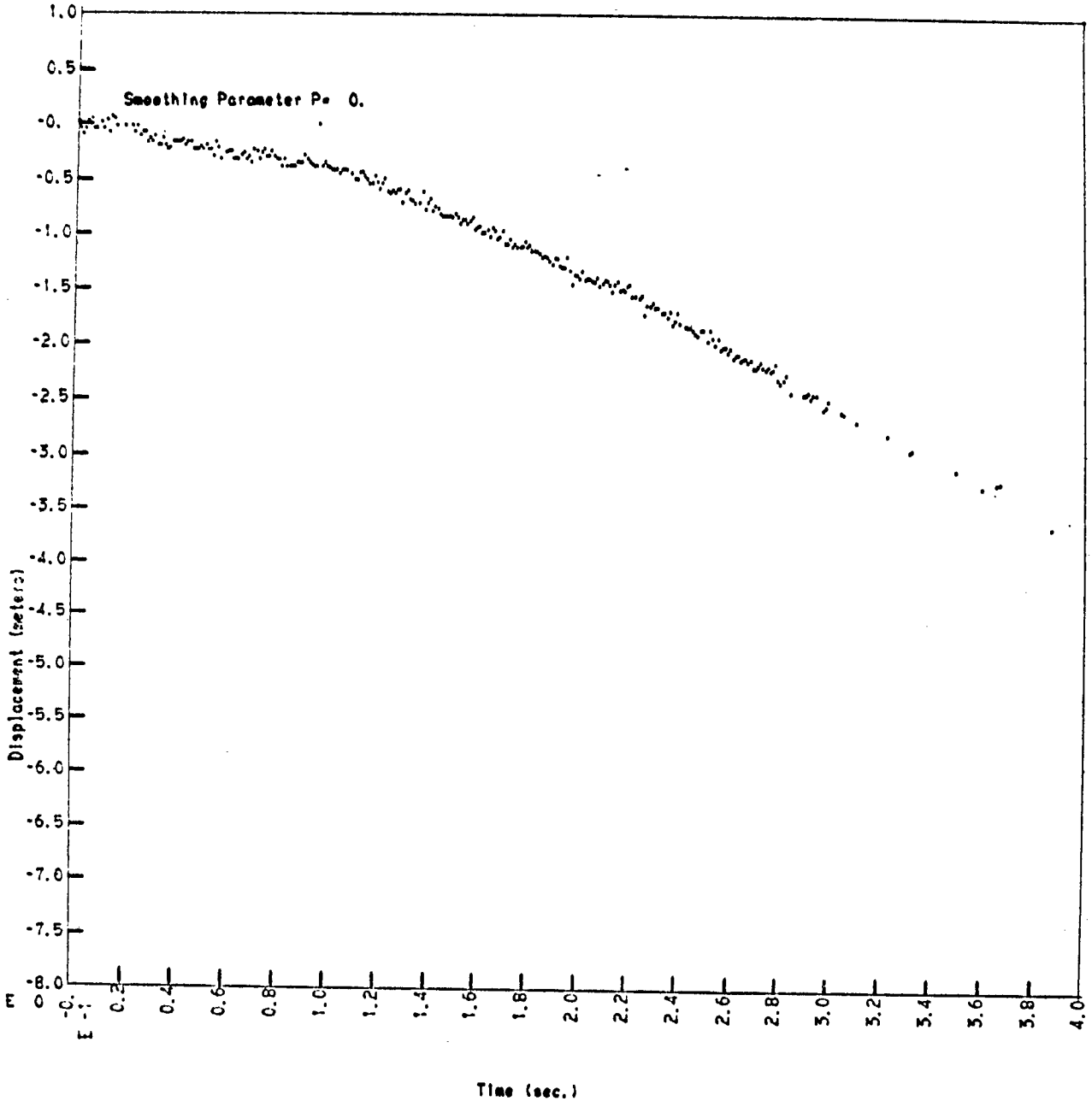

FIGURE C-3
Horizontal Displacement Target 2

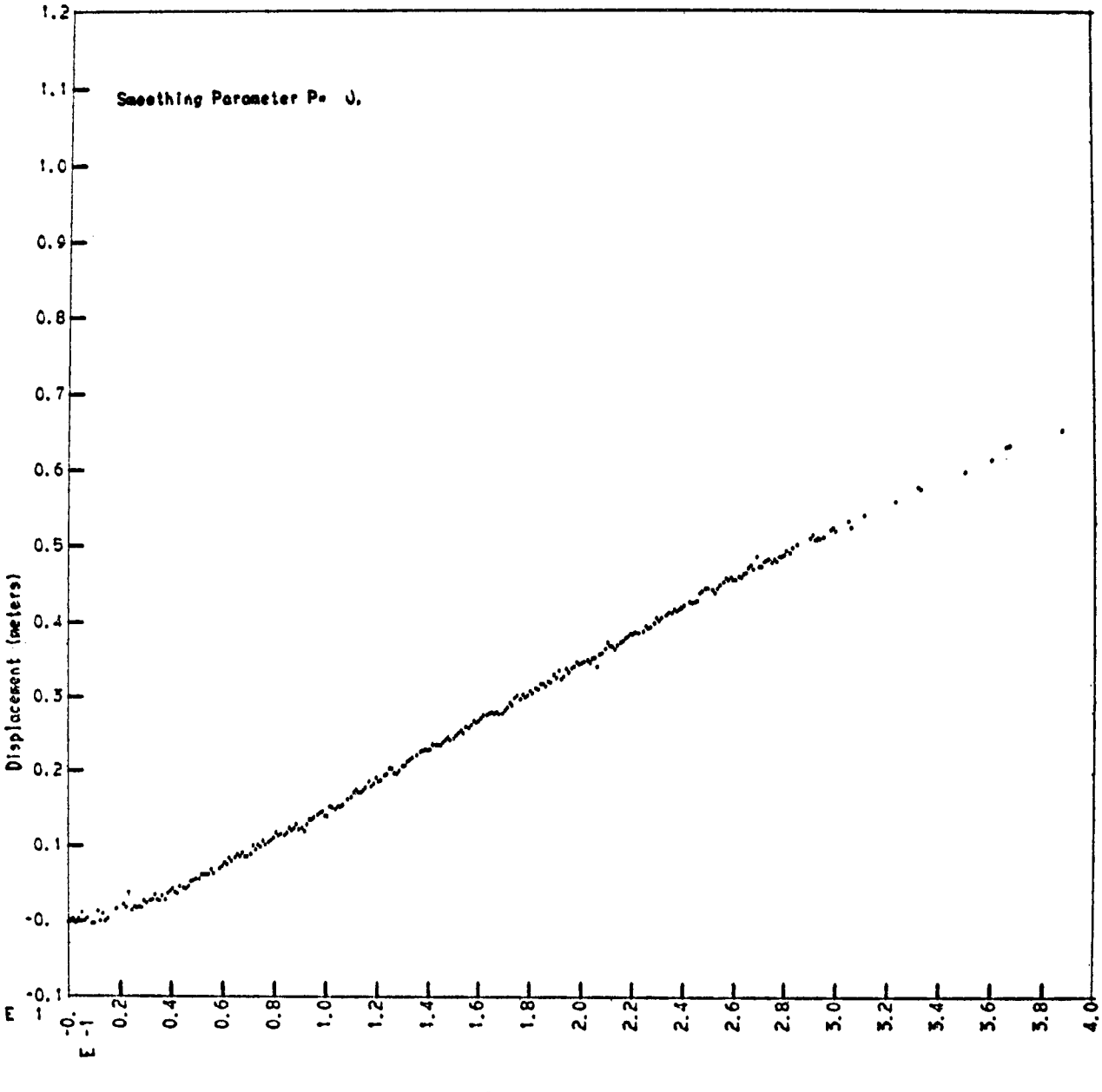

FIGURE C-4
Vertical Displacement Target 2

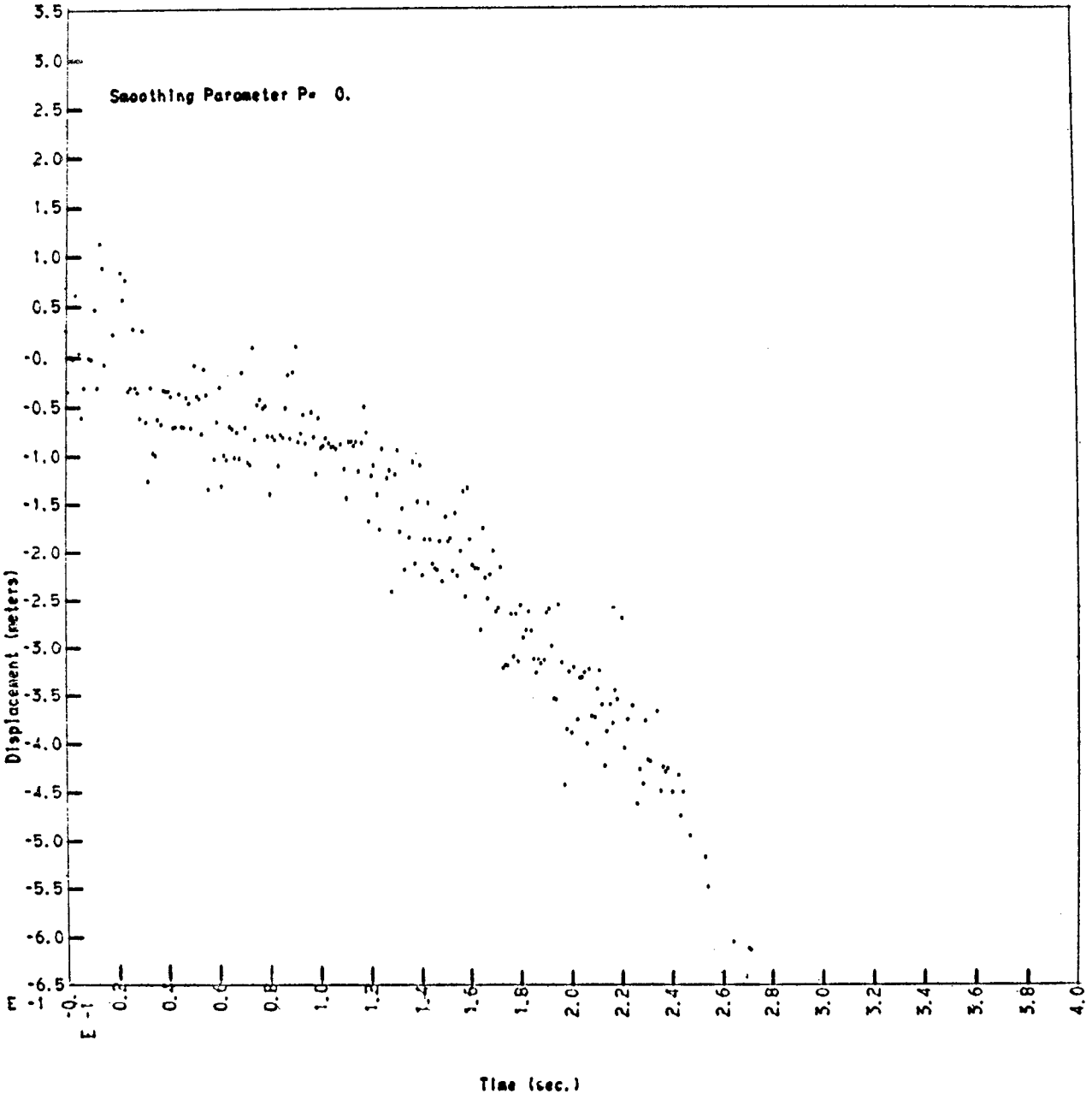

FIGURE C-5
Horizontal Displacement Target 3

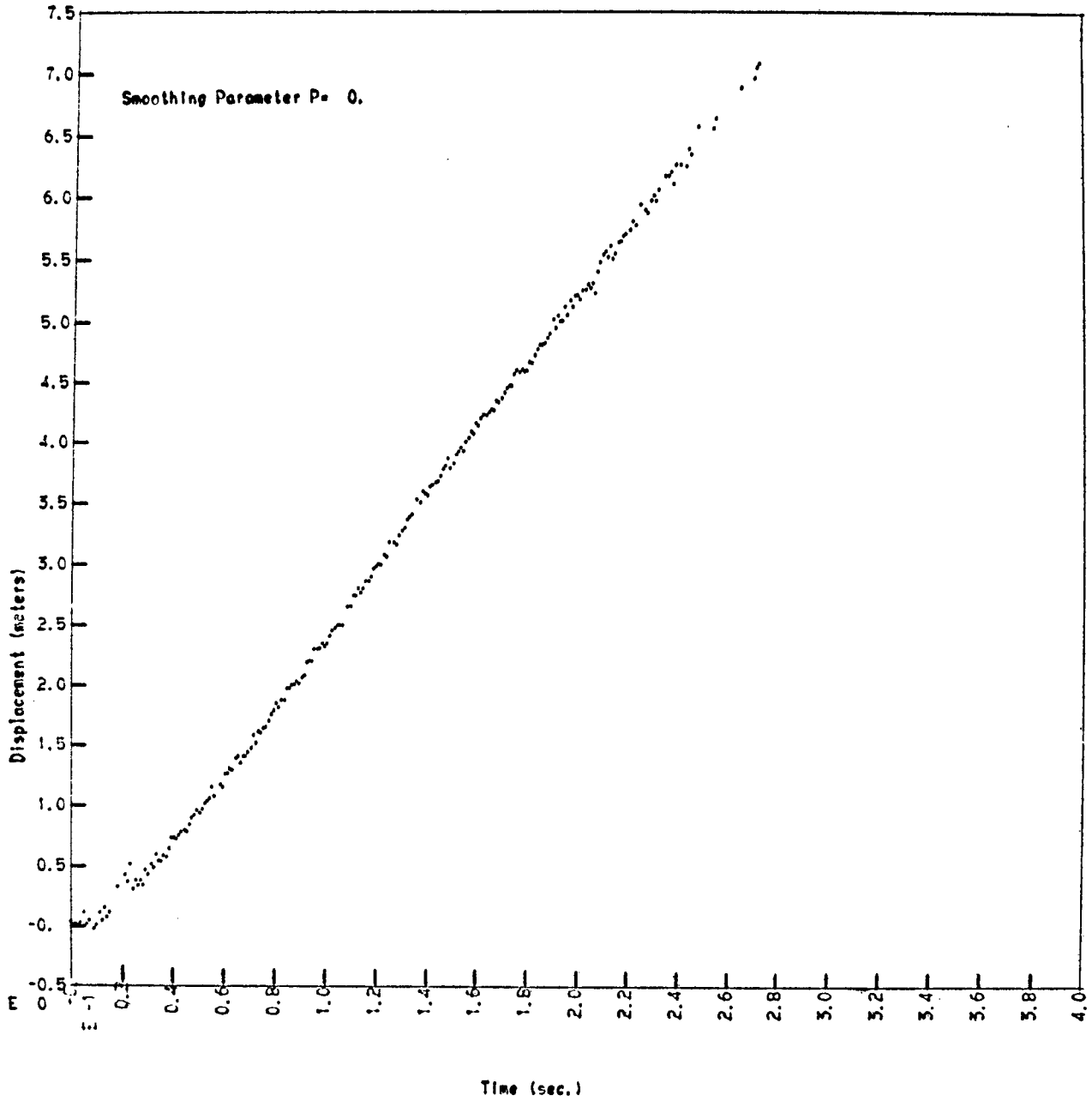

FIGURE C-6
Vertical Displacement Target 3

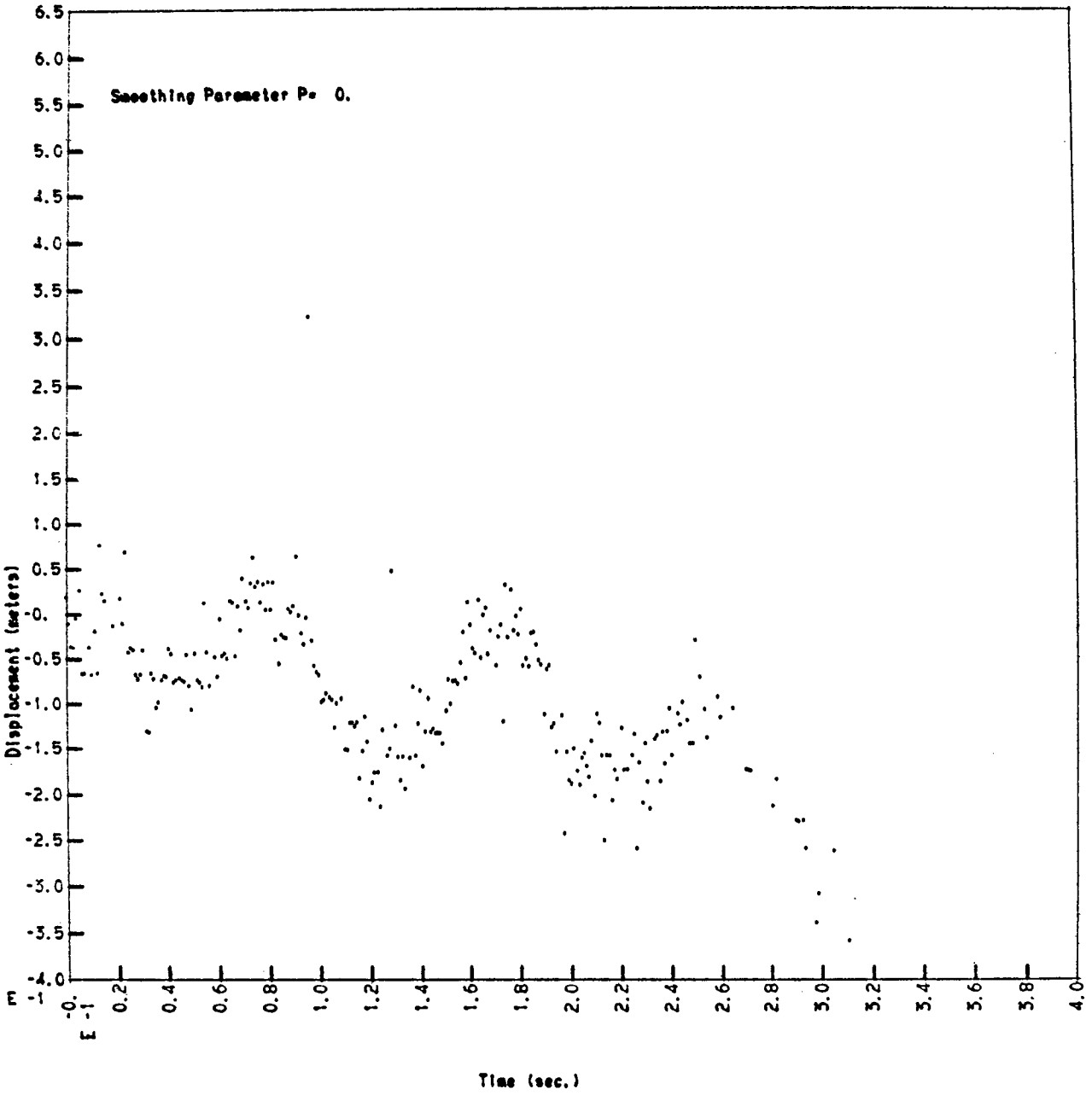

FIGURE C-7
Horizontal Displacement Target 4

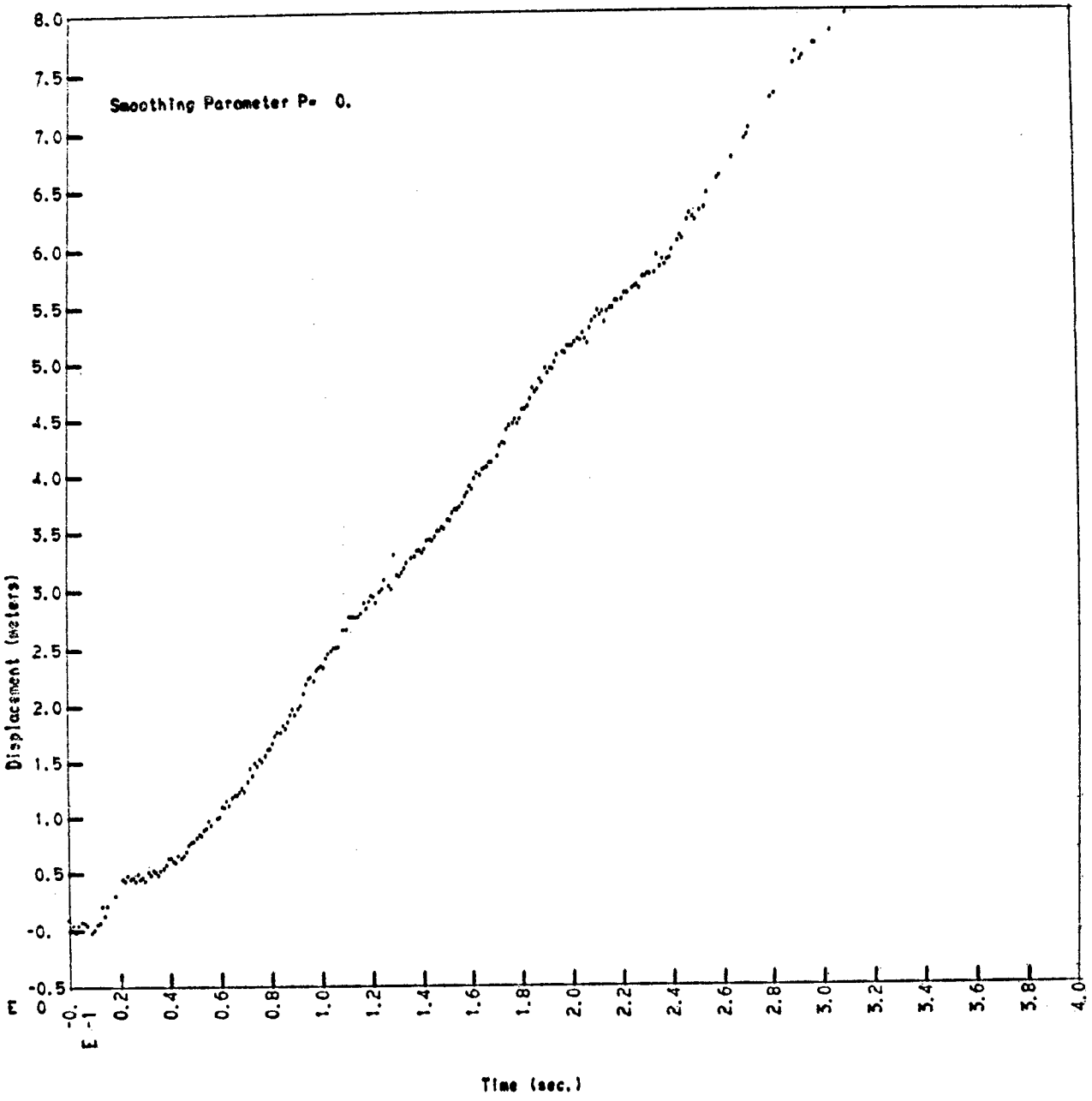

FIGURE C-8
Vertical Displacement Target 4

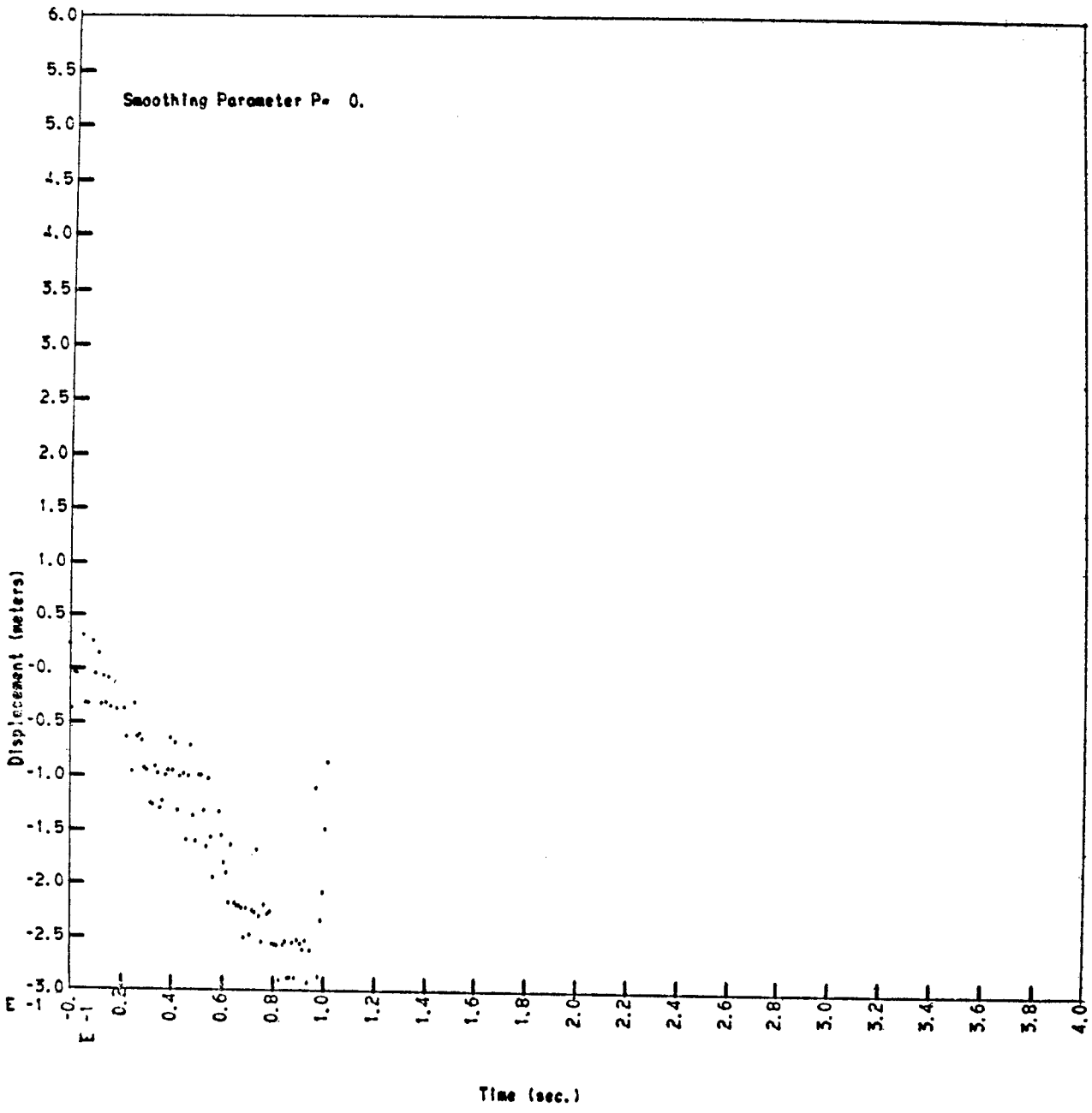

FIGURE C-9
Horizontal Displacement Target 5

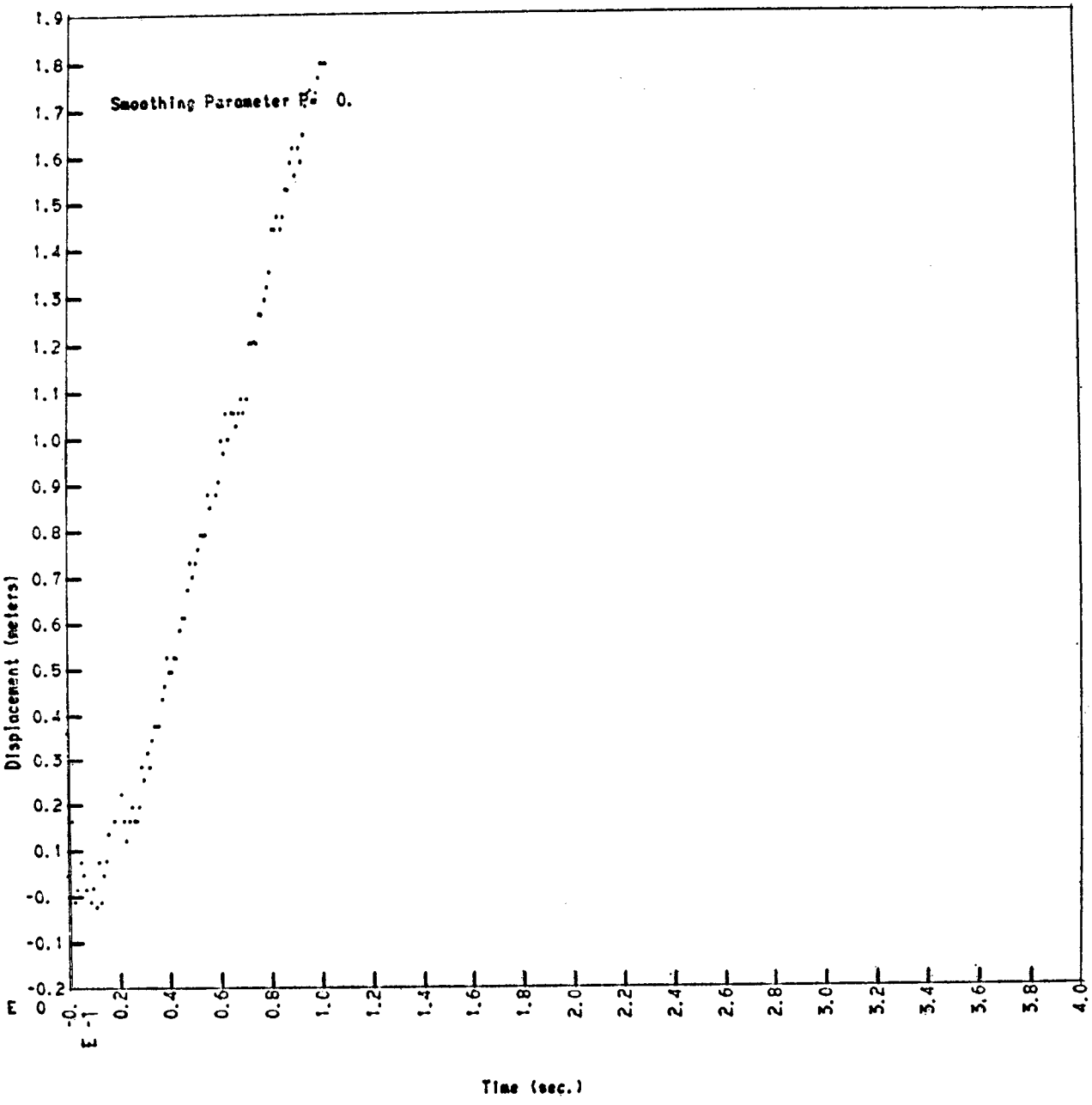

FIGURE C-10
Vertical Displacement Target 5

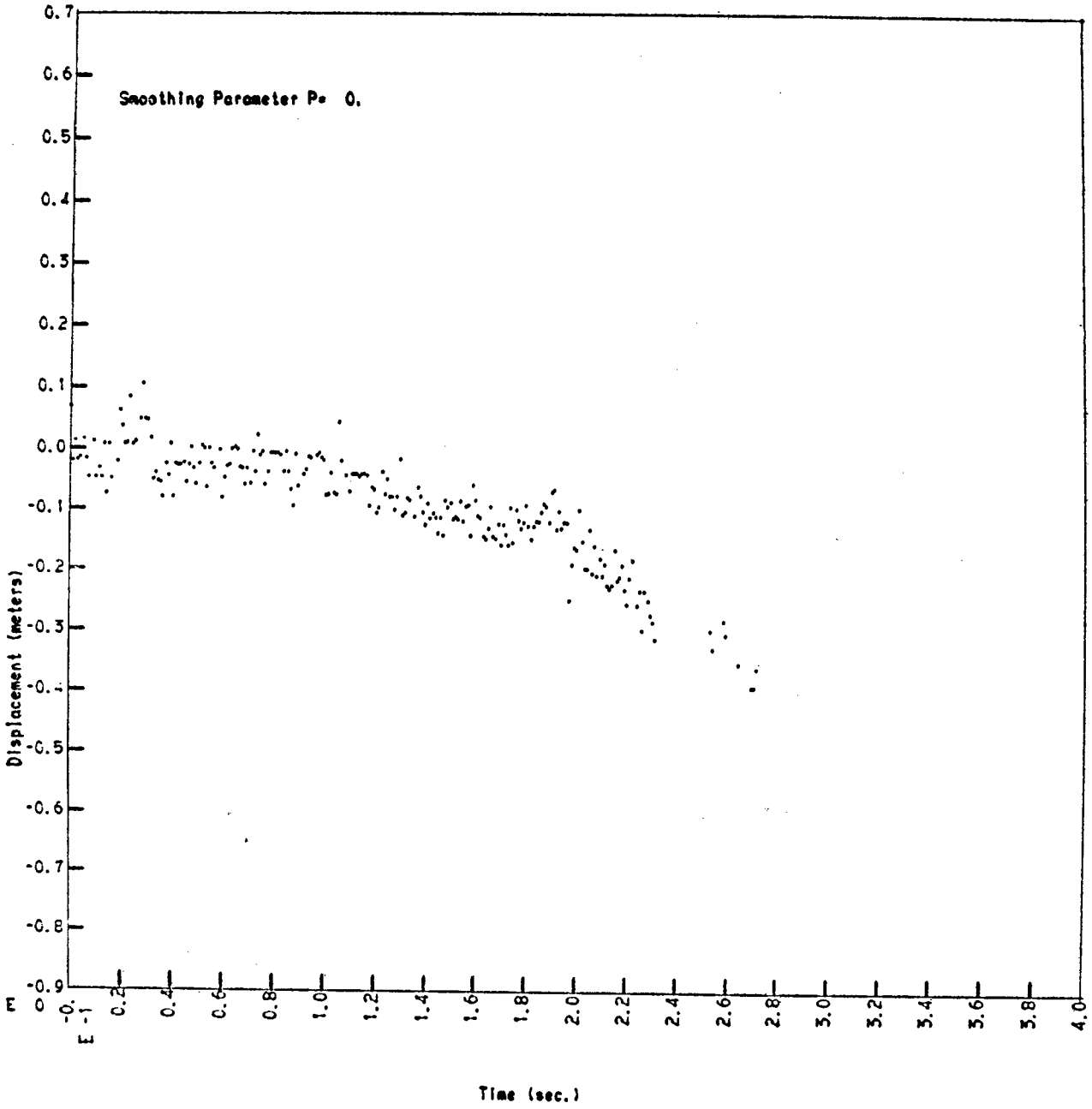

FIGURE C-11
Horizontal Displacement Target 6

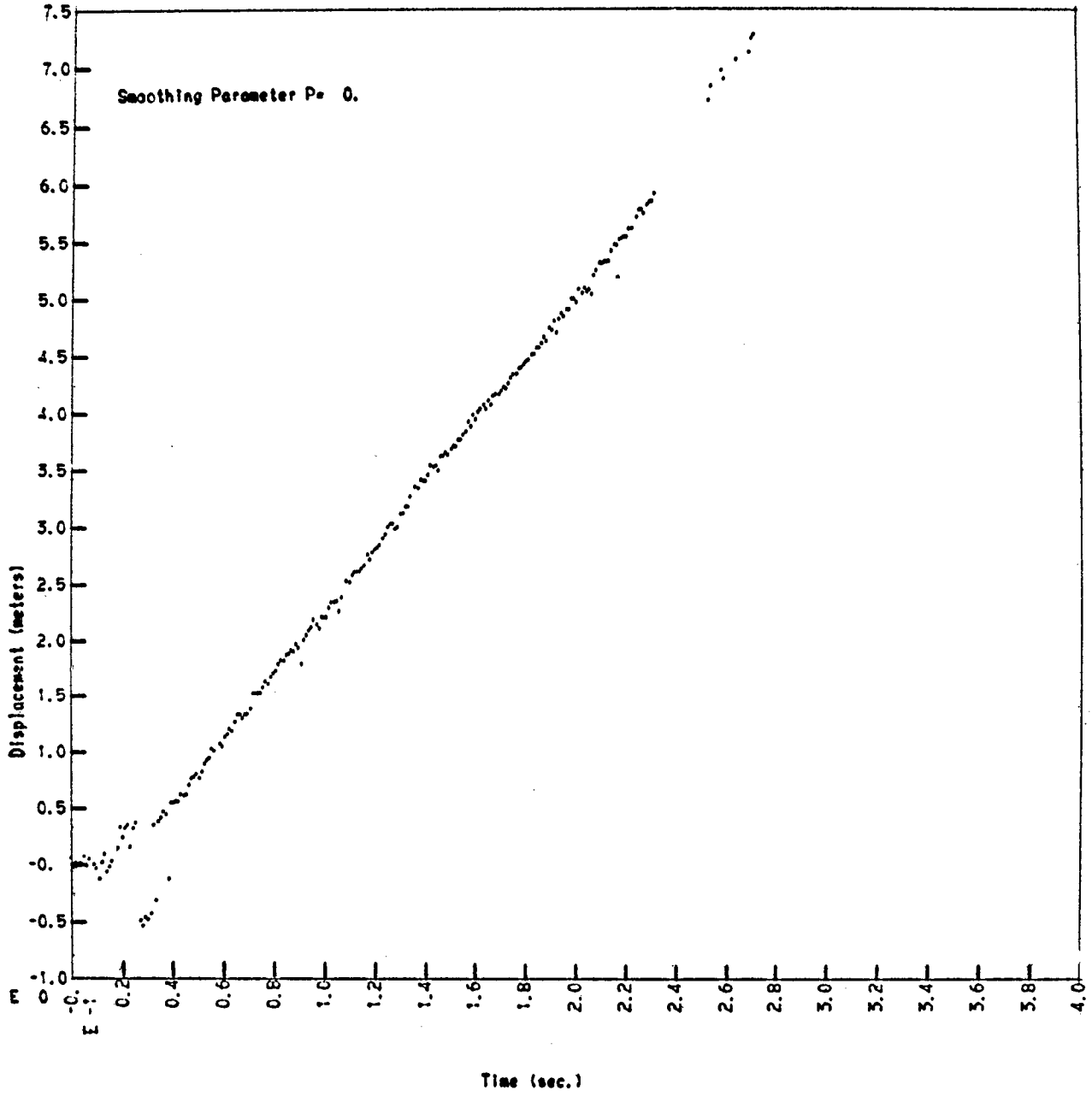

FIGURE C-12
Vertical Displacement Target 6

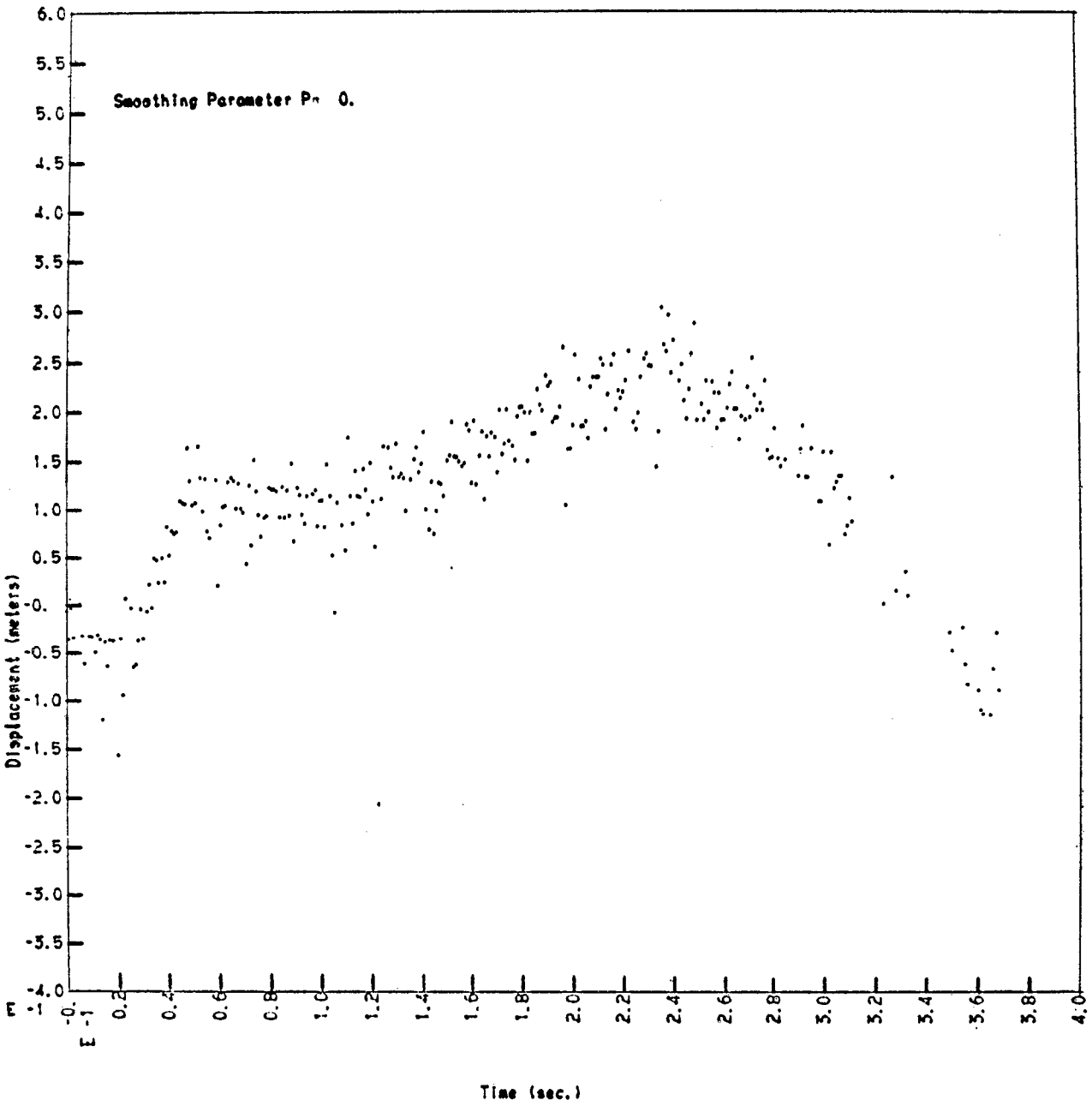

FIGURE C-13
Horizontal Displacement Target 7

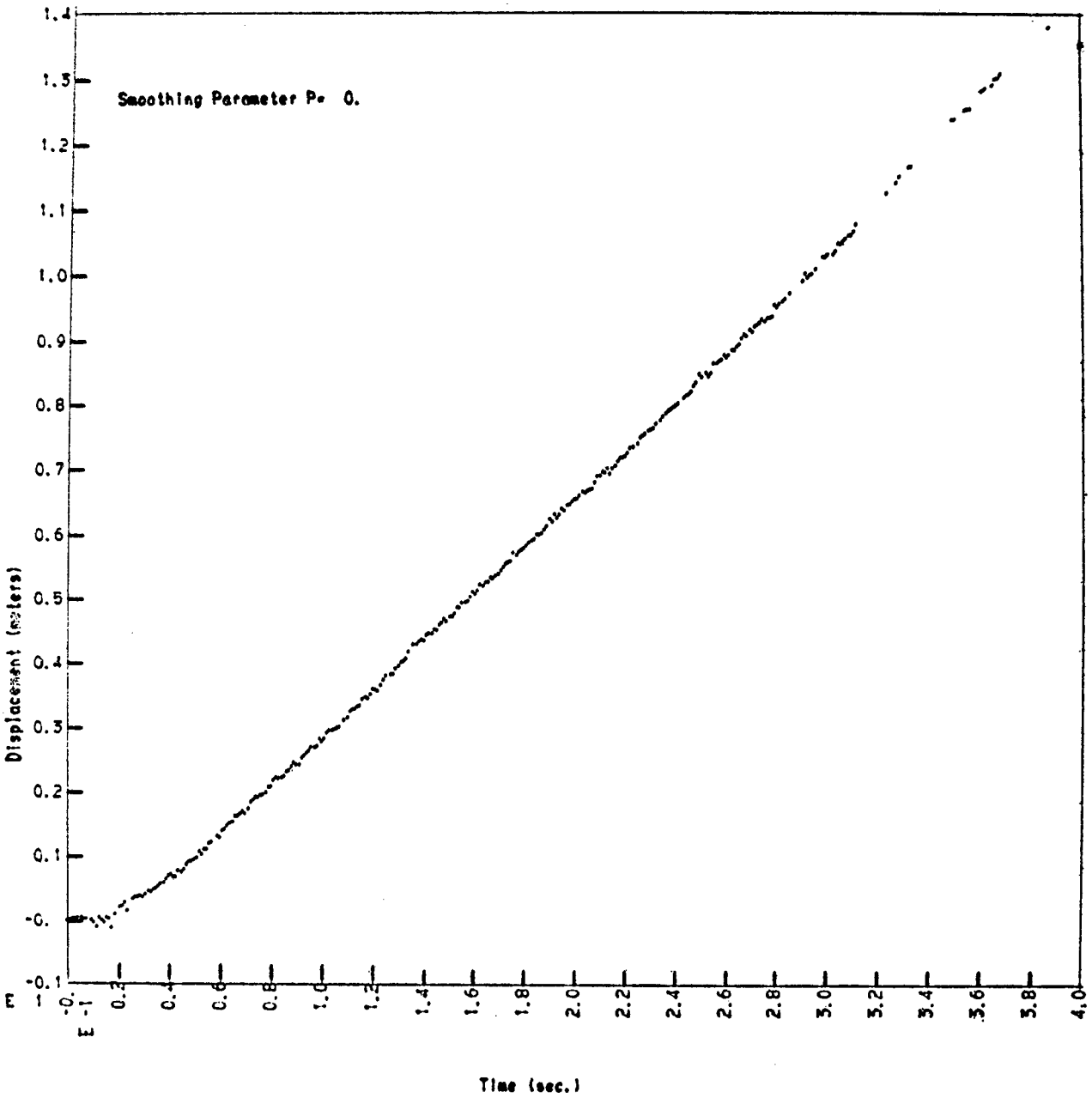

FIGURE C-14
Vertical Displacement Target 7

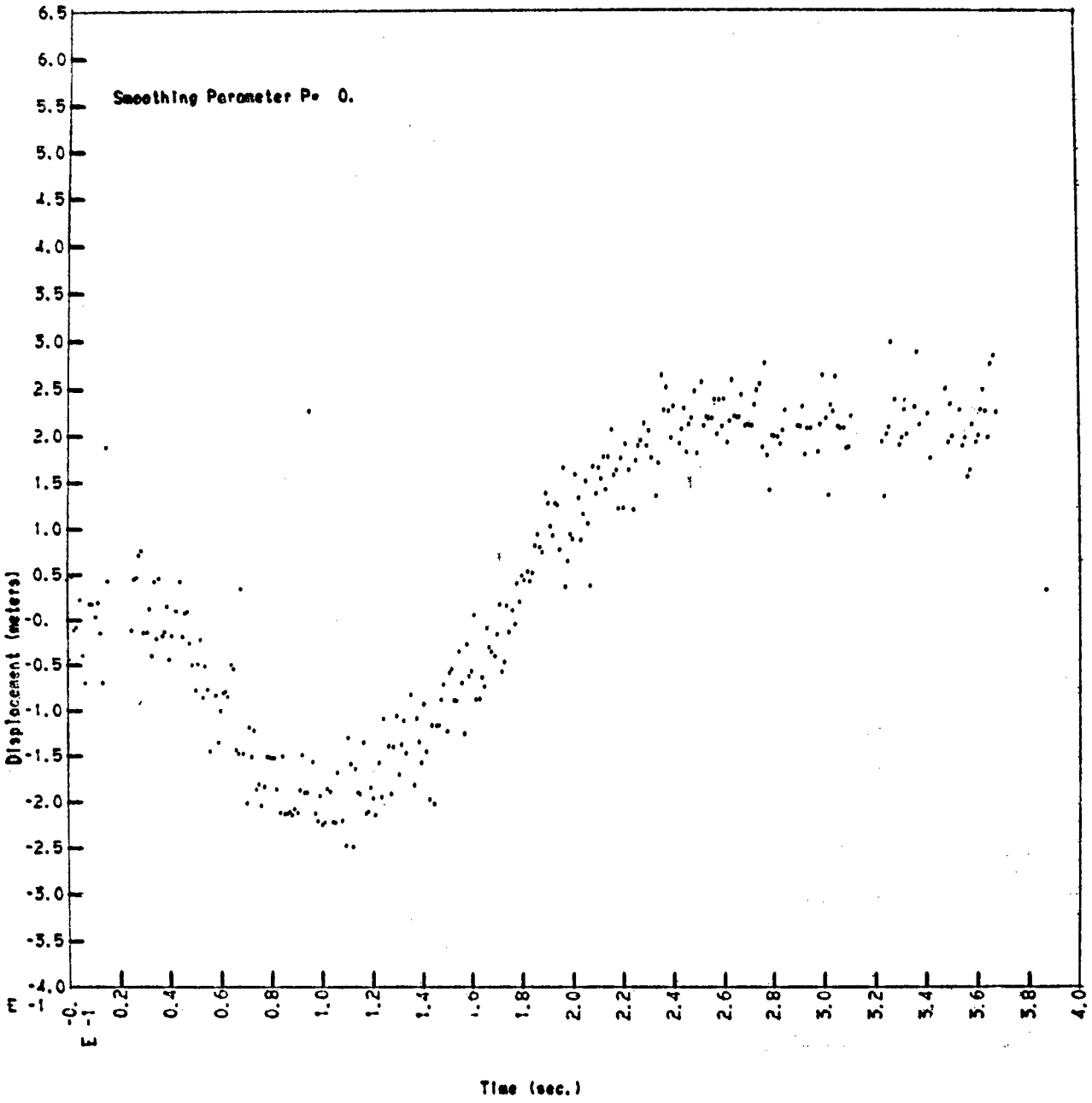

FIGURE C-15
Horizontal Displacement Target 8

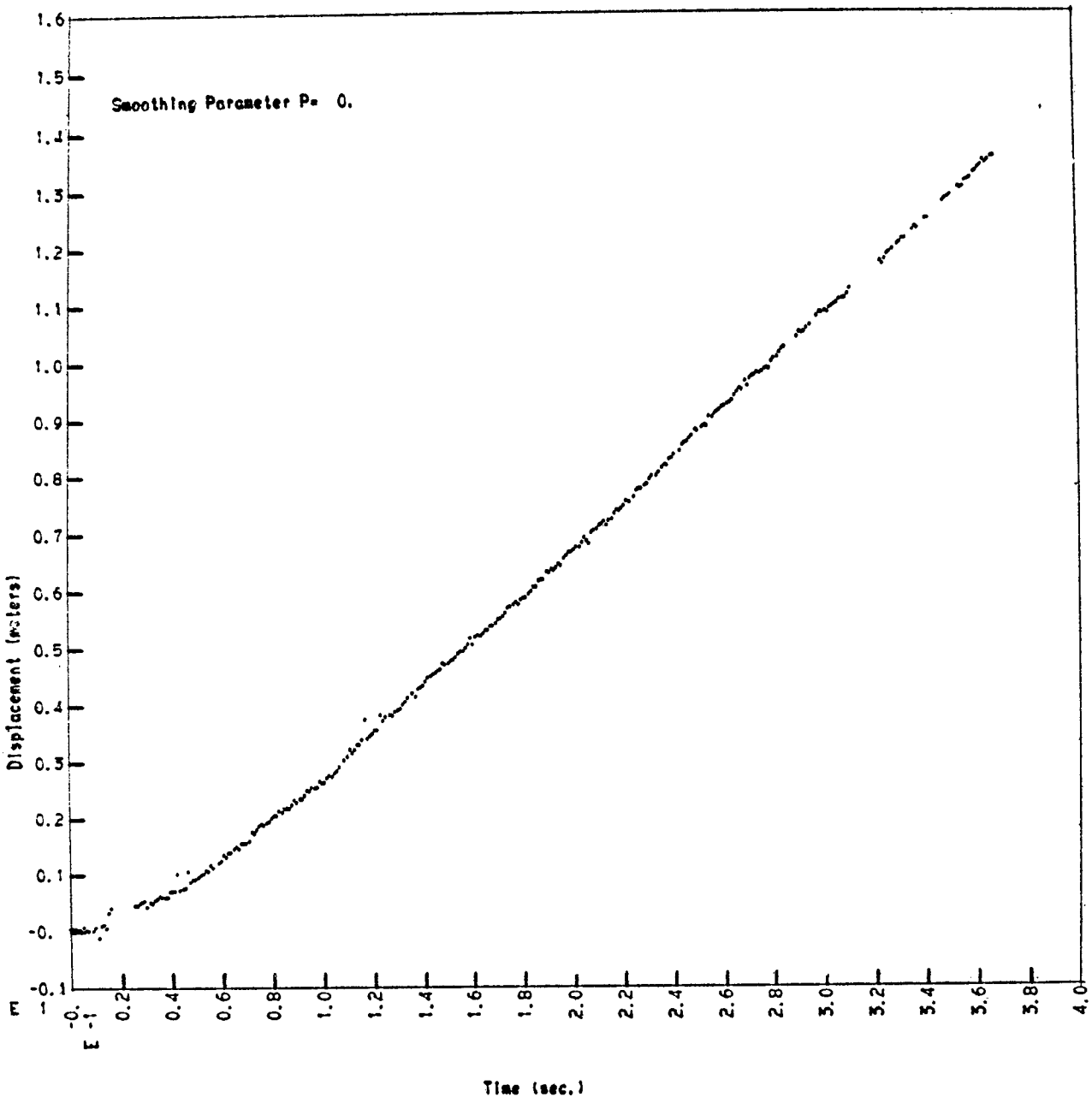

FIGURE C-16
Vertical Displacement Target 8

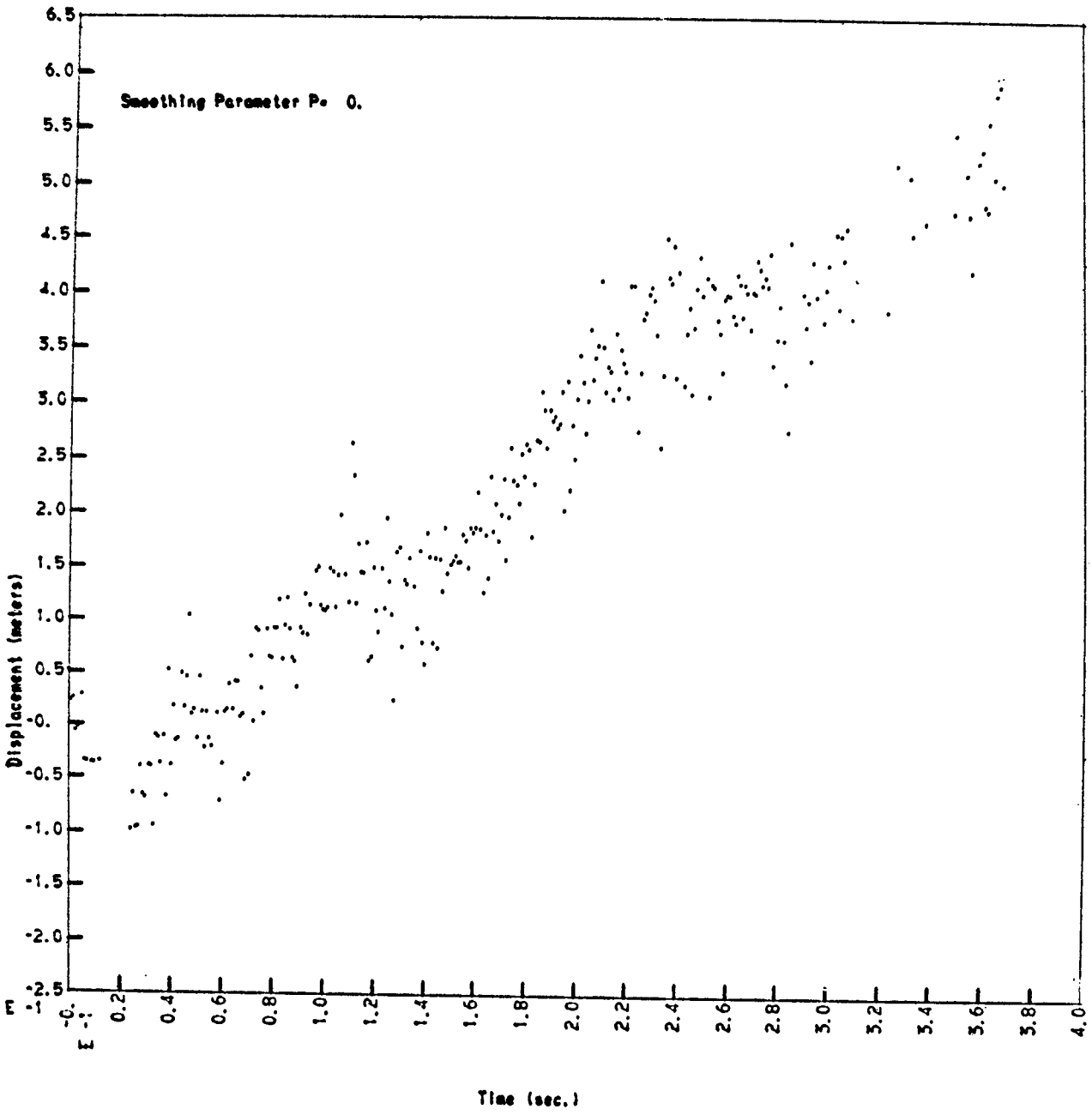

FIGURE C-17
Horizontal Displacement Target 11

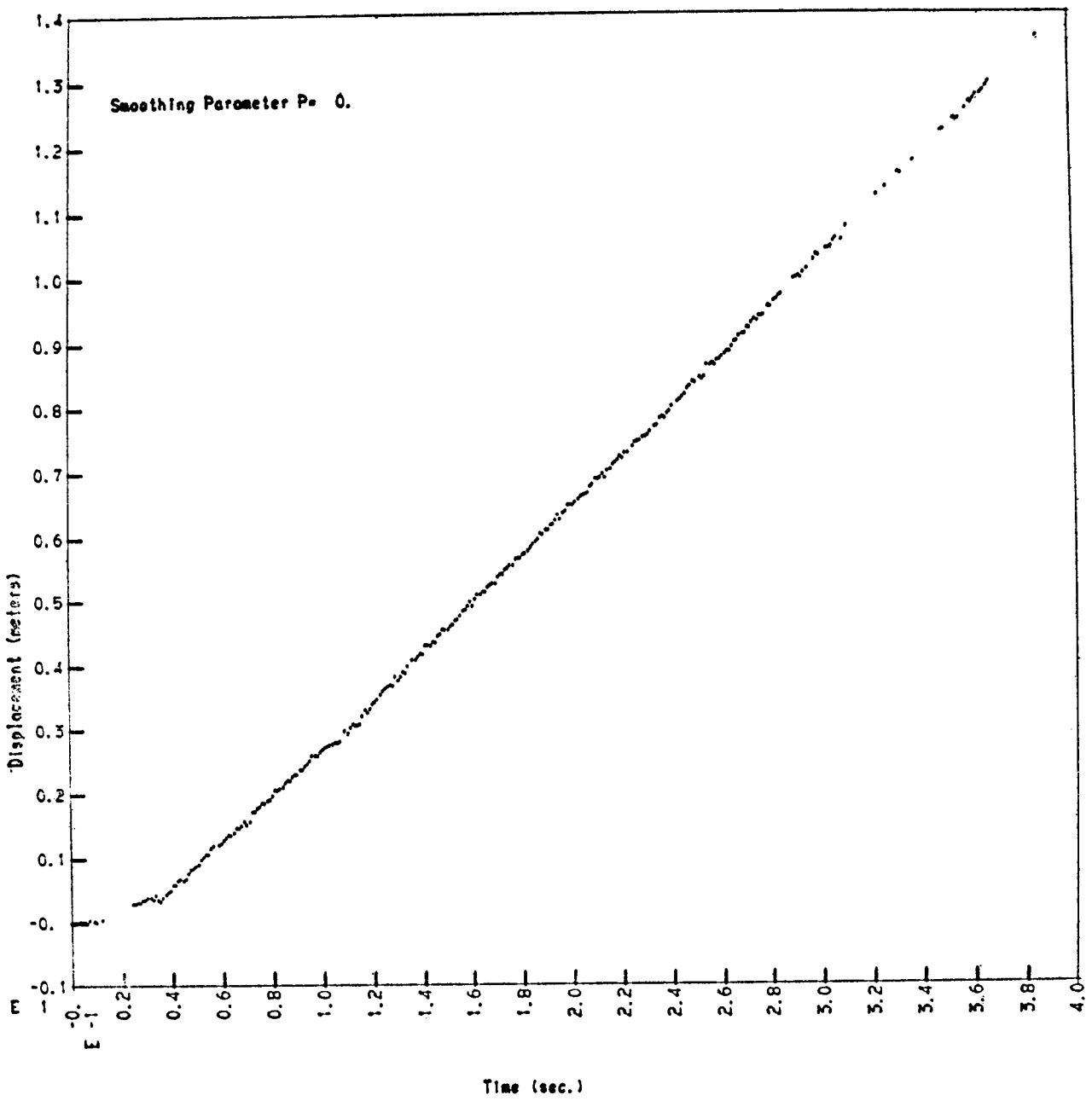

FIGURE C-18
Vertical Displacement Target 11

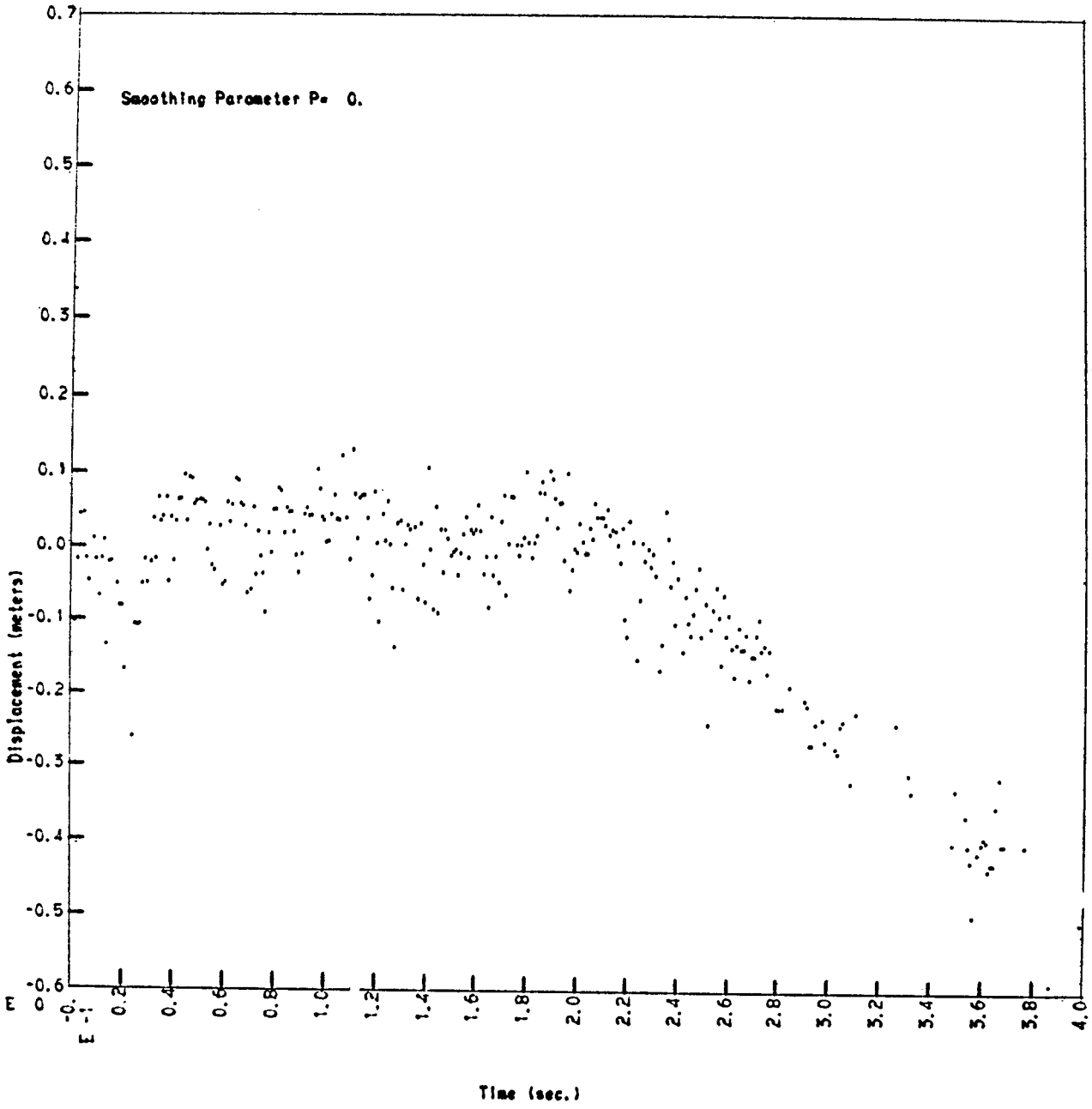

FIGURE C-19
Horizontal Displacement Target 12

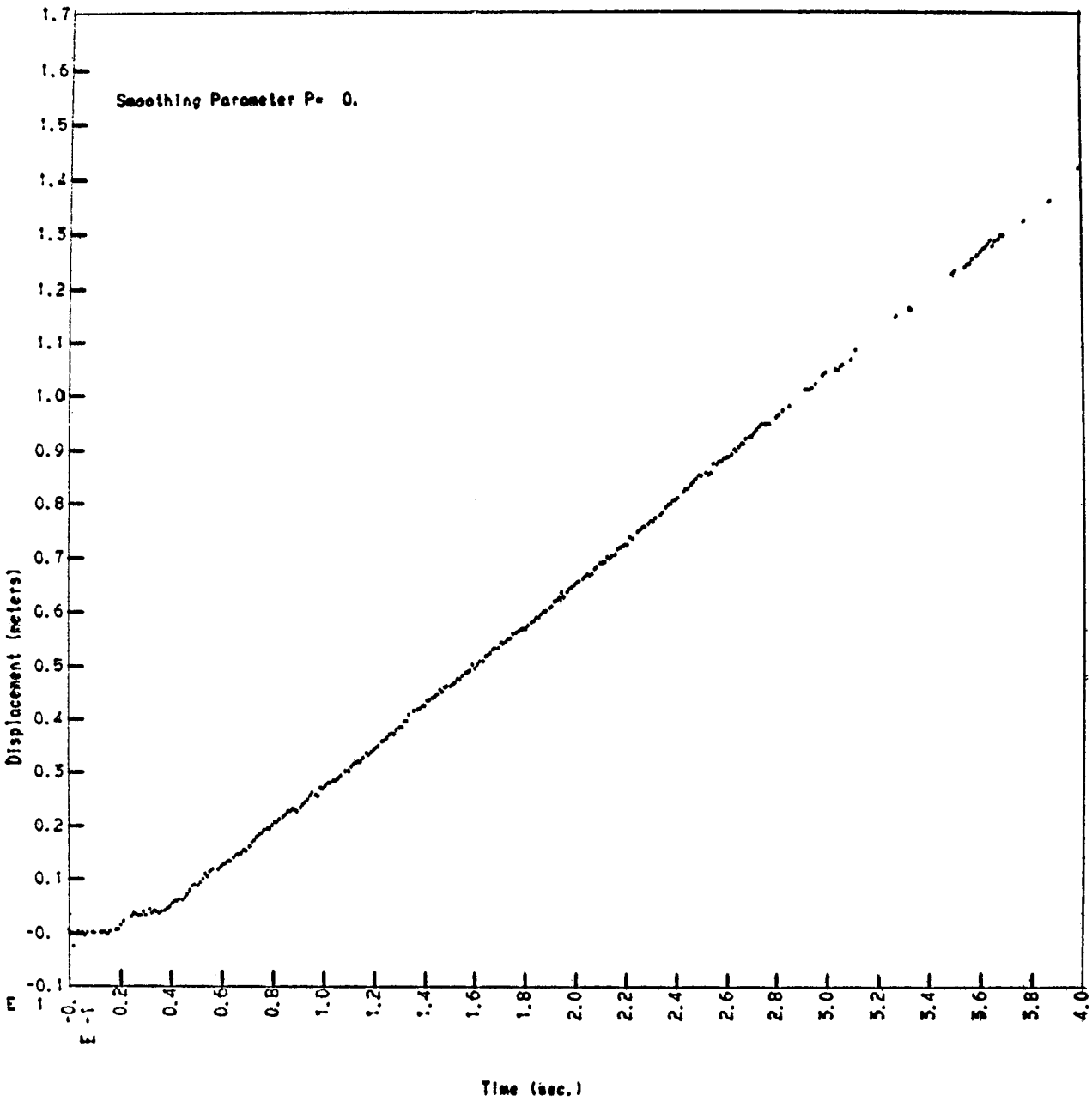

FIGURE C-20
Vertical Displacement Target 12

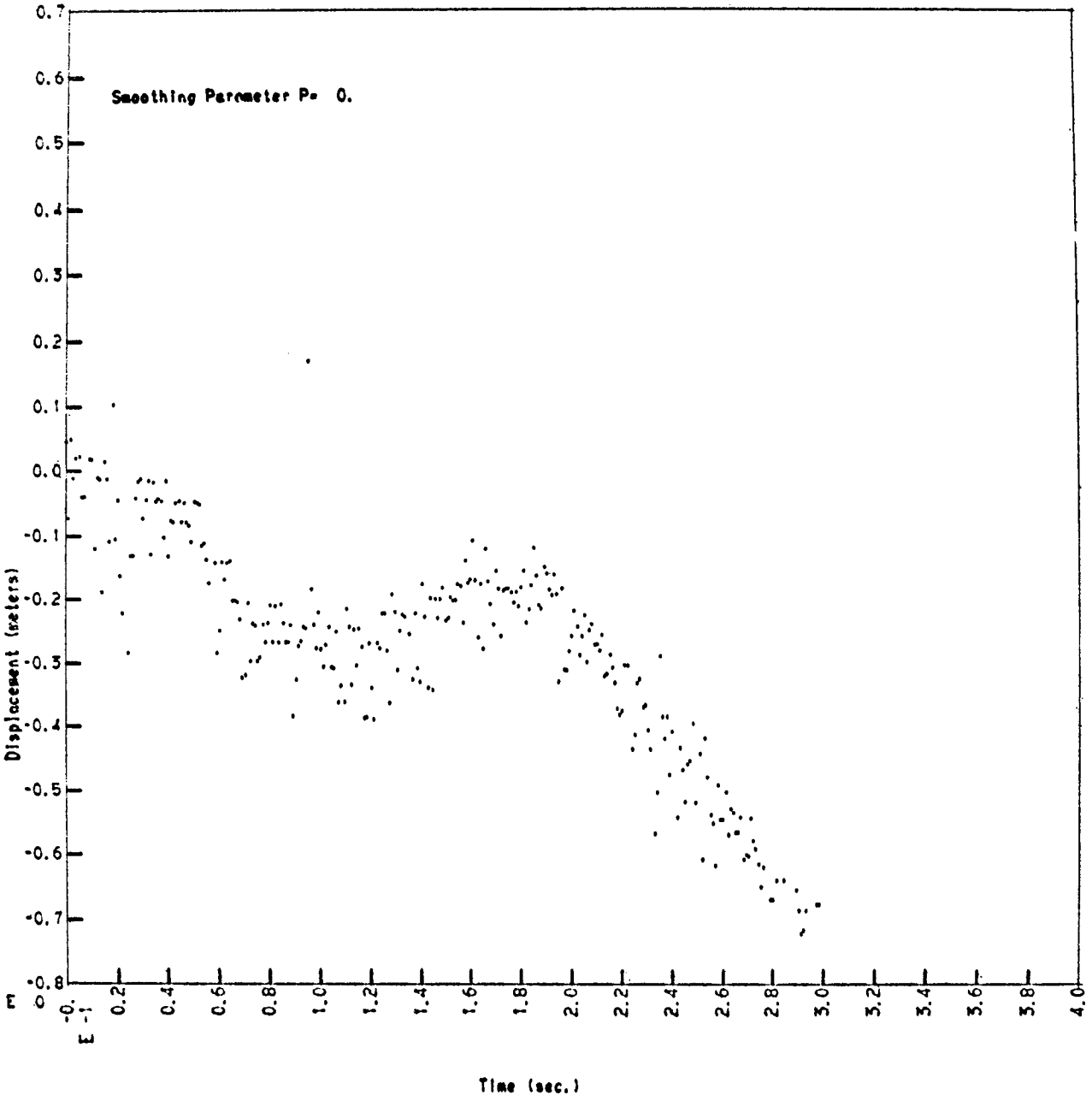

FIGURE C-21
Horizontal Displacement Target 13

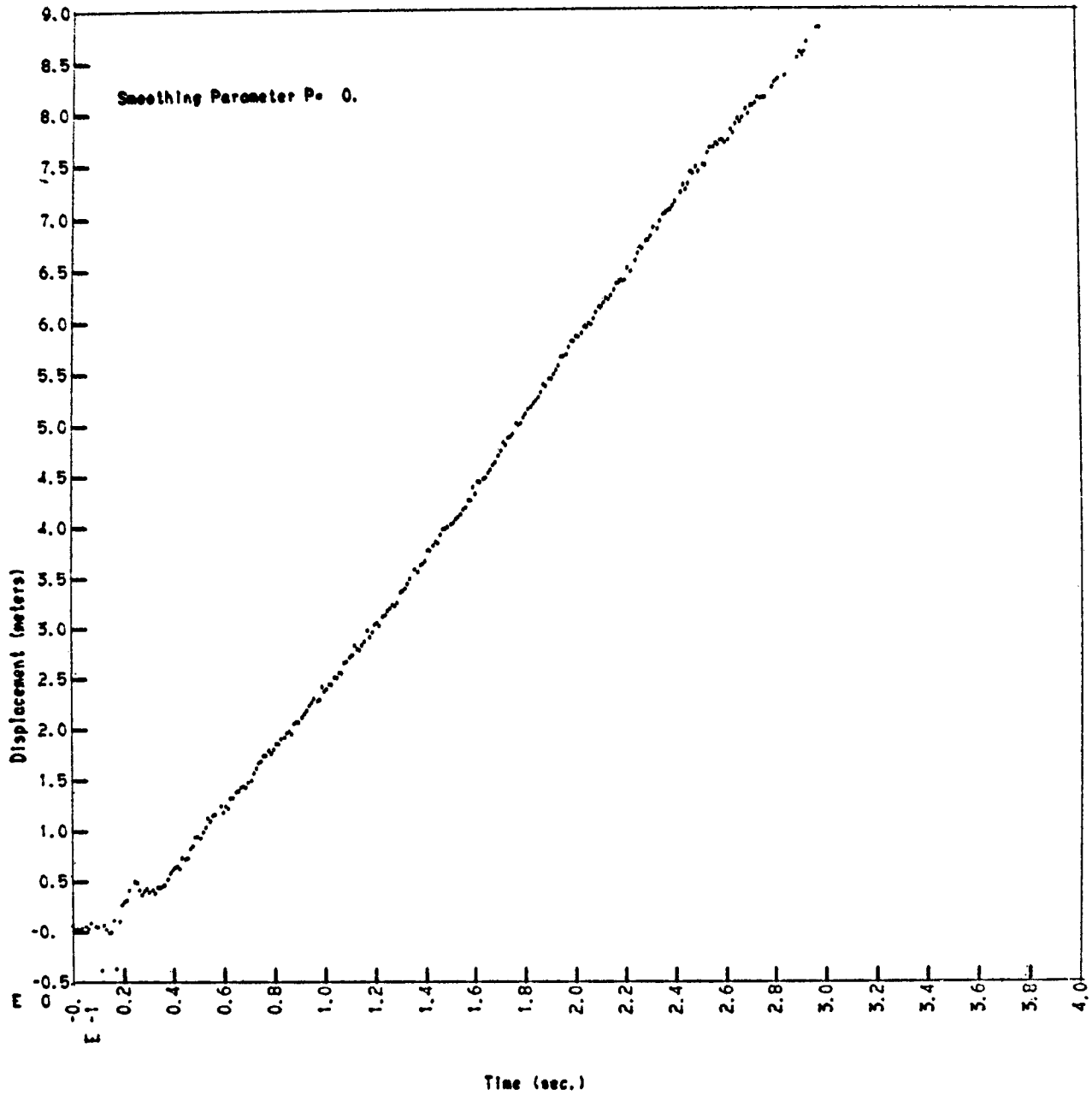

FIGURE C-22
Vertical Displacement Target 13

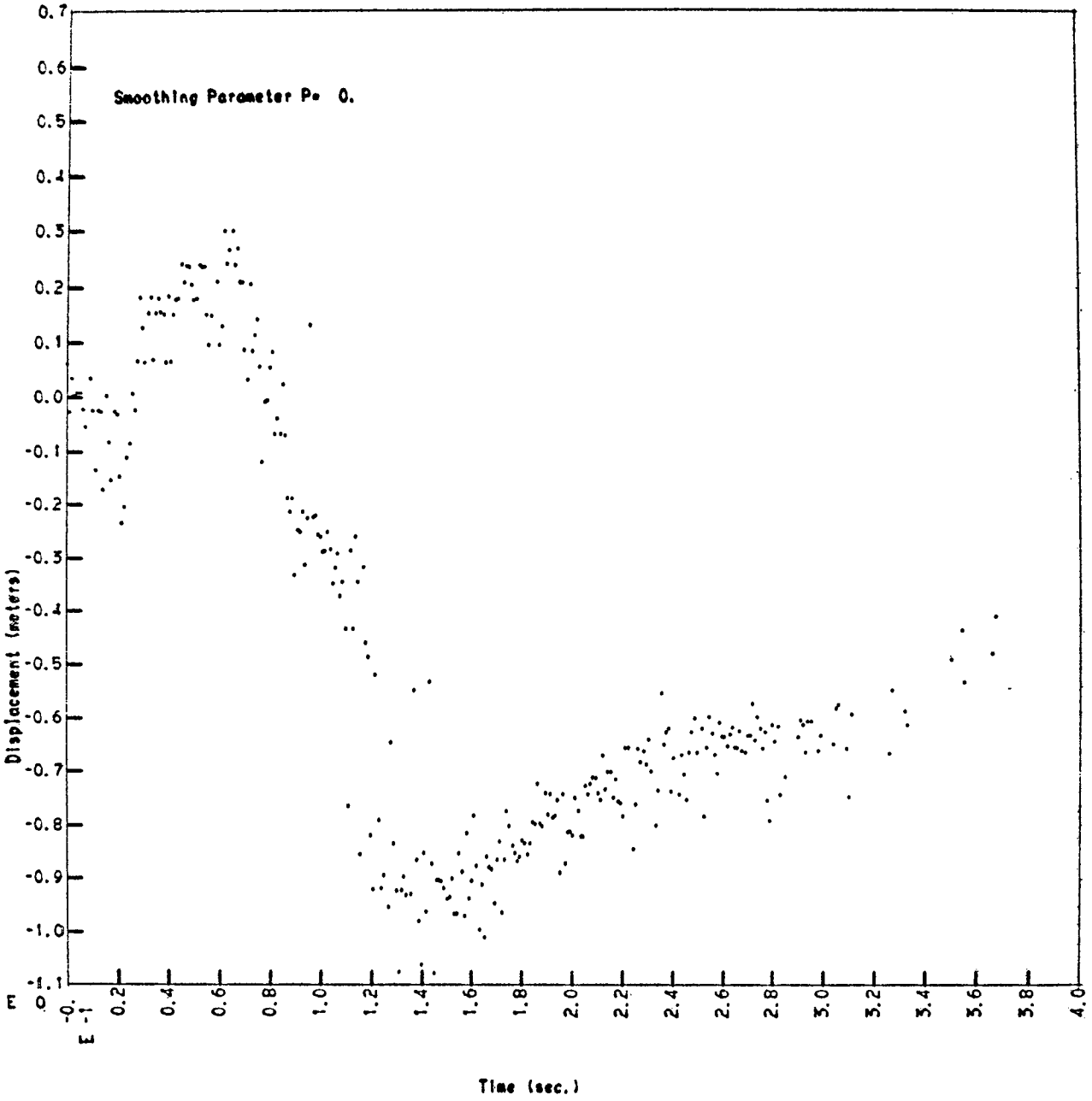

FIGURE C-23
Horizontal Displacement Target 14

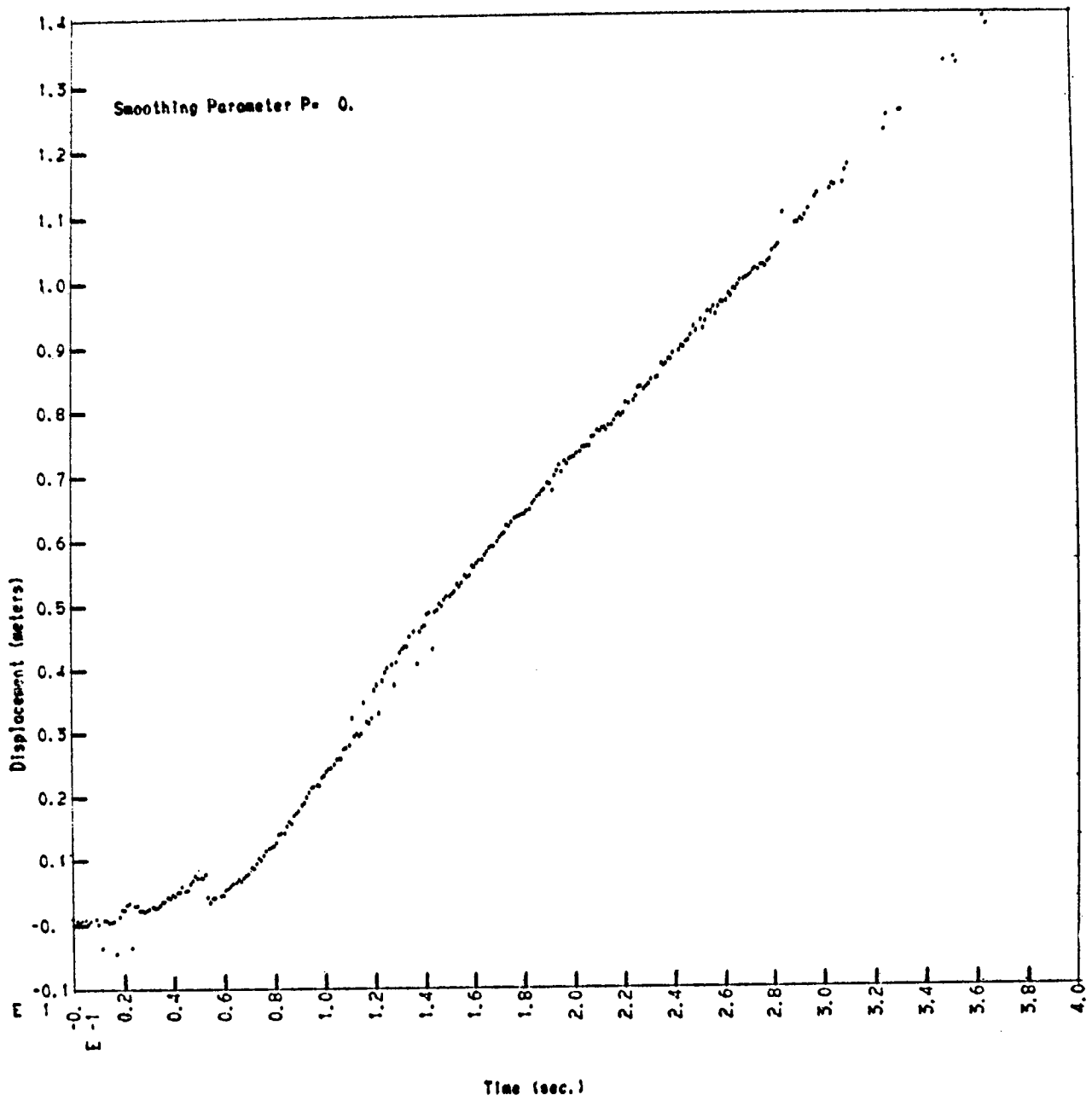

FIGURE C-24
Vertical Displacement Target 14

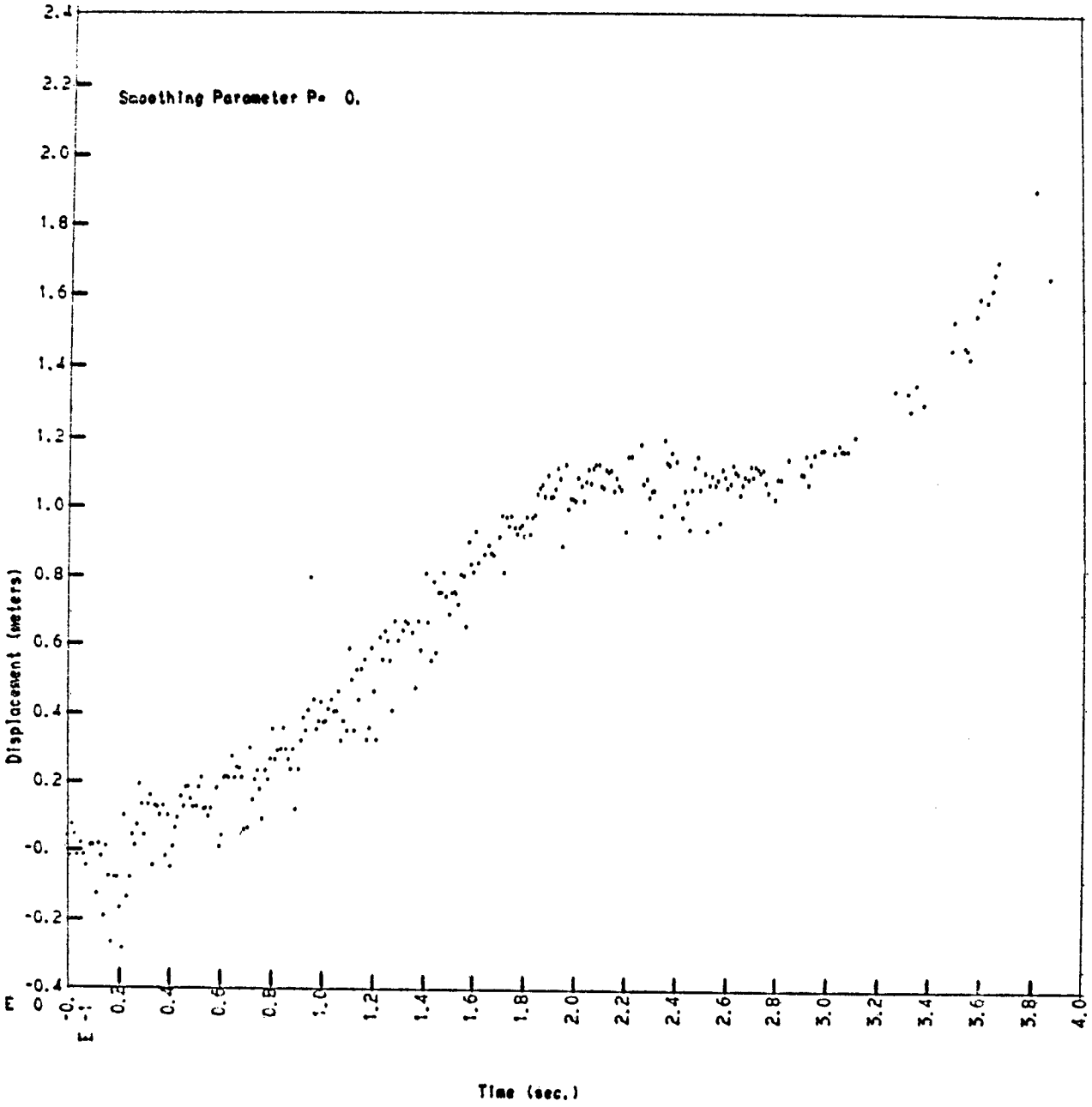

FIGURE C-25
Horizontal Displacement Target 15

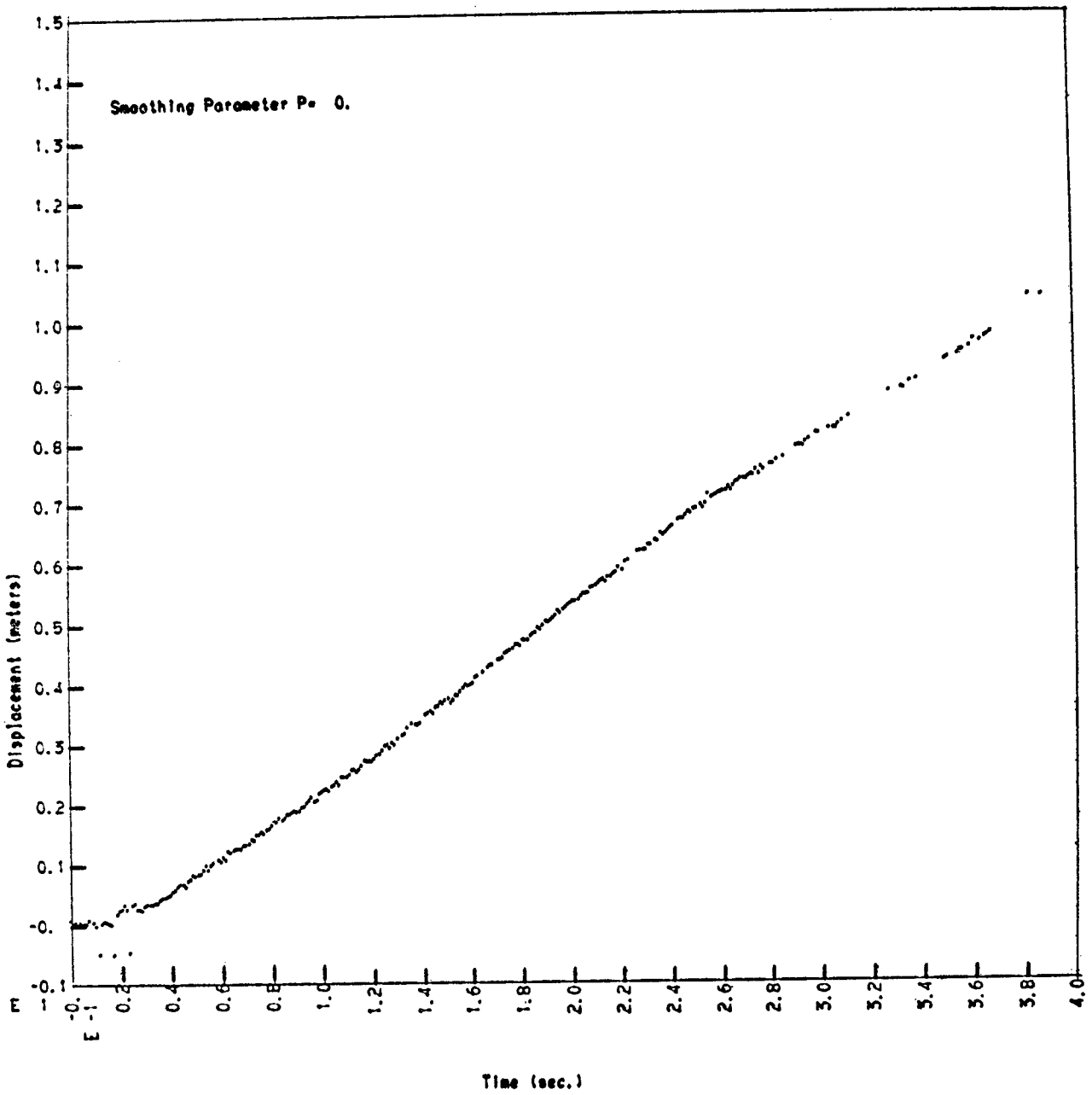

FIGURE C-26
Vertical Displacement Target 15

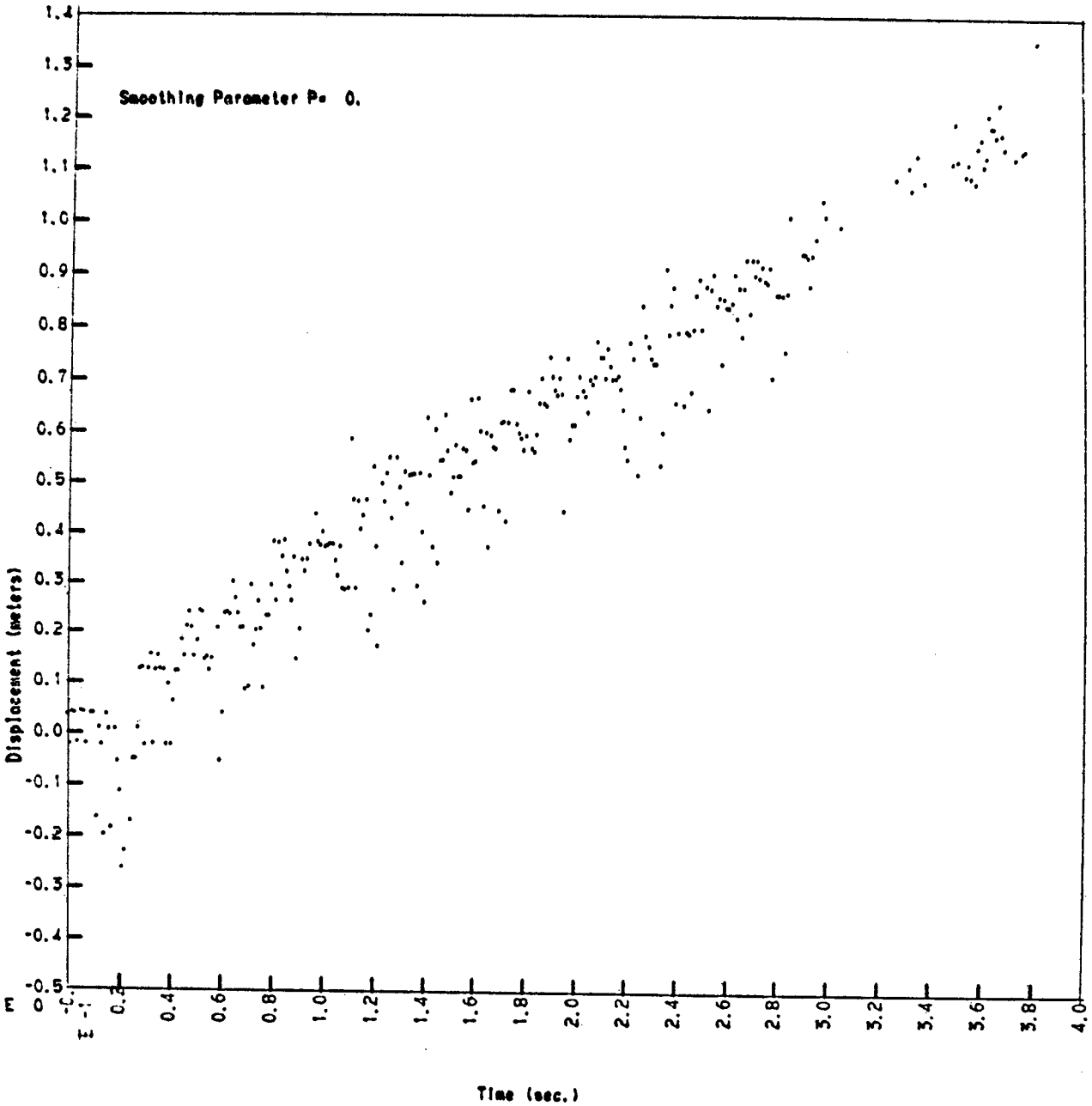

FIGURE C-27
Horizontal Displacement Target 16

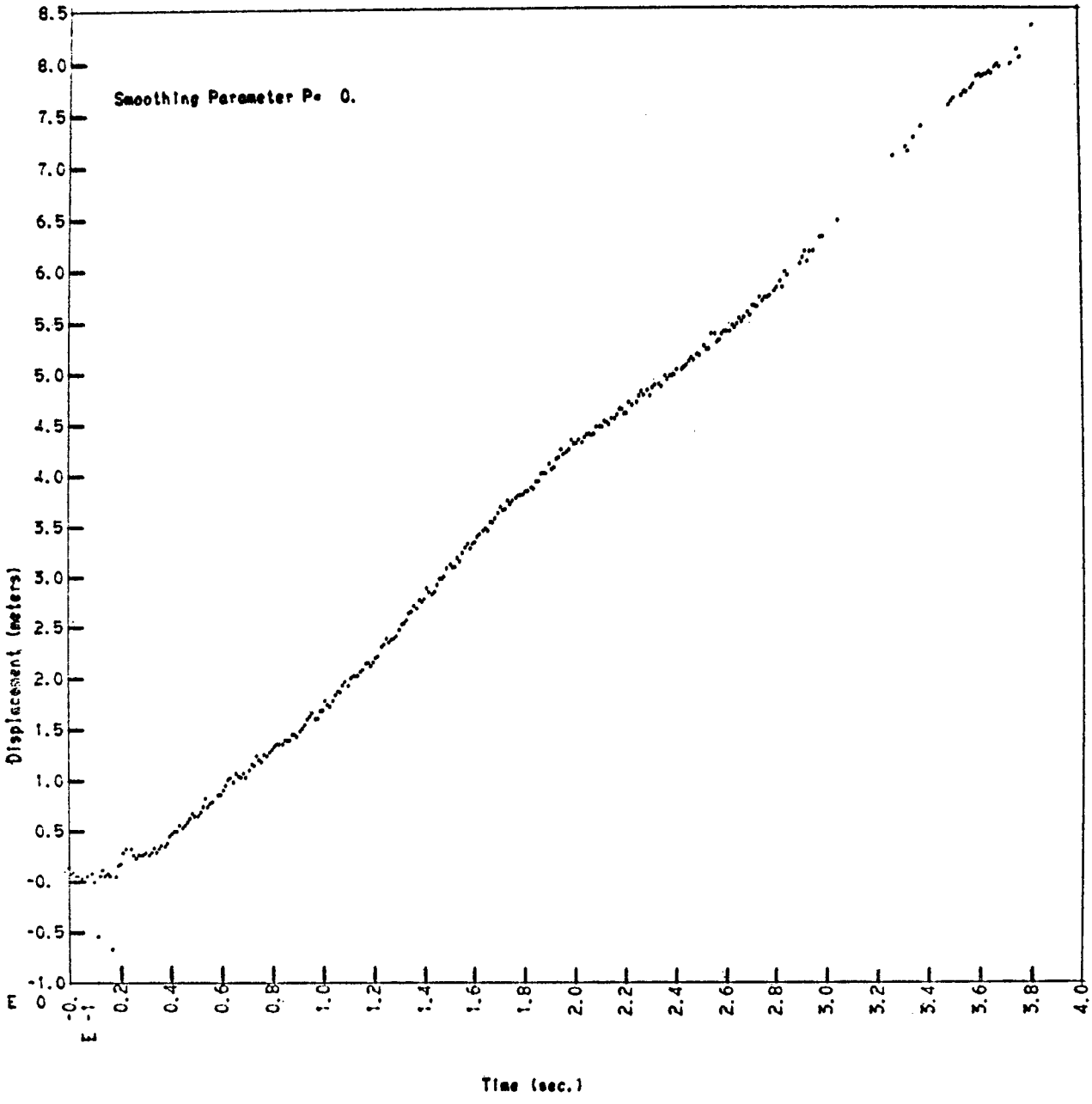

FIGURE C-28
Vertical Displacement Target 16

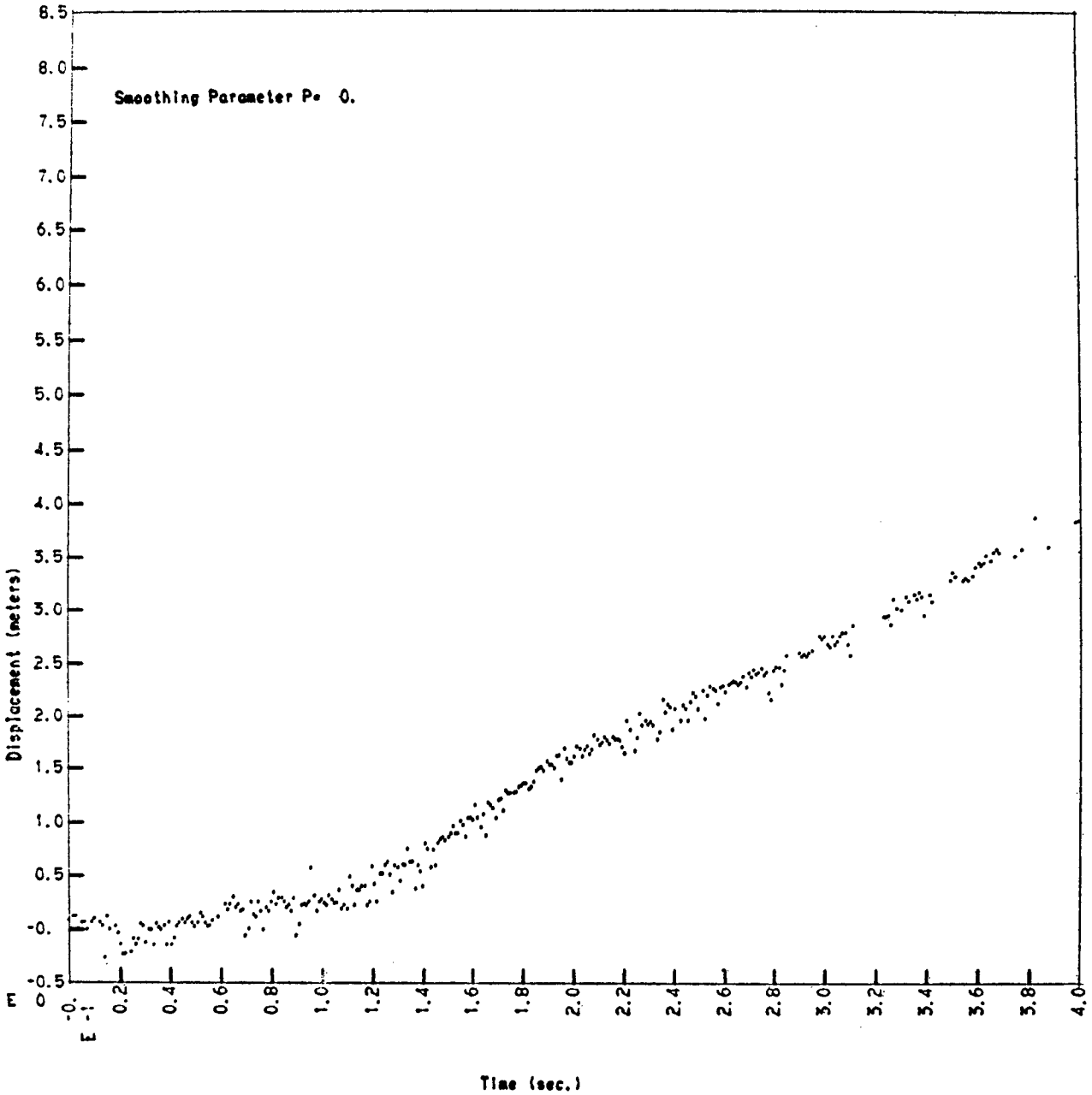

FIGURE C-29
Horizontal Displacement Target 17

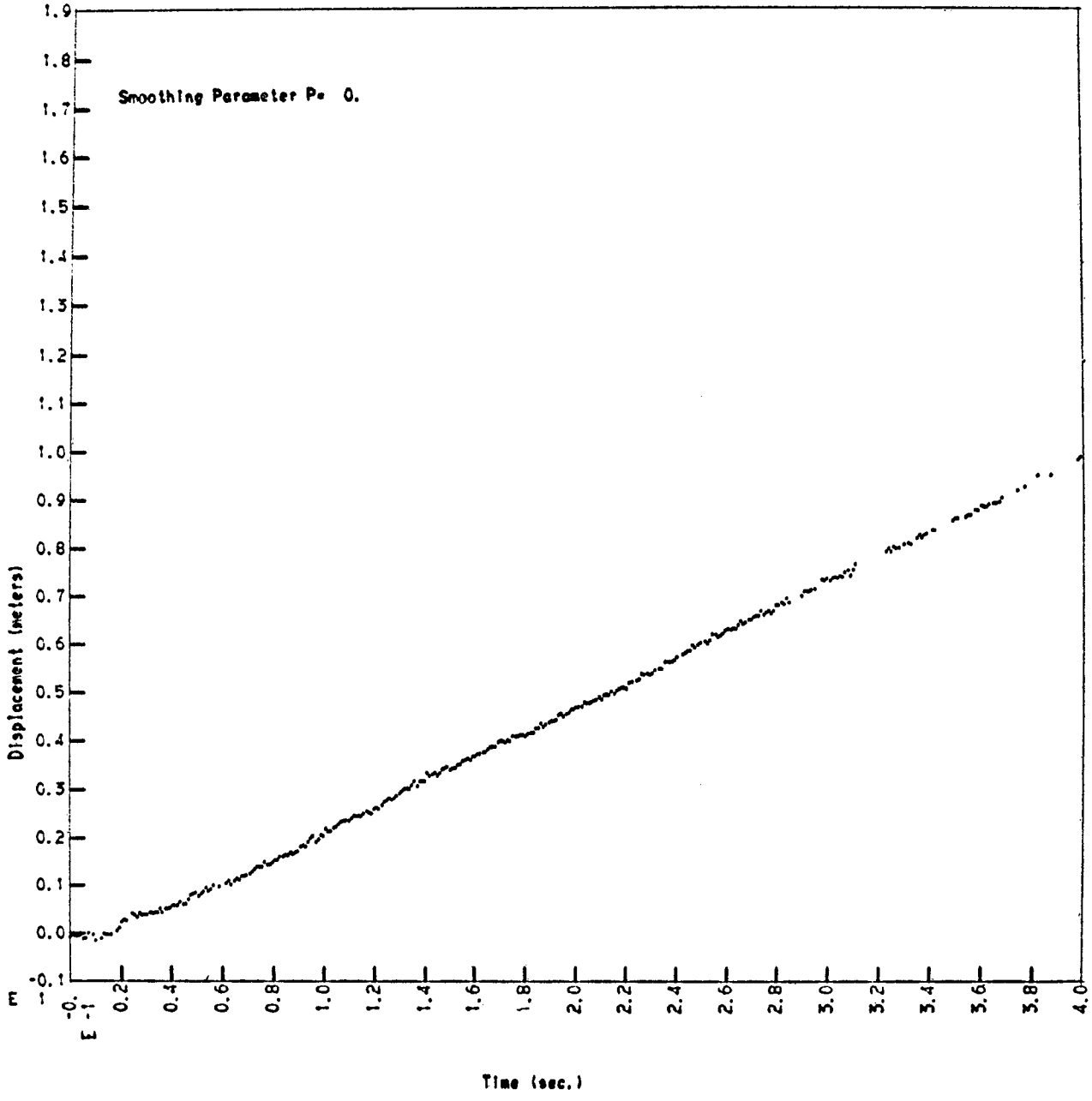

FIGURE C-30
Vertical Displacement Target 17

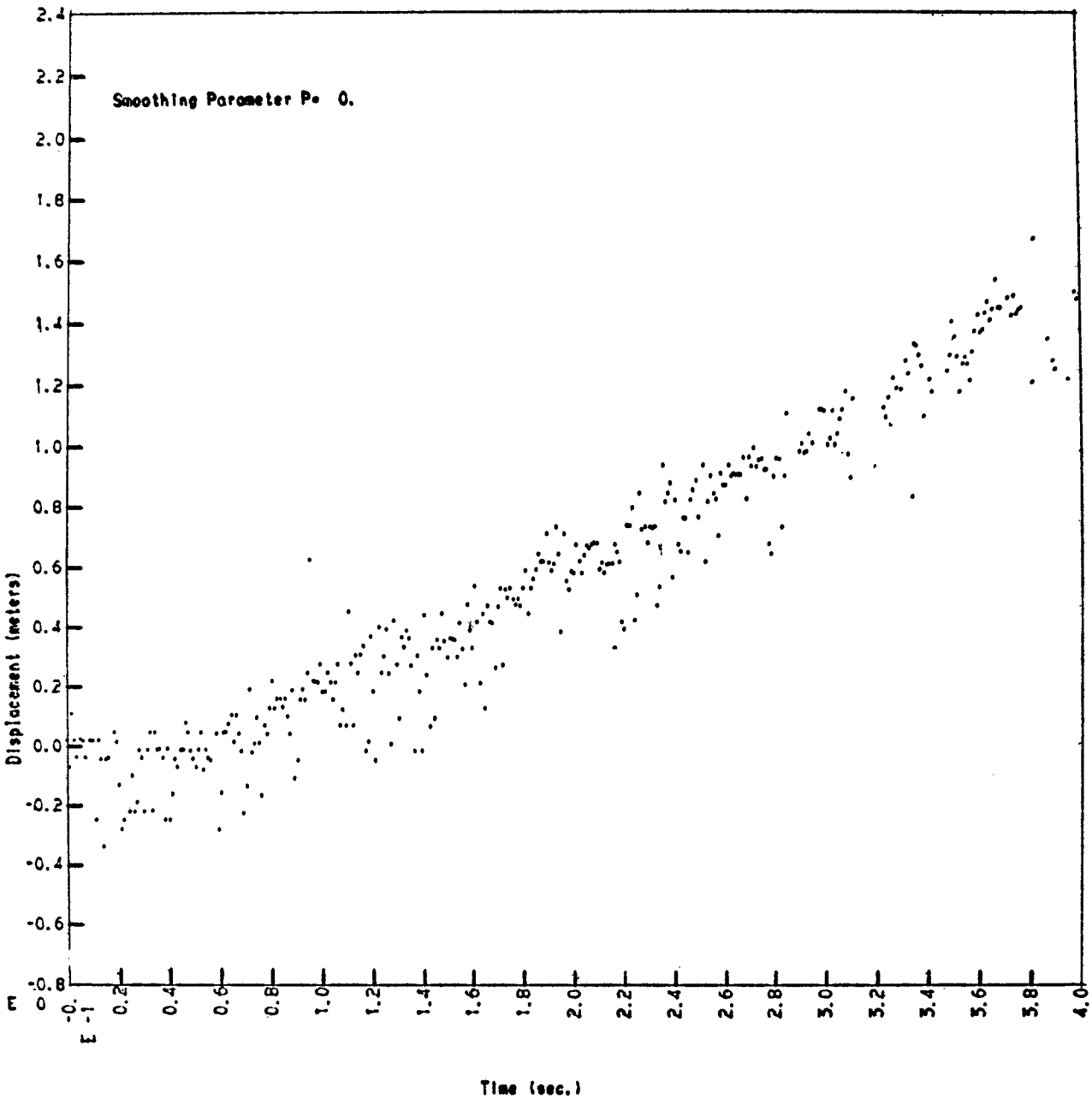

FIGURE C-31
Horizontal Displacement Target 19

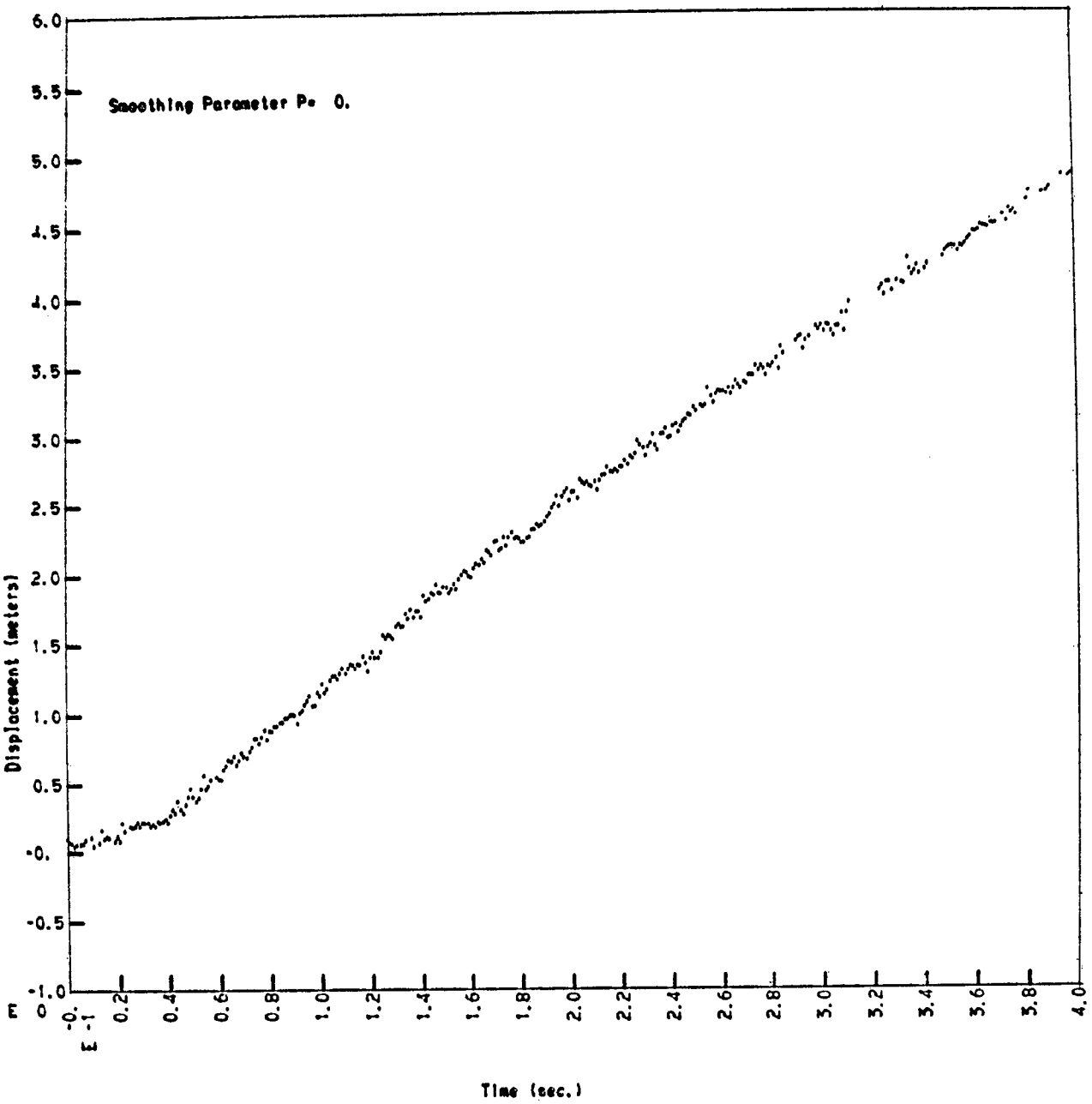

FIGURE C-32
Vertical Displacement Target 19

APPENDIX D

SURFACE MOTION TARGETS, HORIZONTAL AND VERTICAL VELOCITIES

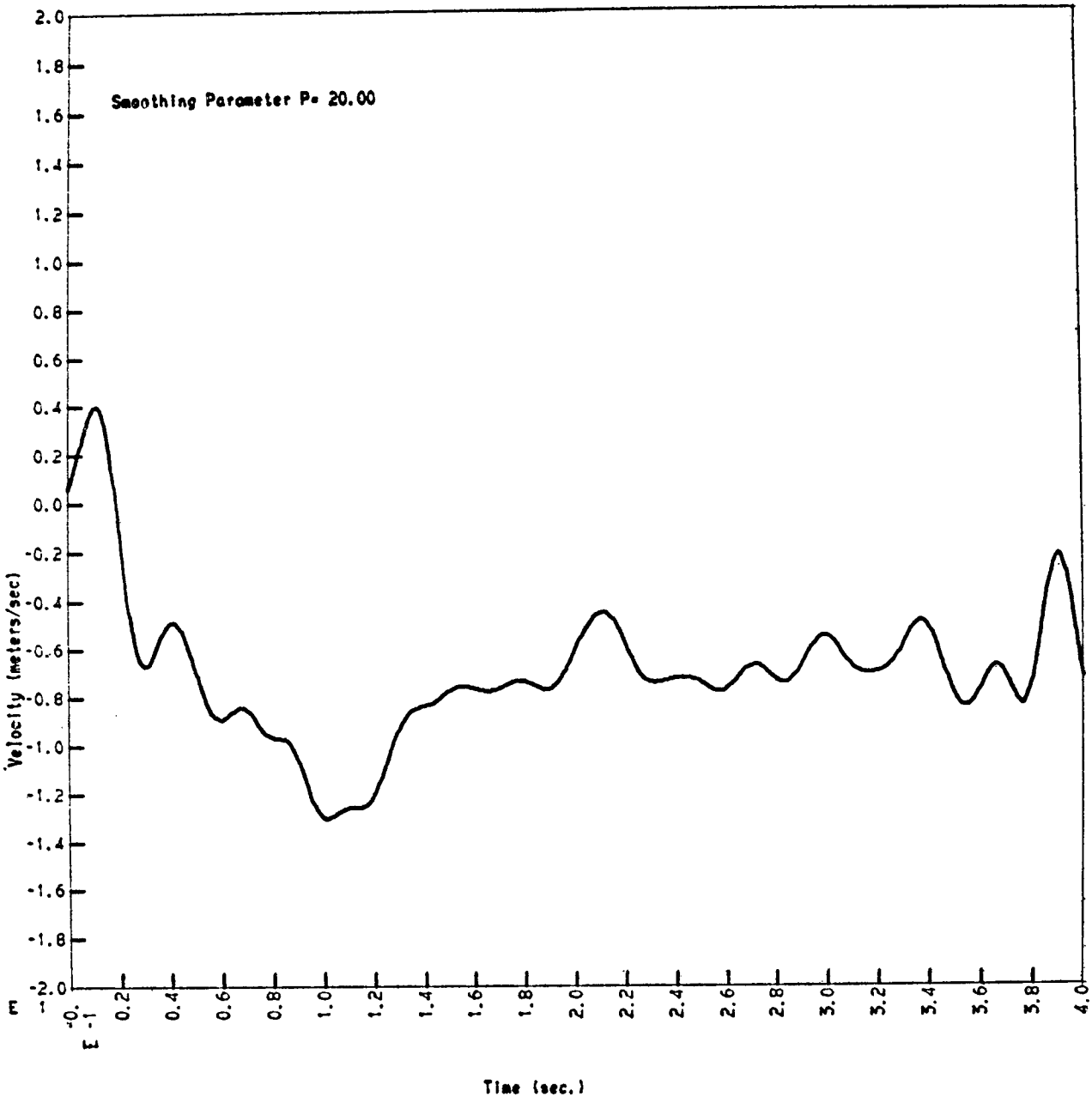

FIGURE D-1
Horizontal Velocity Target 1

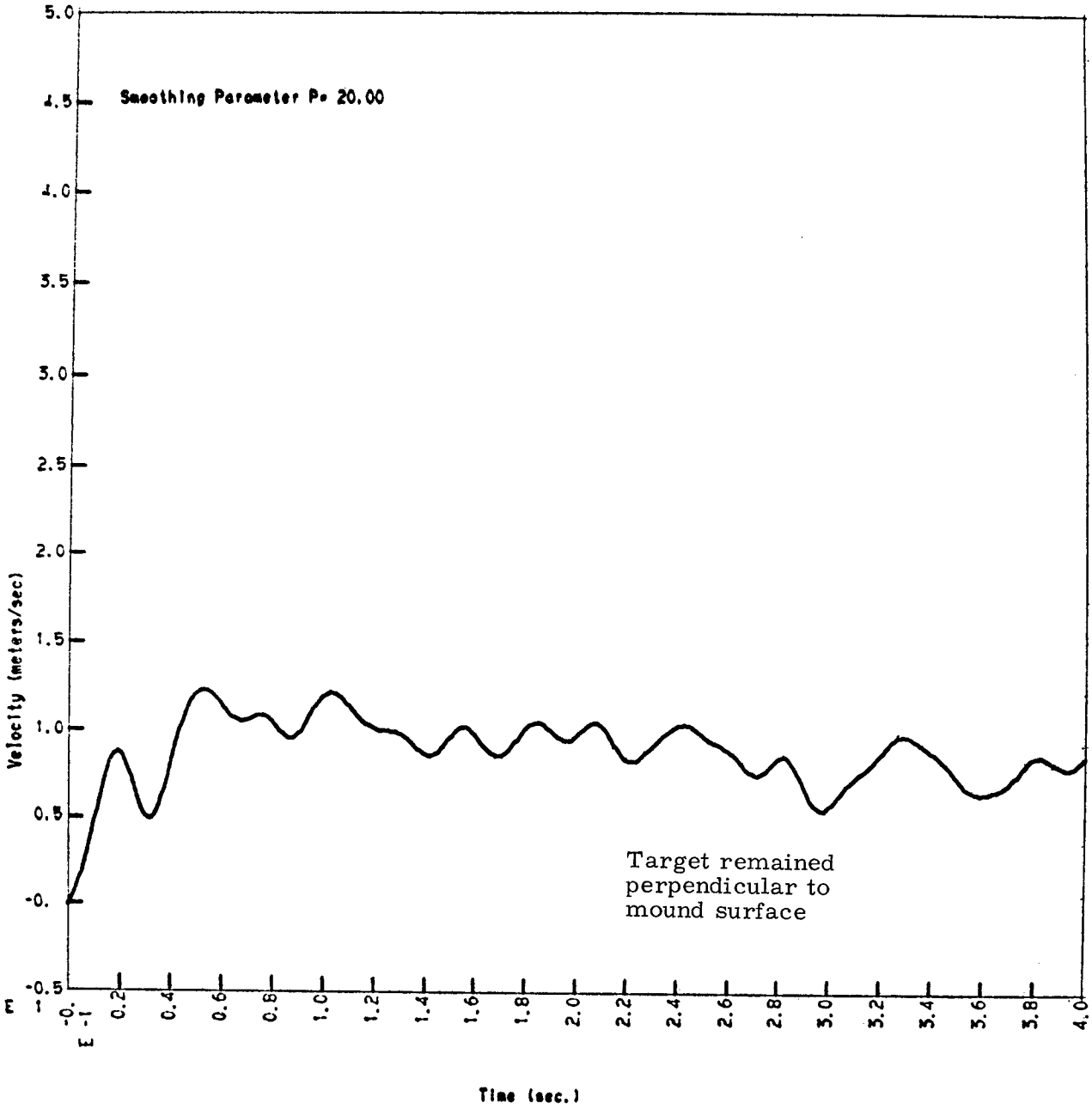

FIGURE D-2
Vertical Velocity Target 1

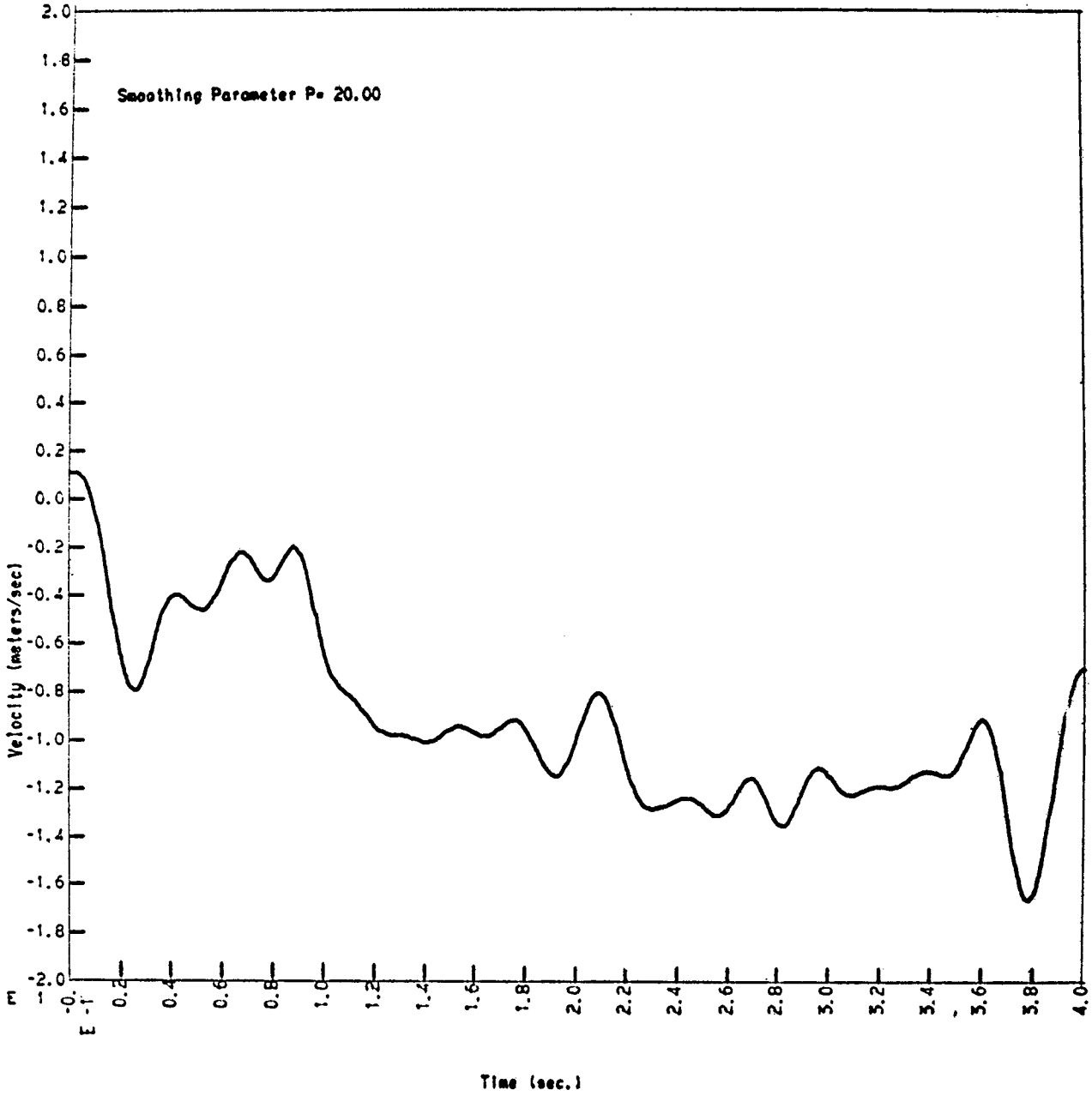

FIGURE D-3
Horizontal Velocity Target 2

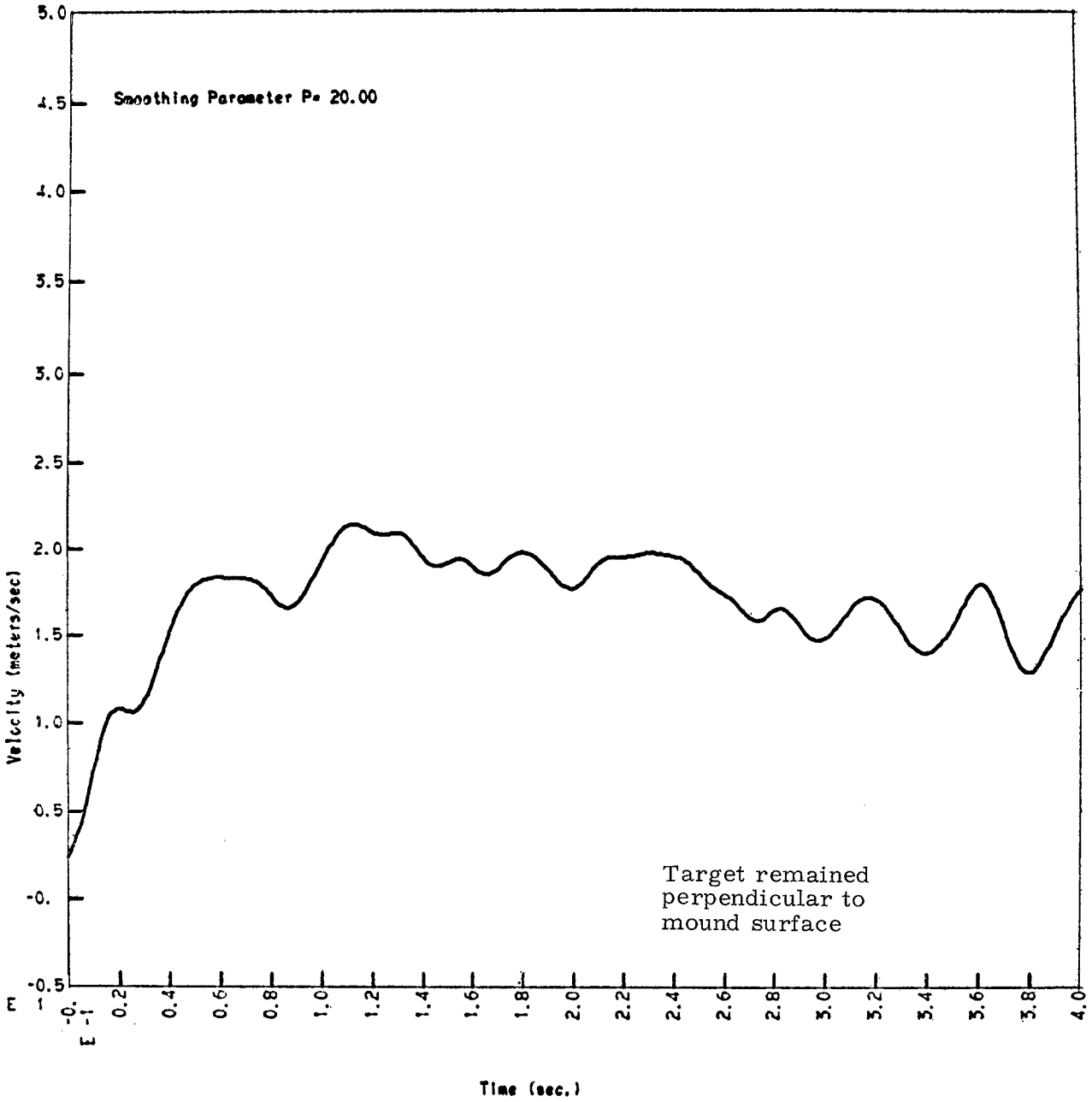

FIGURE D-4
Vertical Velocity Target 2

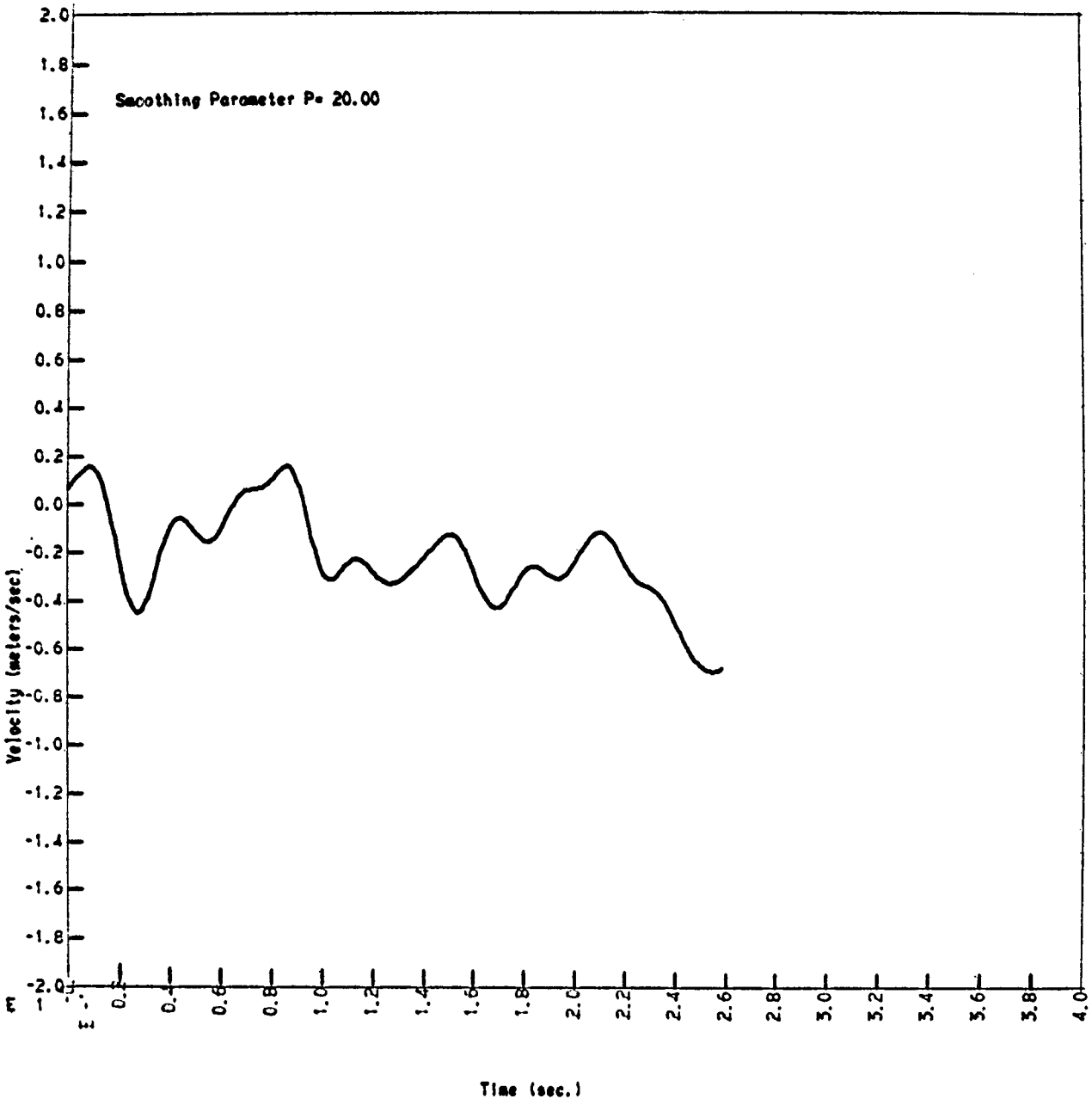

FIGURE D-5
Horizontal Velocity Target 3

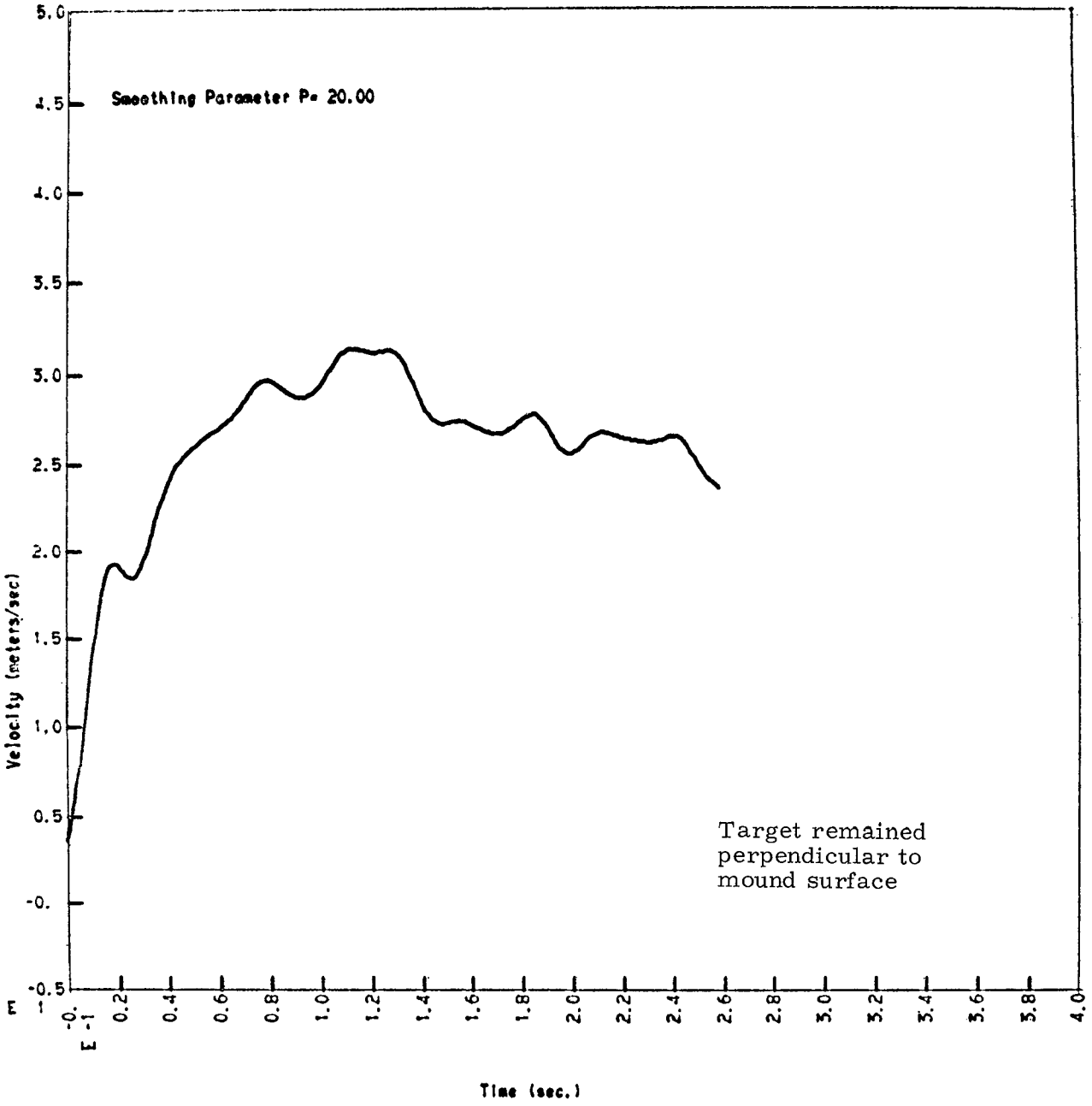

FIGURE D-6
Vertical Velocity Target 3

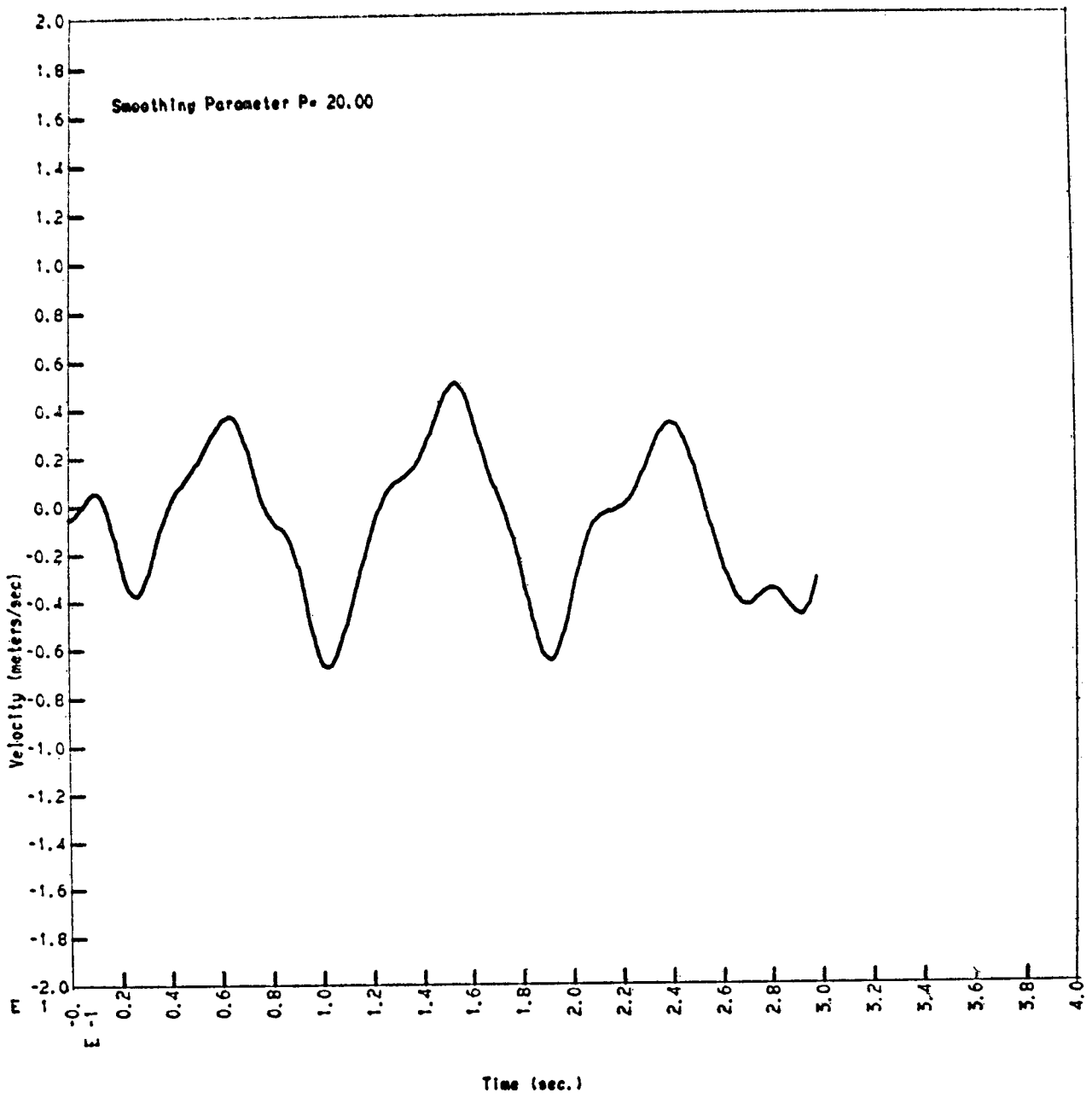

FIGURE D-7
Horizontal Velocity Target 4

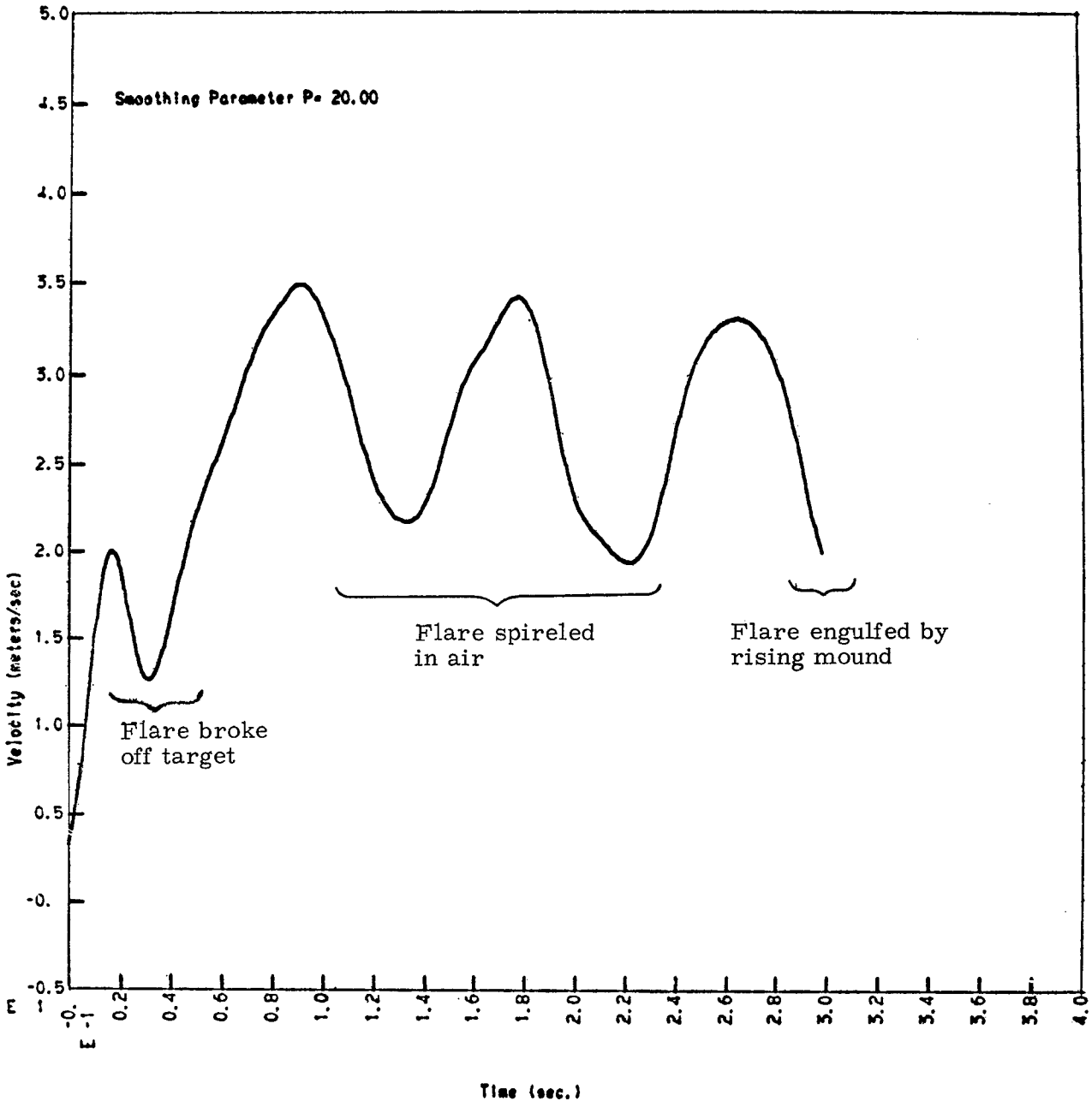

FIGURE D-8
Vertical Velocity Target 4

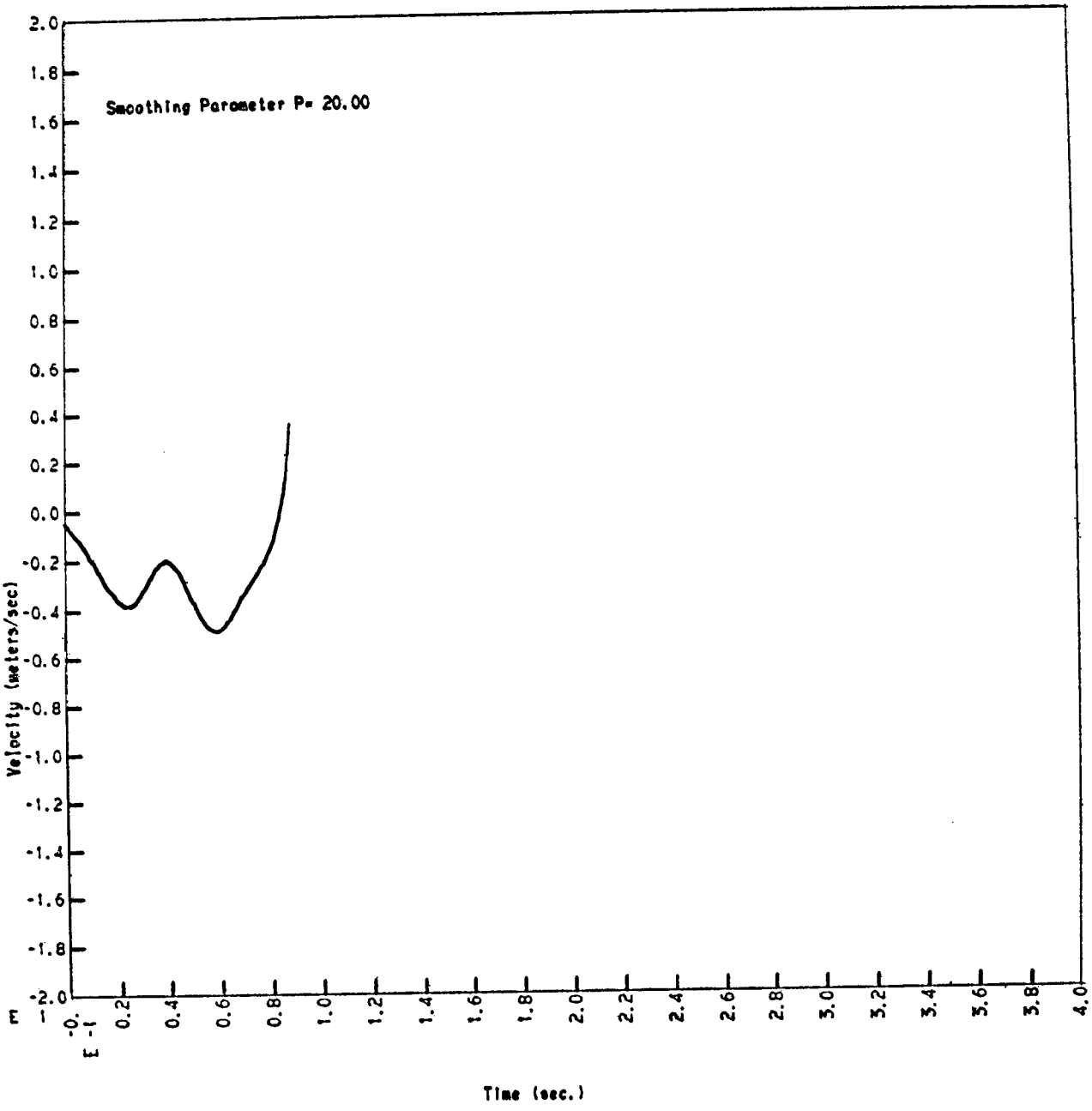

FIGURE D-9
Horizontal Velocity Target 5

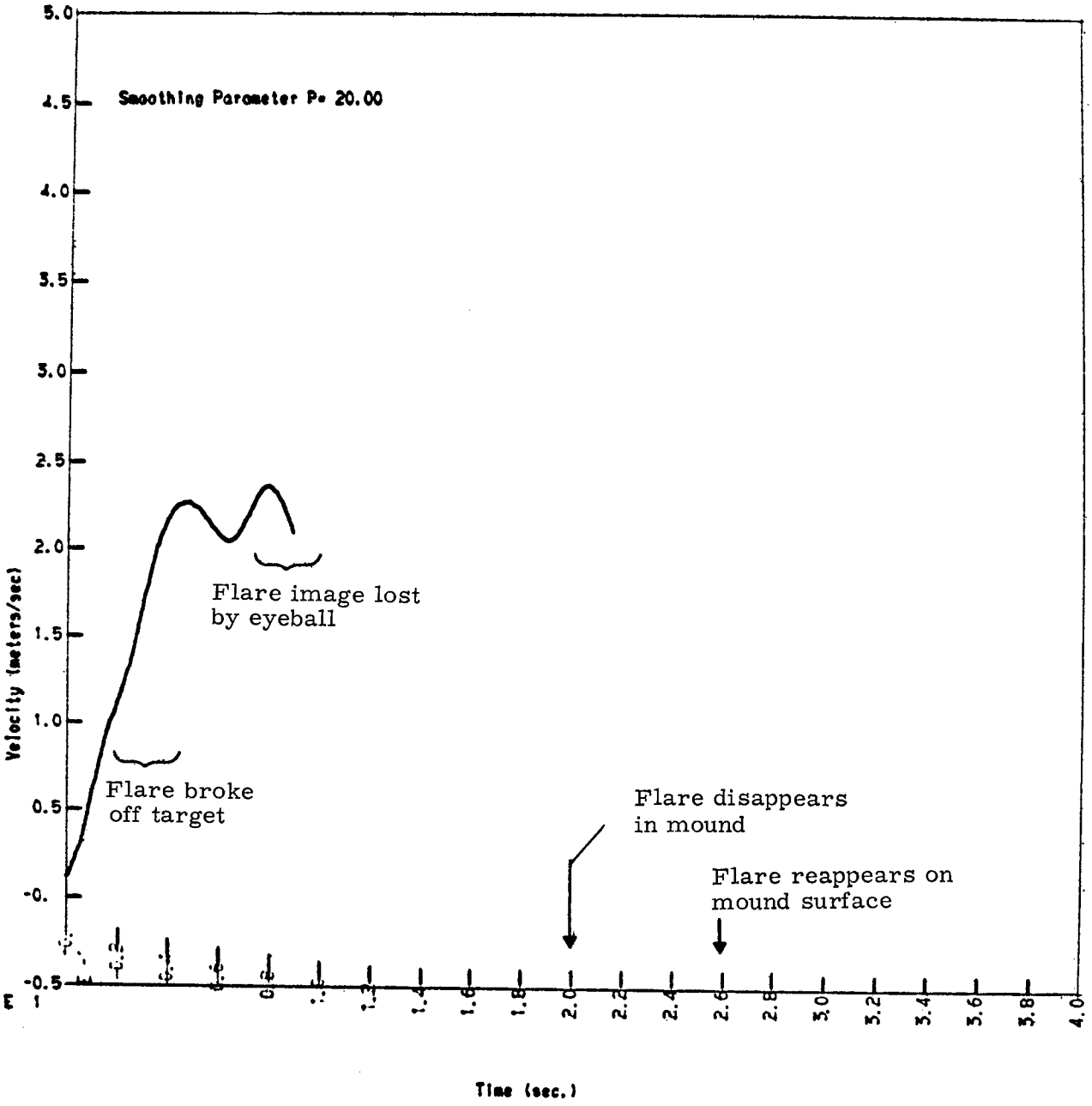

FIGURE D-10
Vertical Velocity Target 5

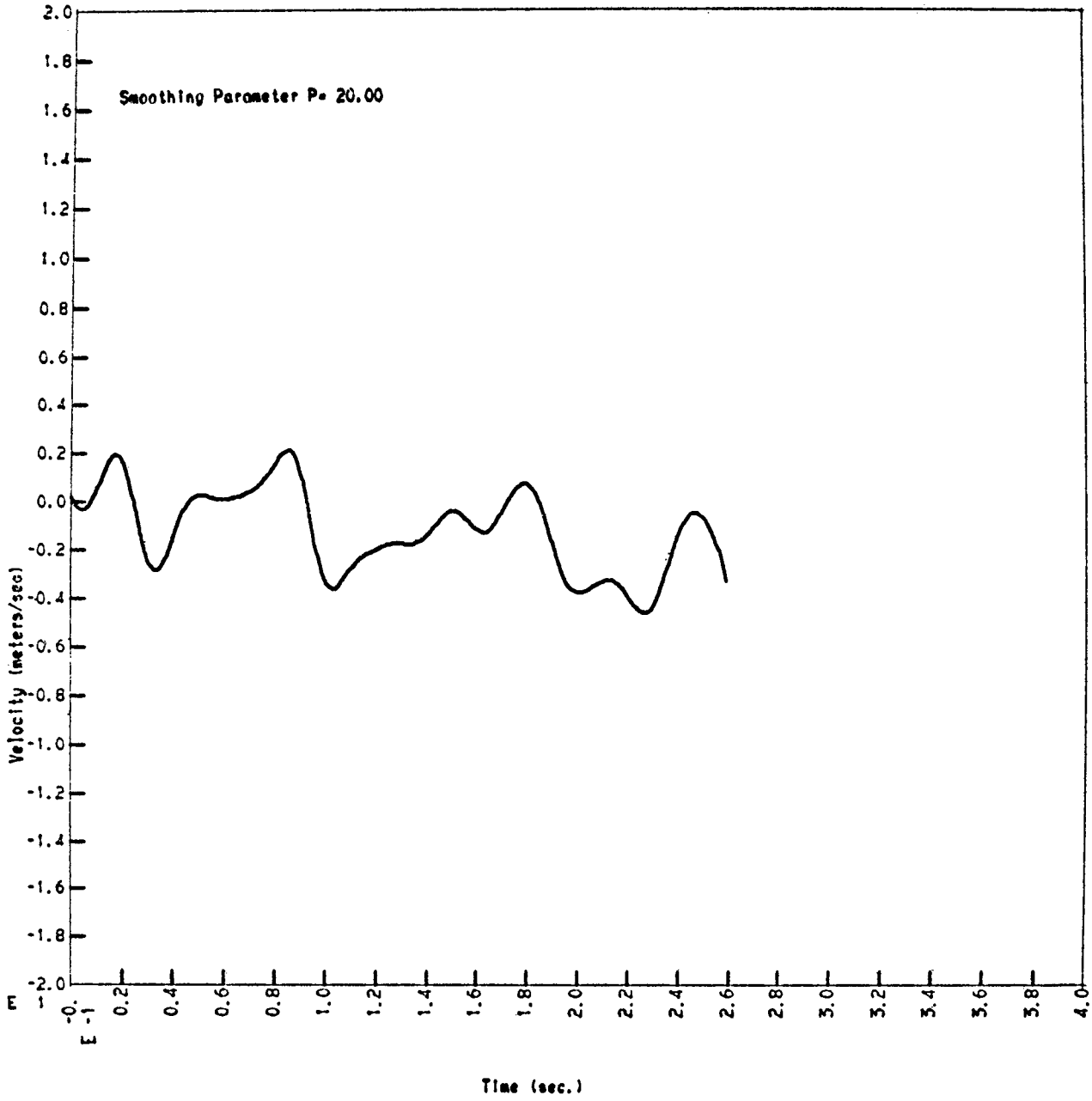

FIGURE D-11
Horizontal Velocity Target 6

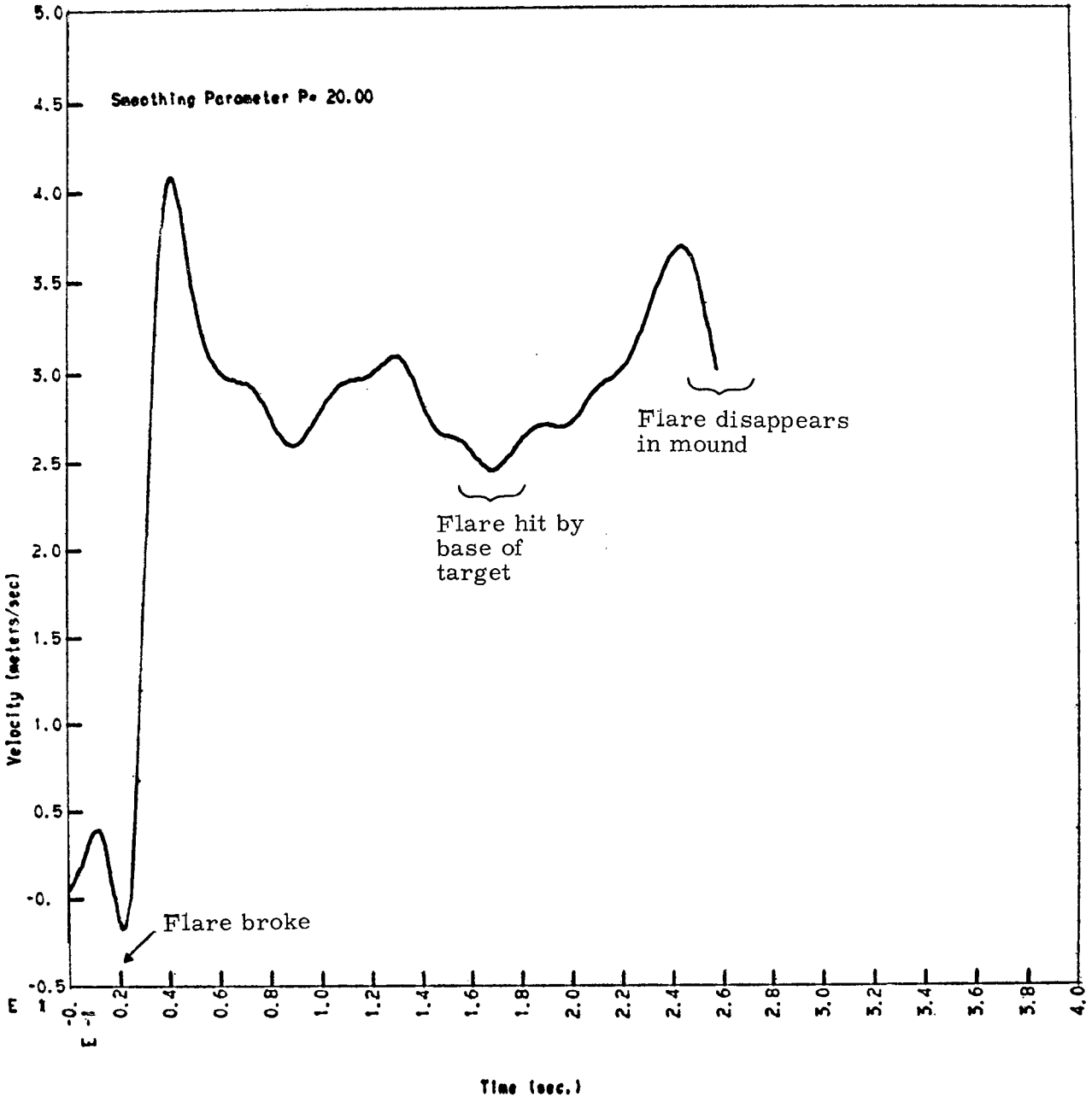

FIGURE D-12
Vertical Velocity Target 6

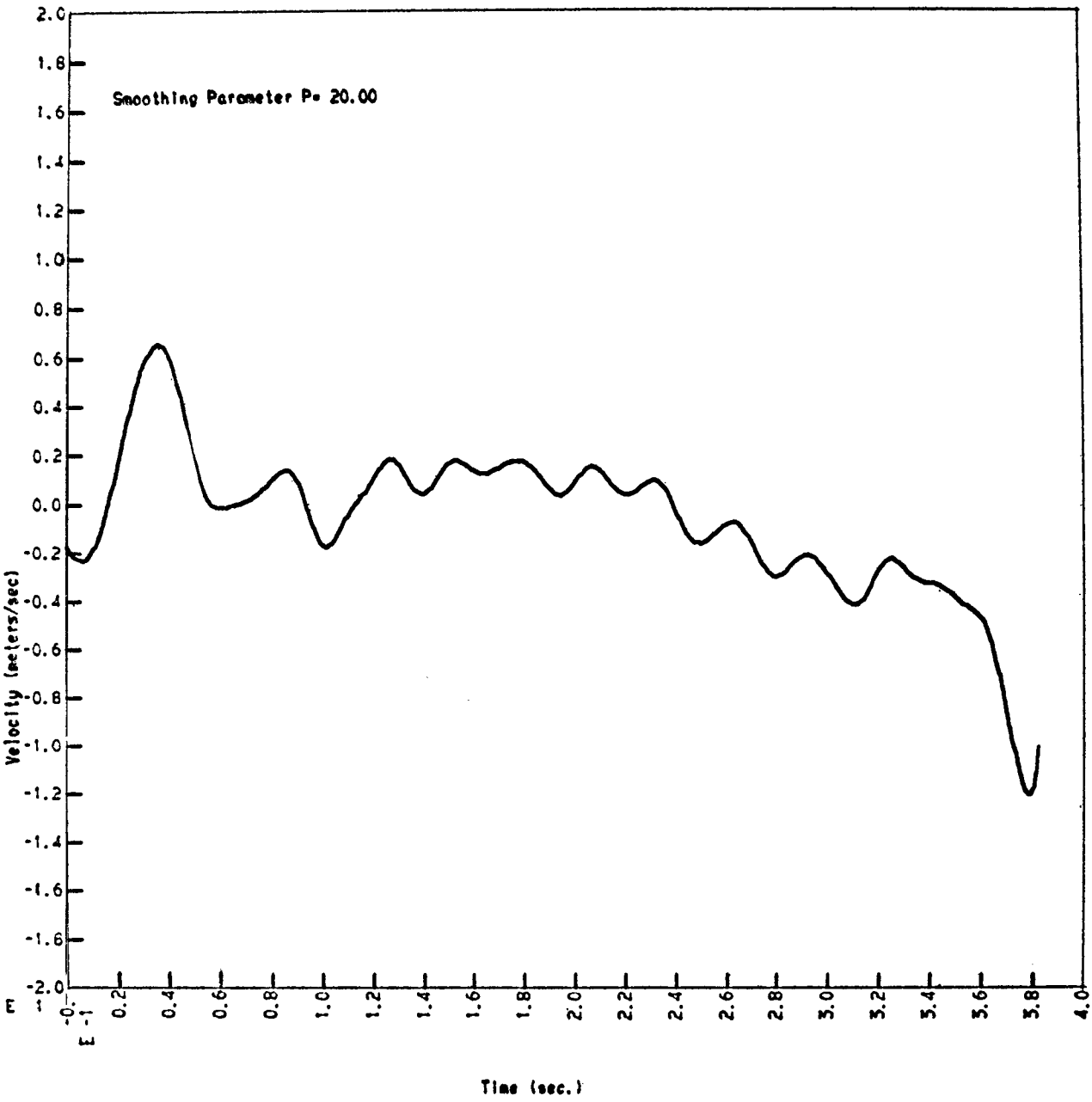

FIGURE D-13
Horizontal Velocity Target 7

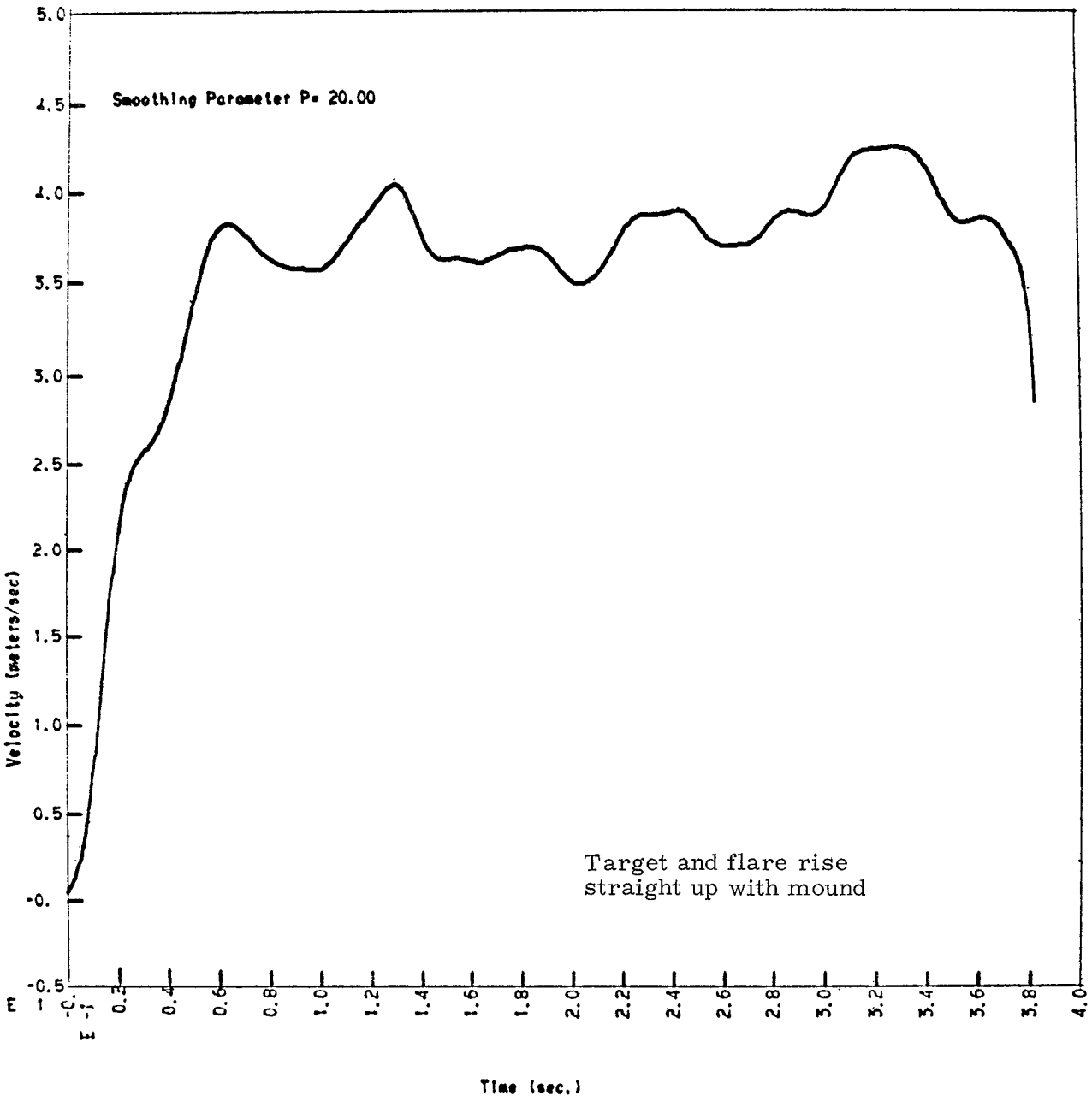

FIGURE D-14
Vertical Velocity Target 7

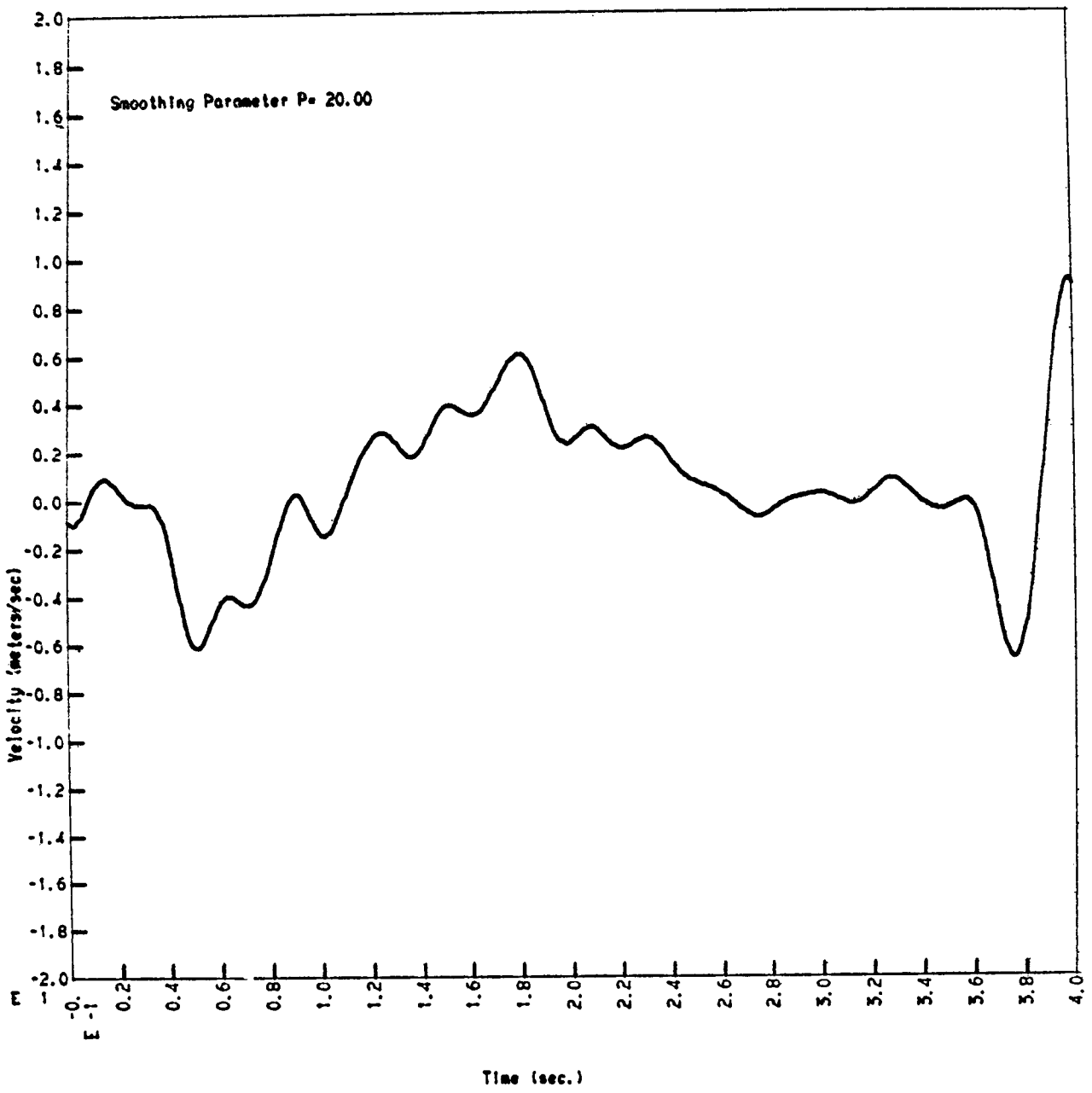

FIGURE D-15
Horizontal Velocity Target 8

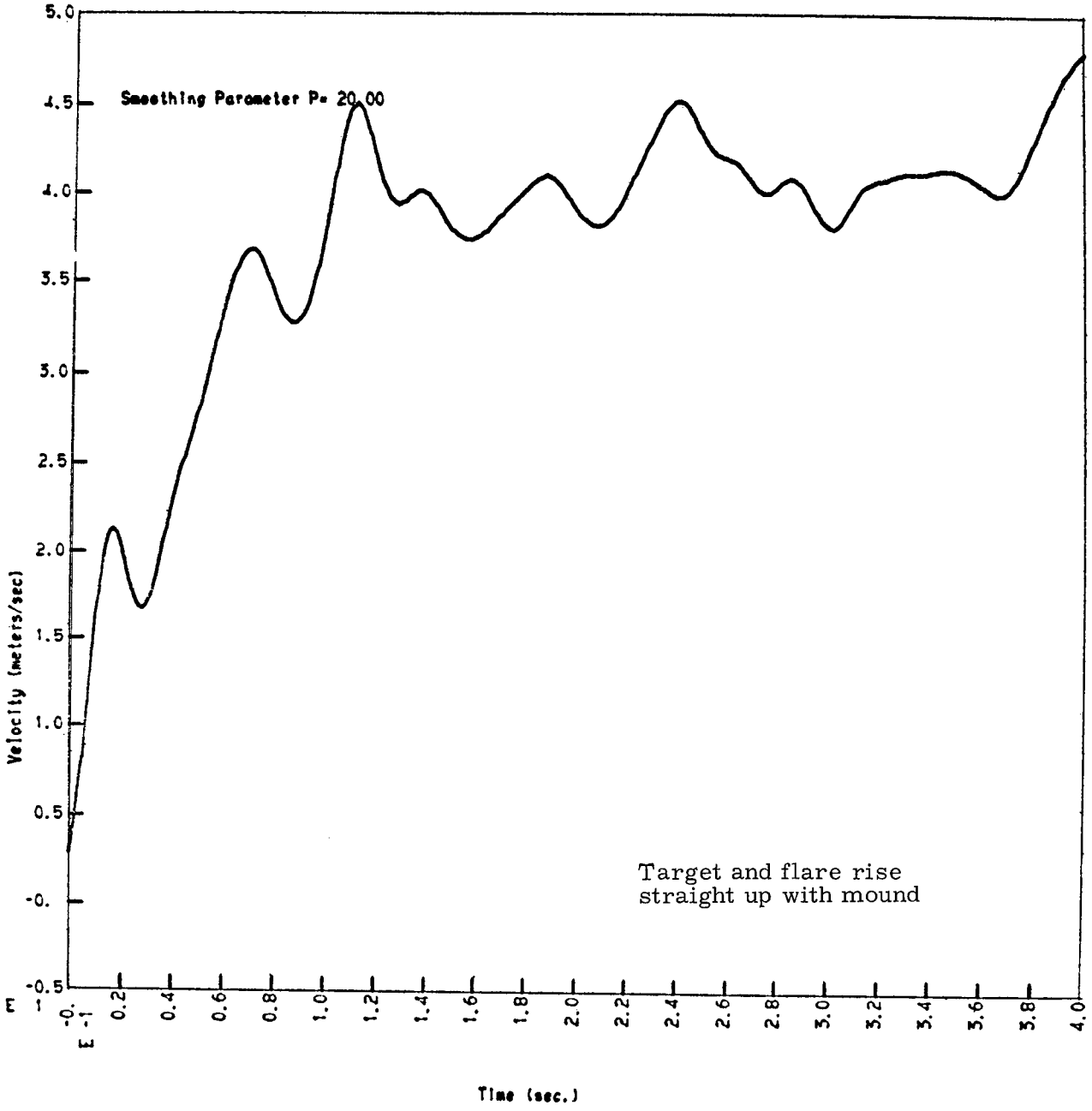

FIGURE D-16
Vertical Velocity Target 8

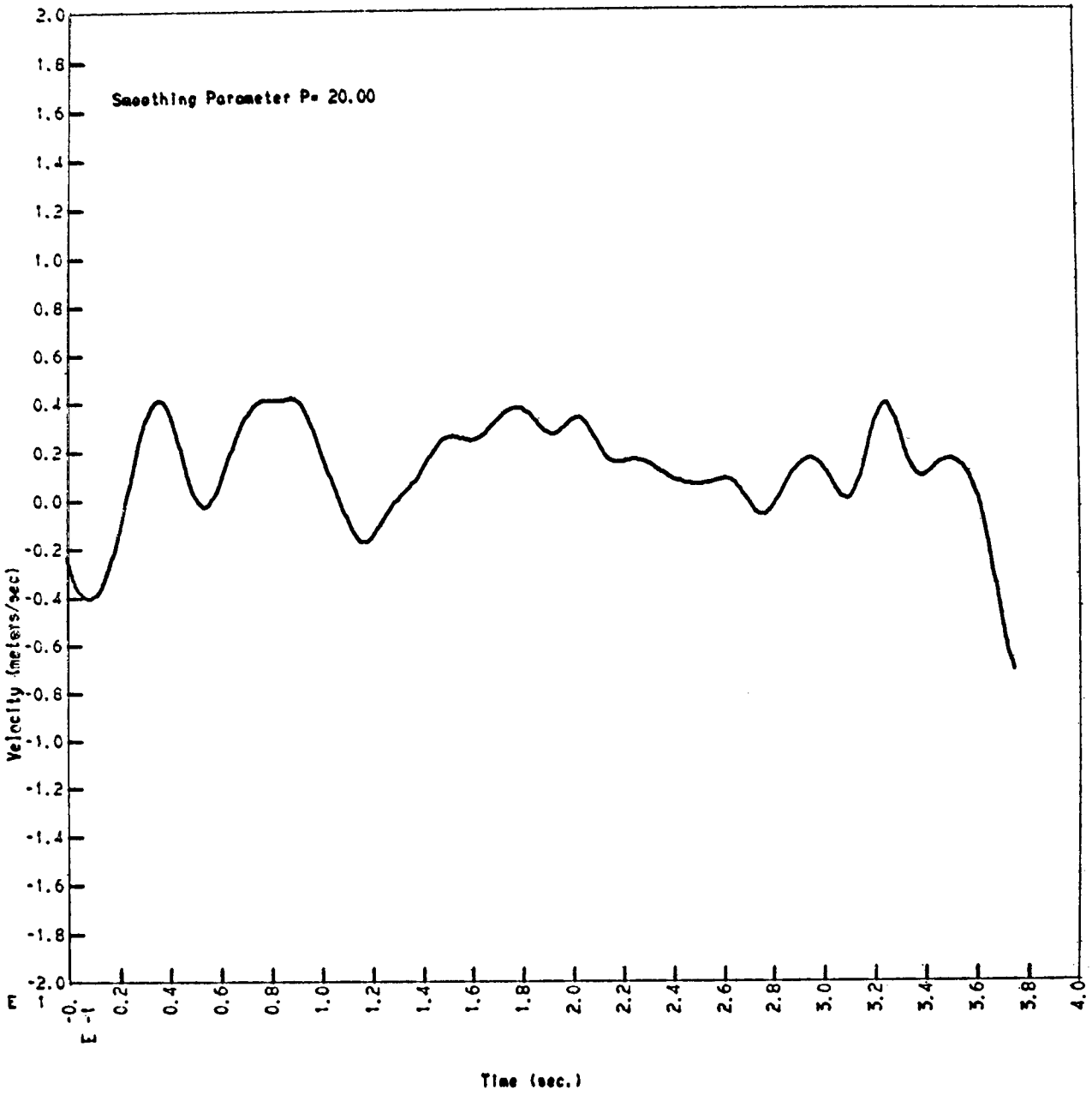

FIGURE D-17
Horizontal Velocity Target 11

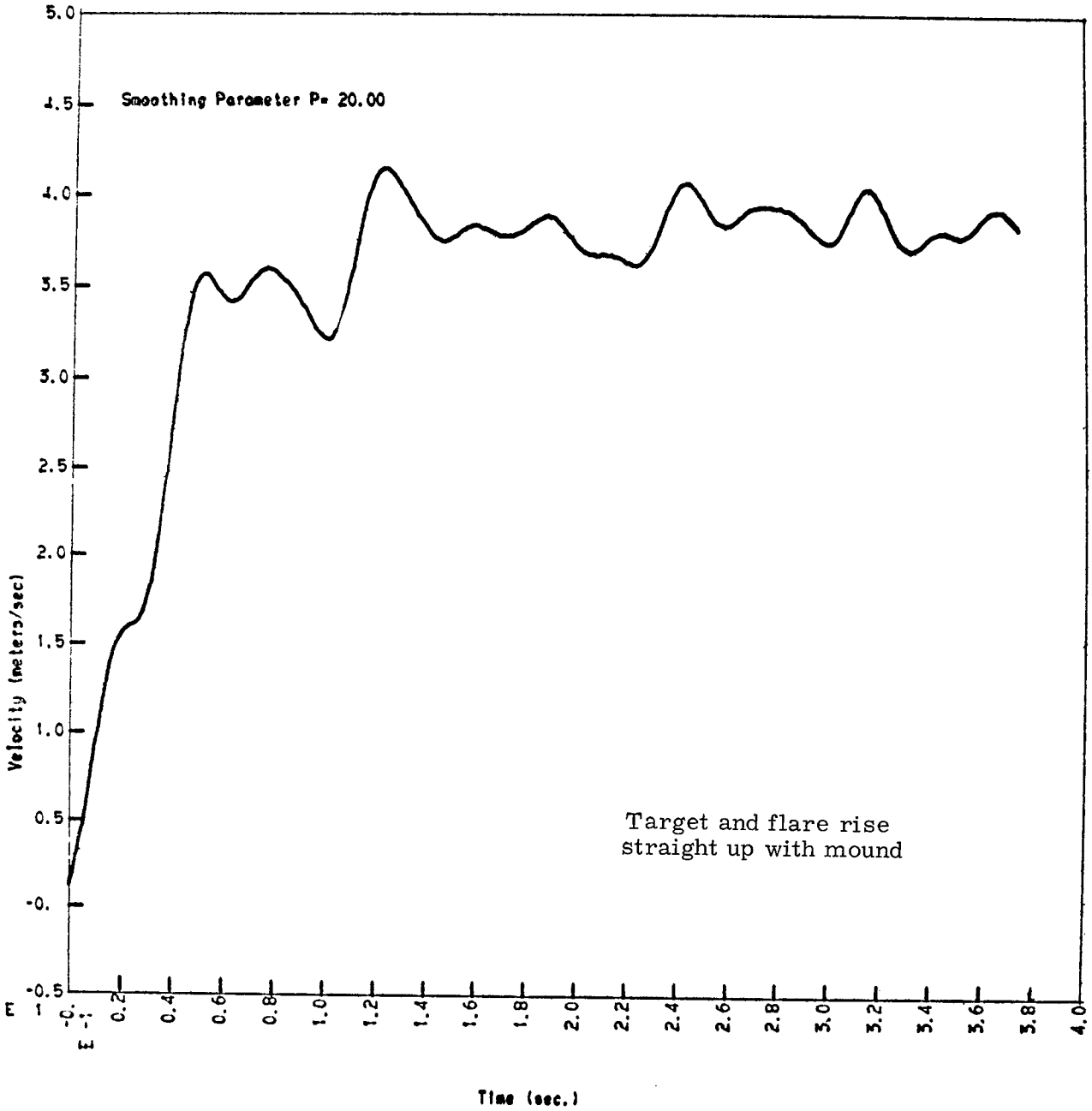

FIGURE D-18
Vertical Velocity Target 11

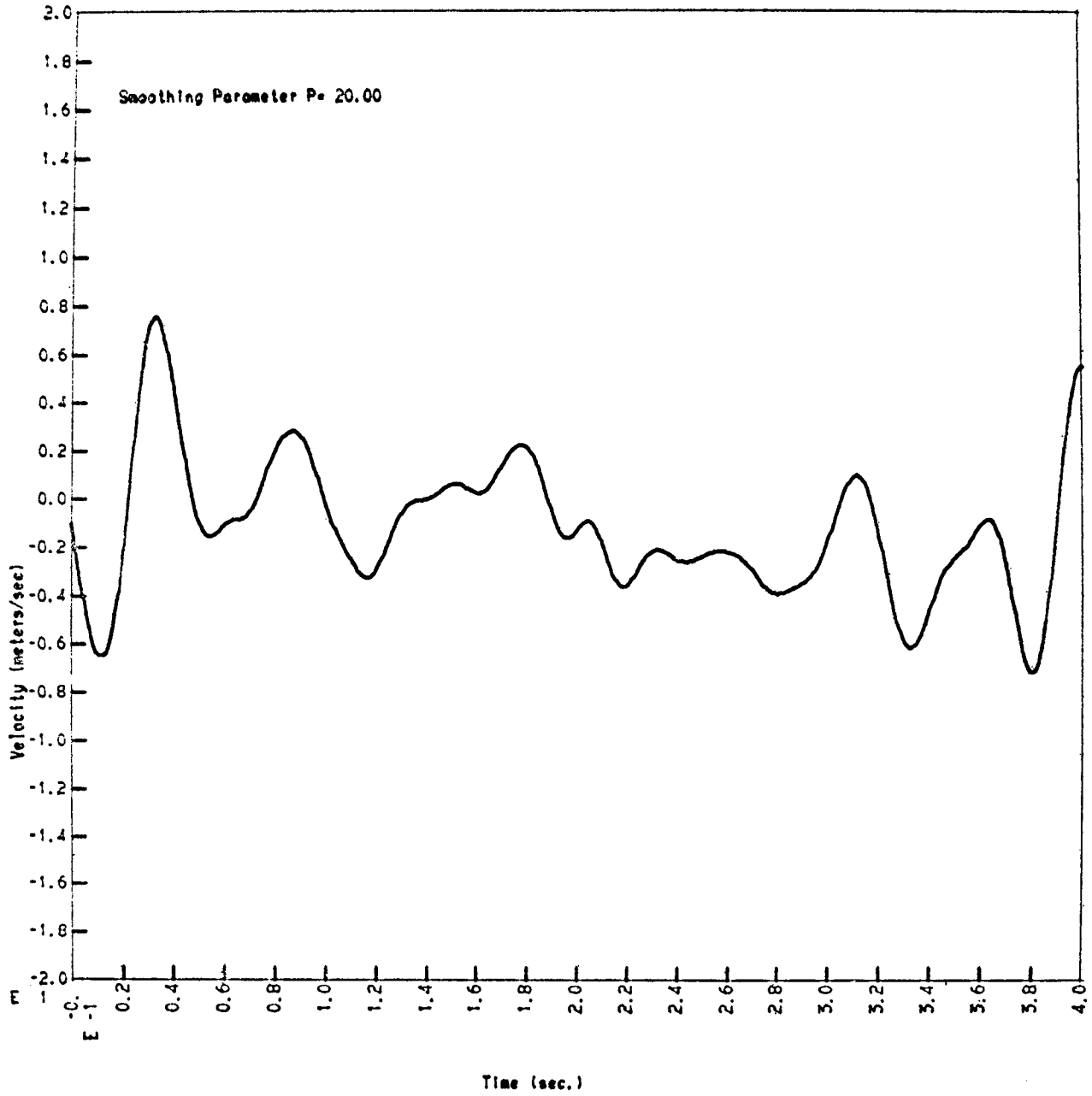

FIGURE D-19
Horizontal Velocity Target 12

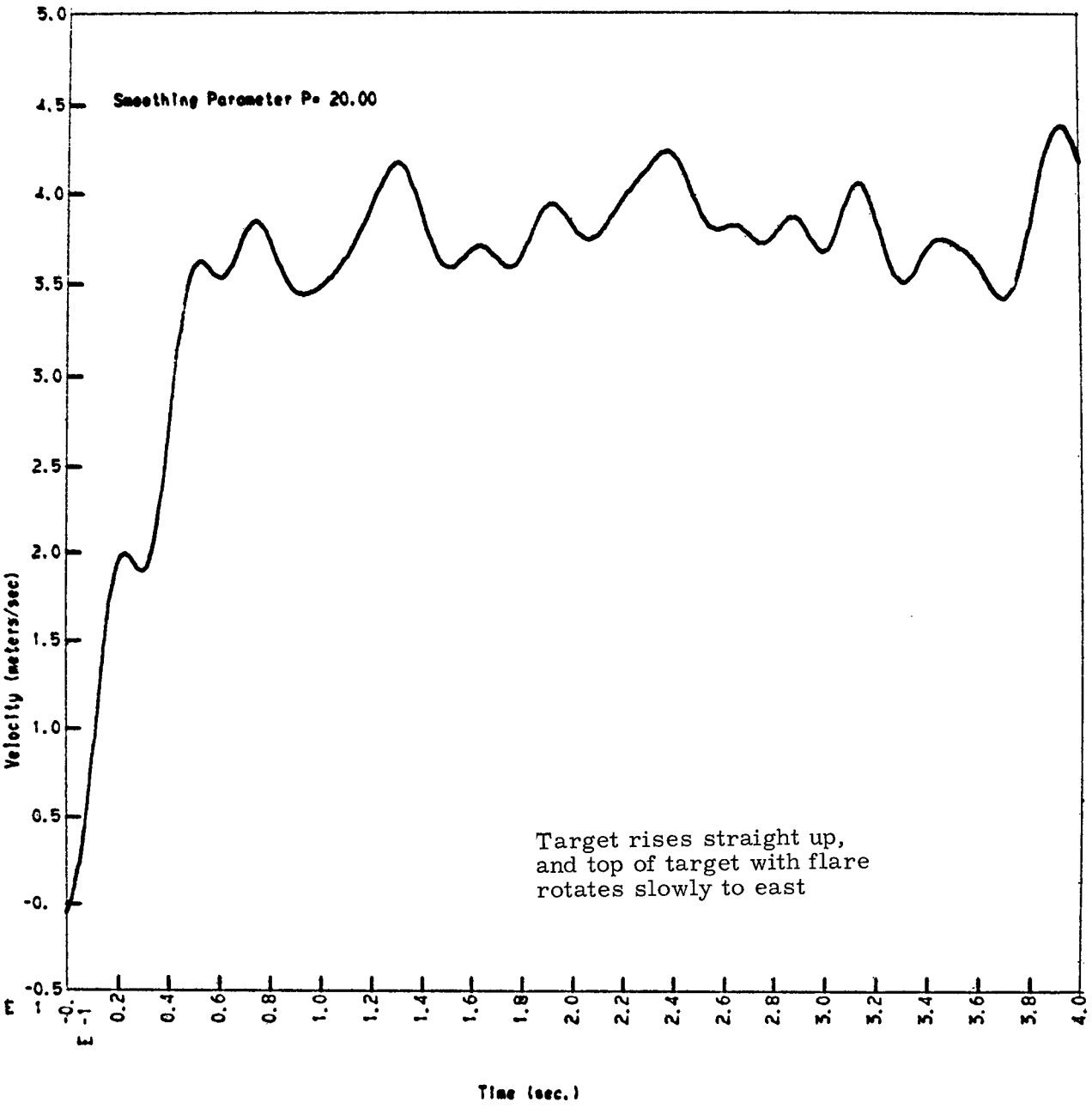

FIGURE D-20
Vertical Velocity Target 12

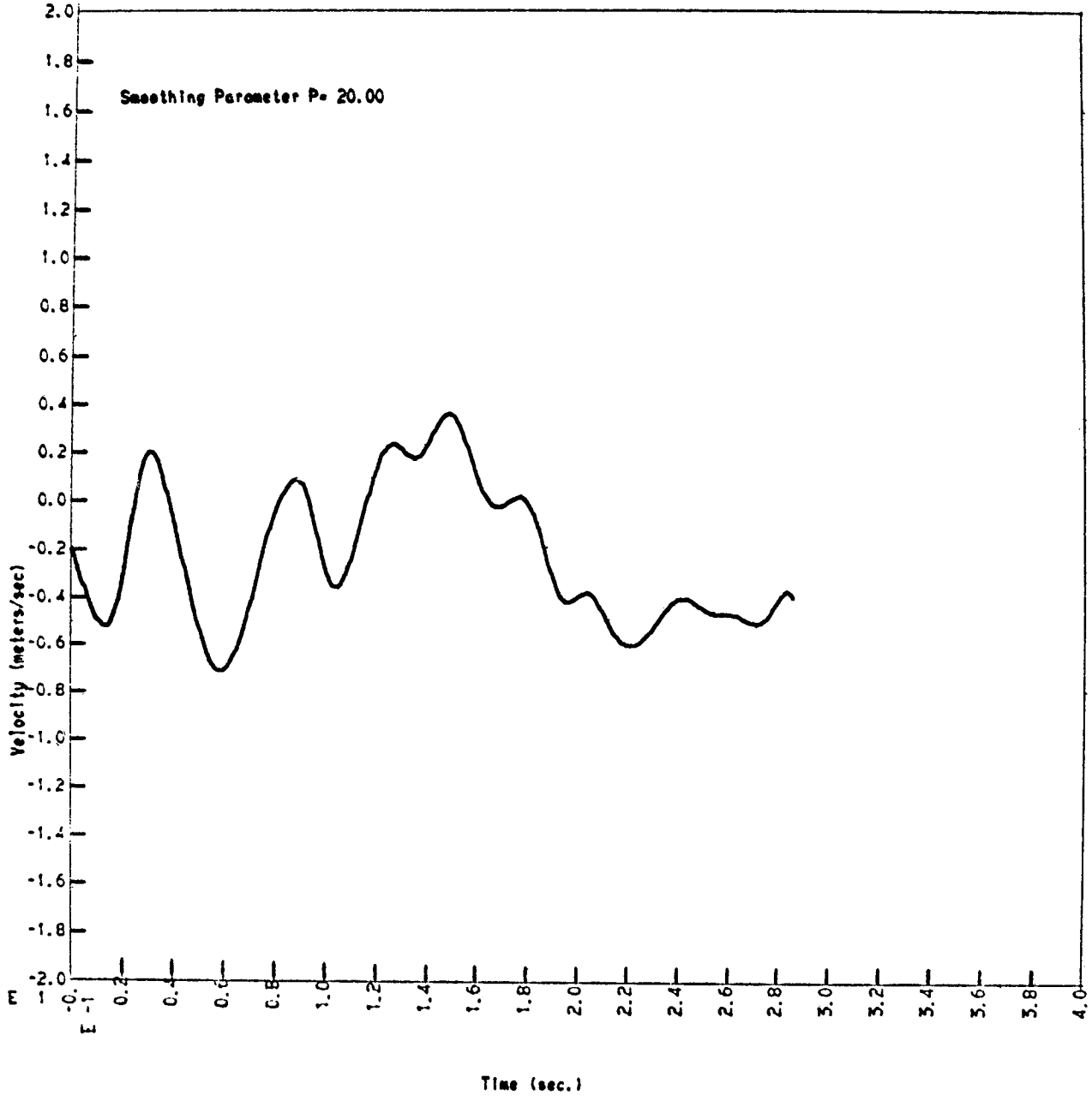

FIGURE D-21
Horizontal Velocity Target 13

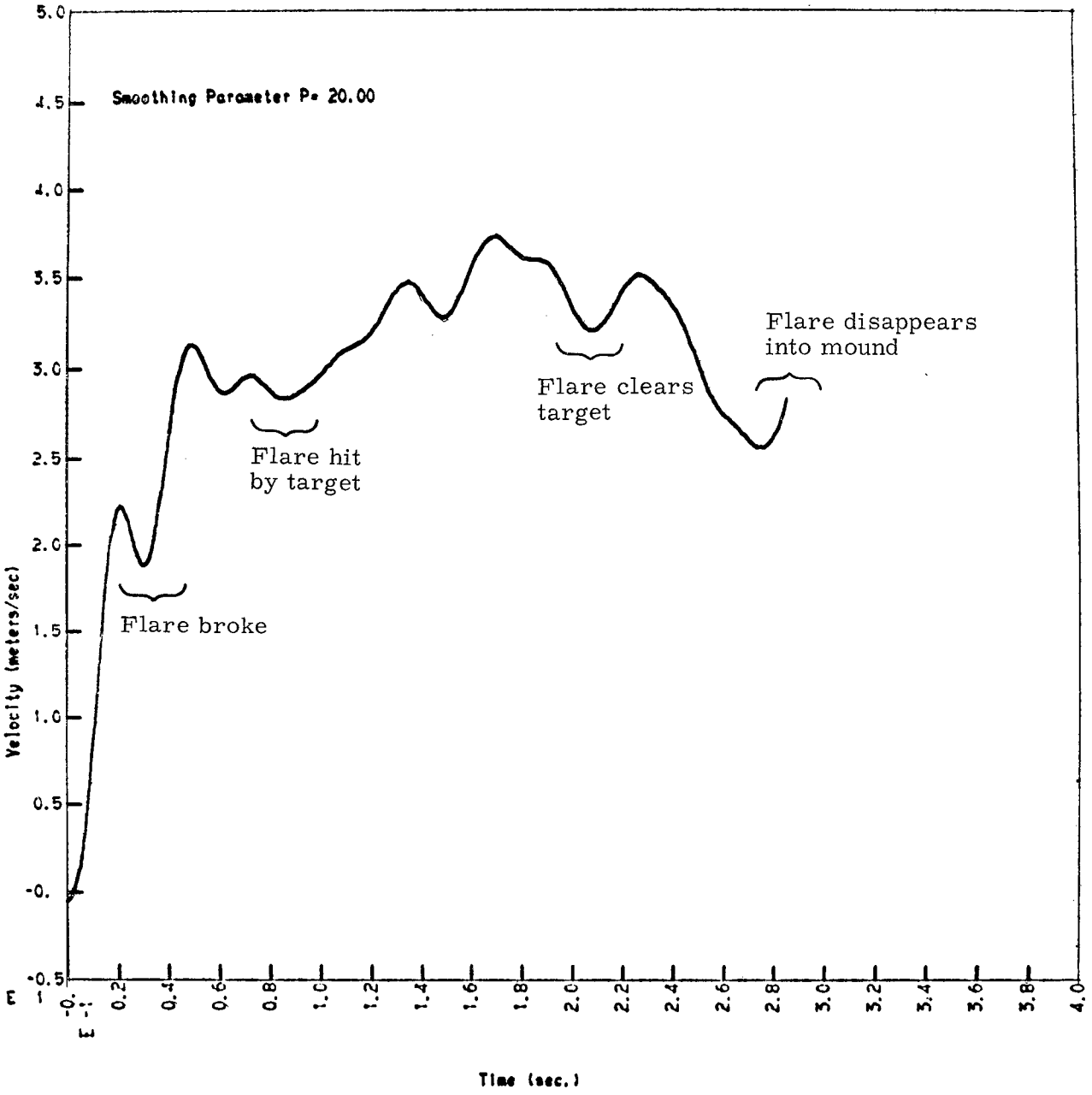

FIGURE D-22
Vertical Velocity Target 13

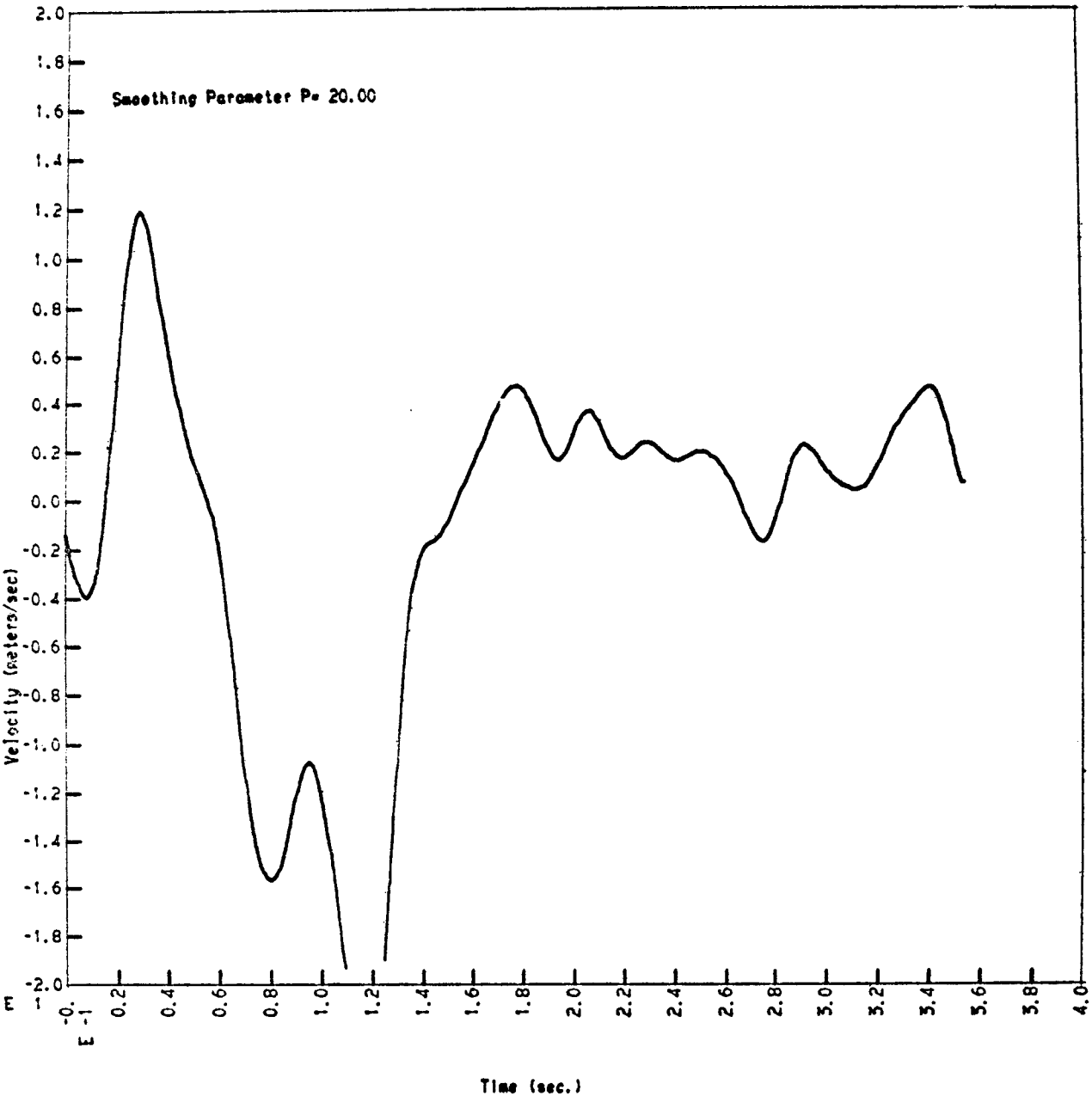

FIGURE D-23
Horizontal Velocity Target 14

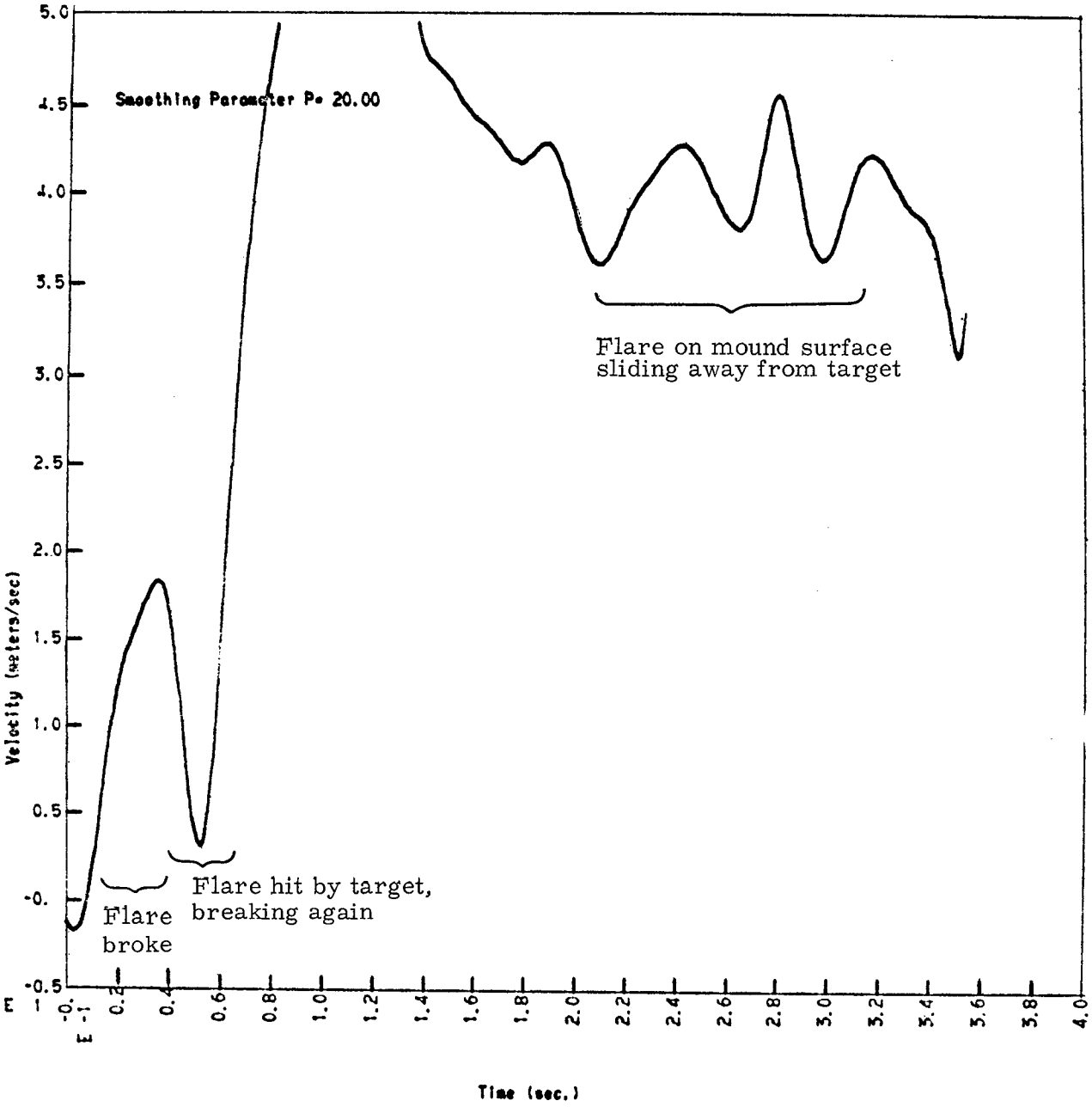

FIGURE D-24
Vertical Velocity Target 14

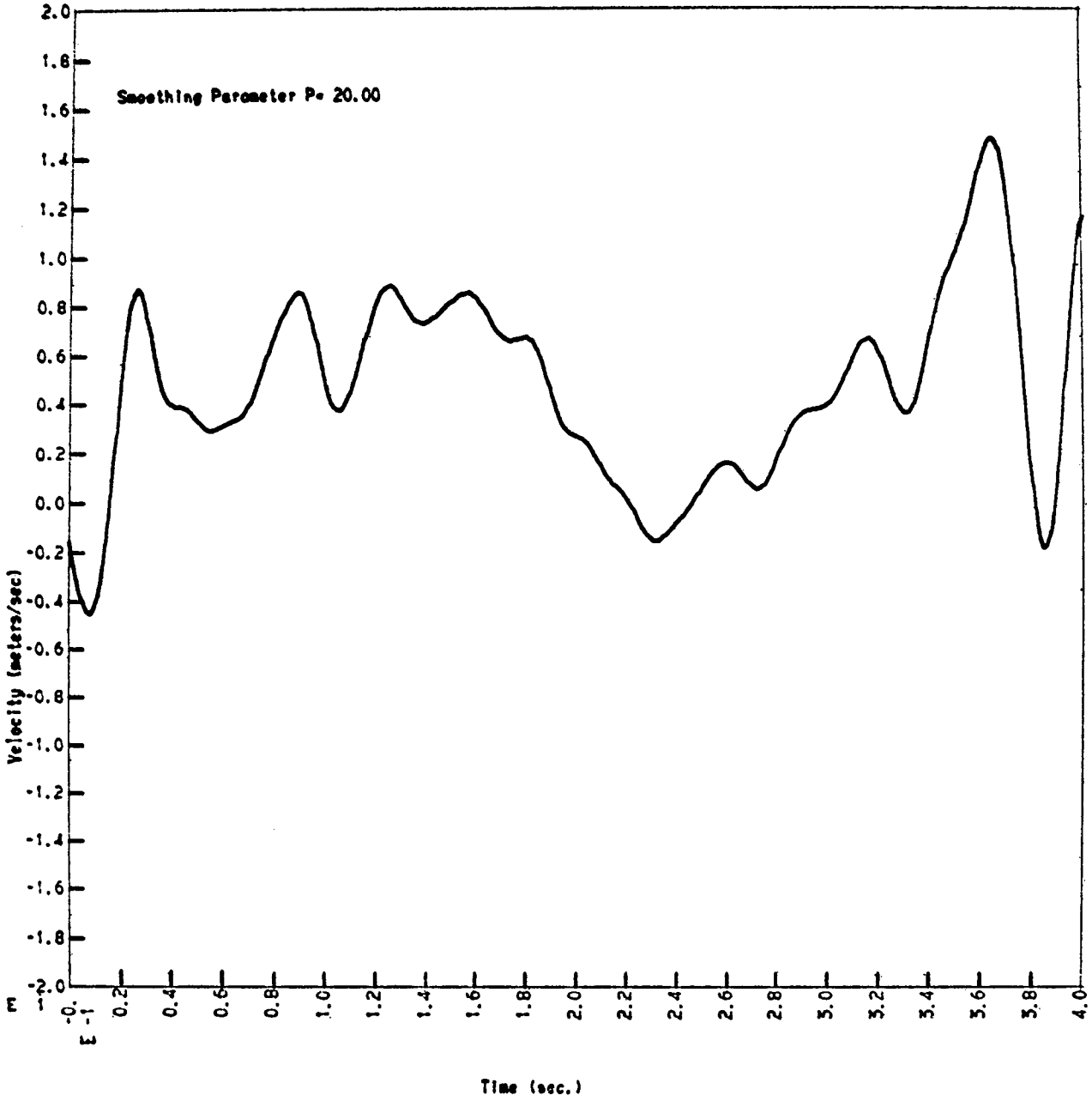

FIGURE D-25
Horizontal Velocity Target 15

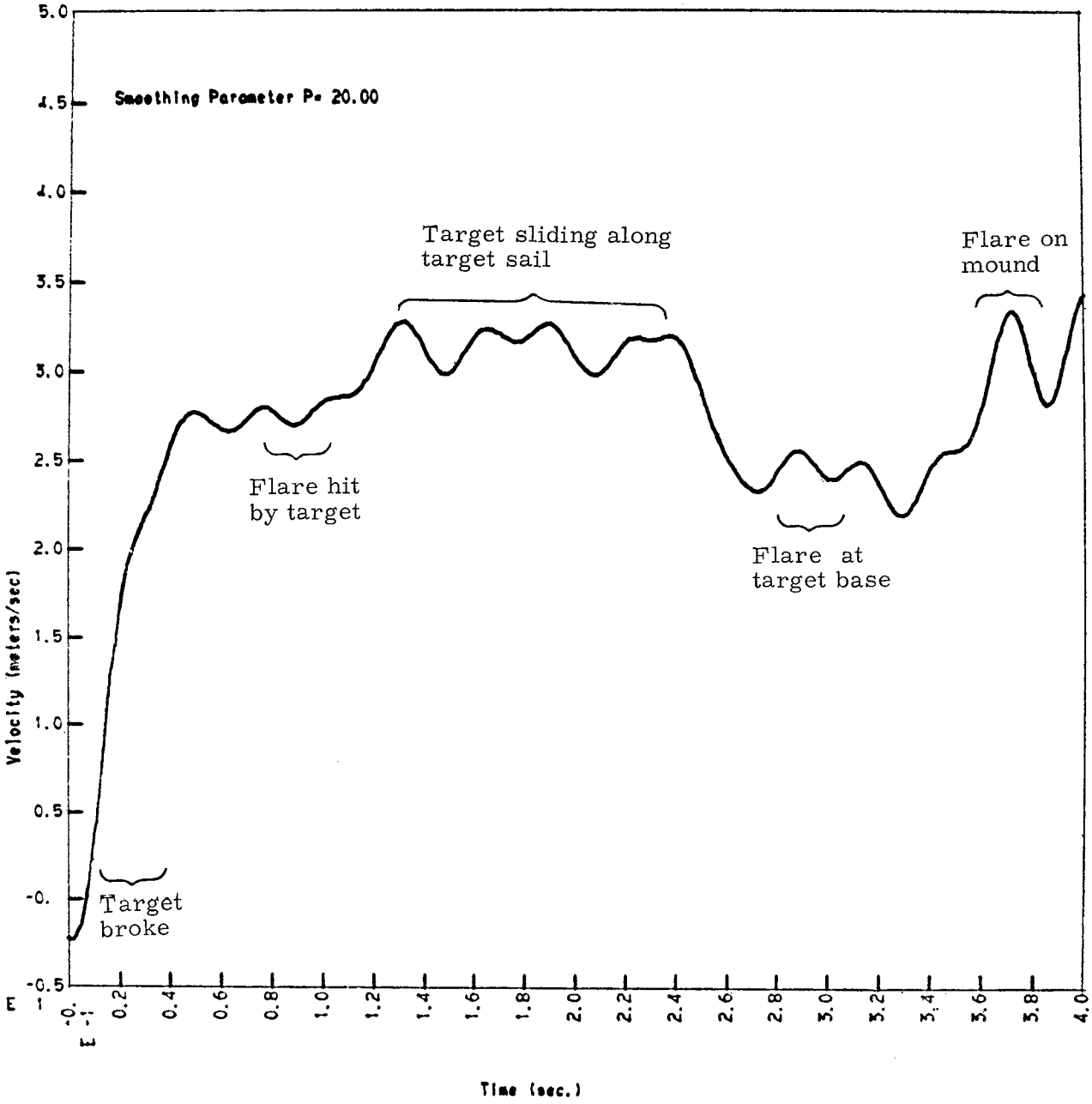

FIGURE D-26
Vertical Velocity Target 15

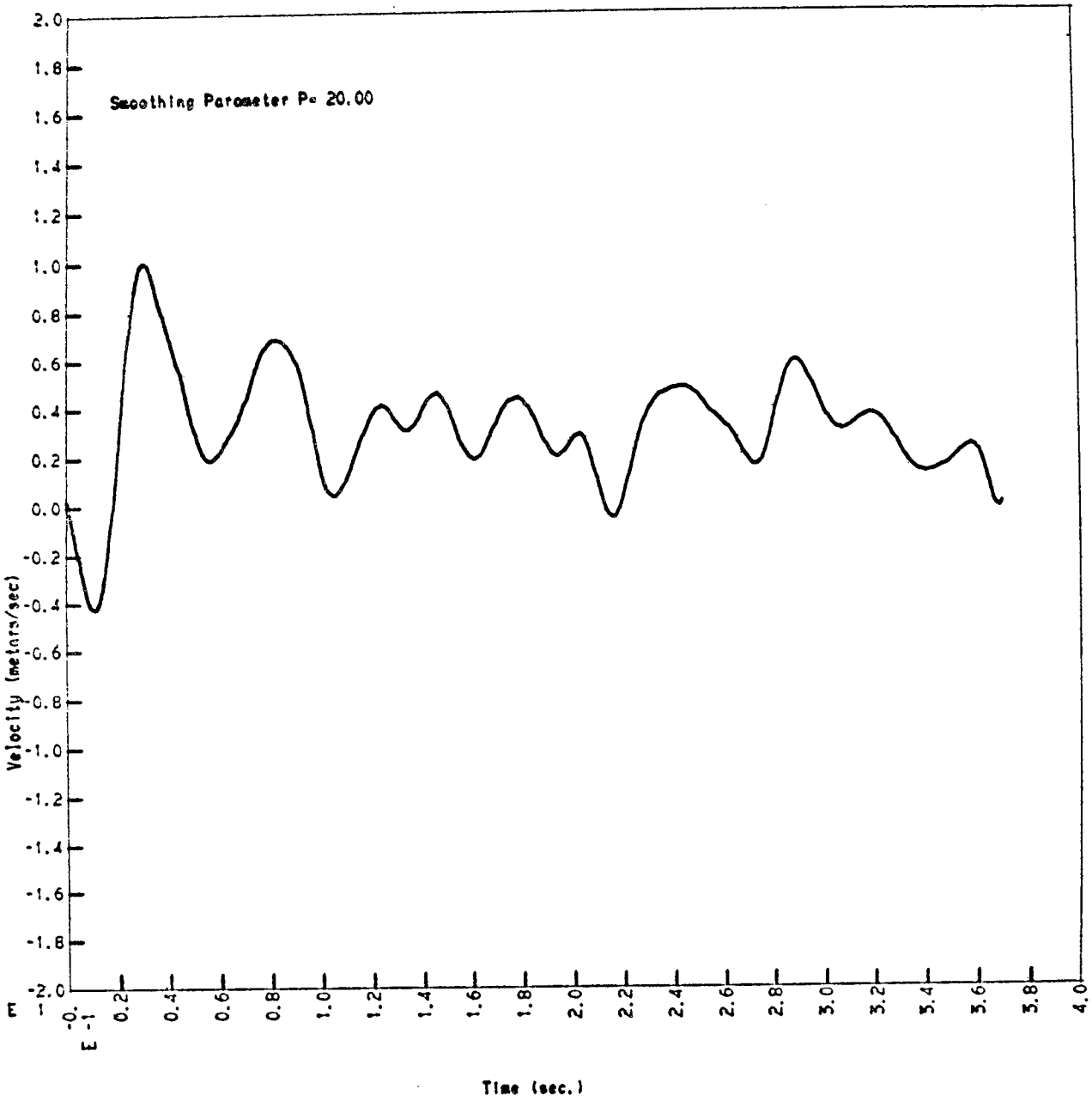

FIGURE D-27
Horizontal Velocity Target 16

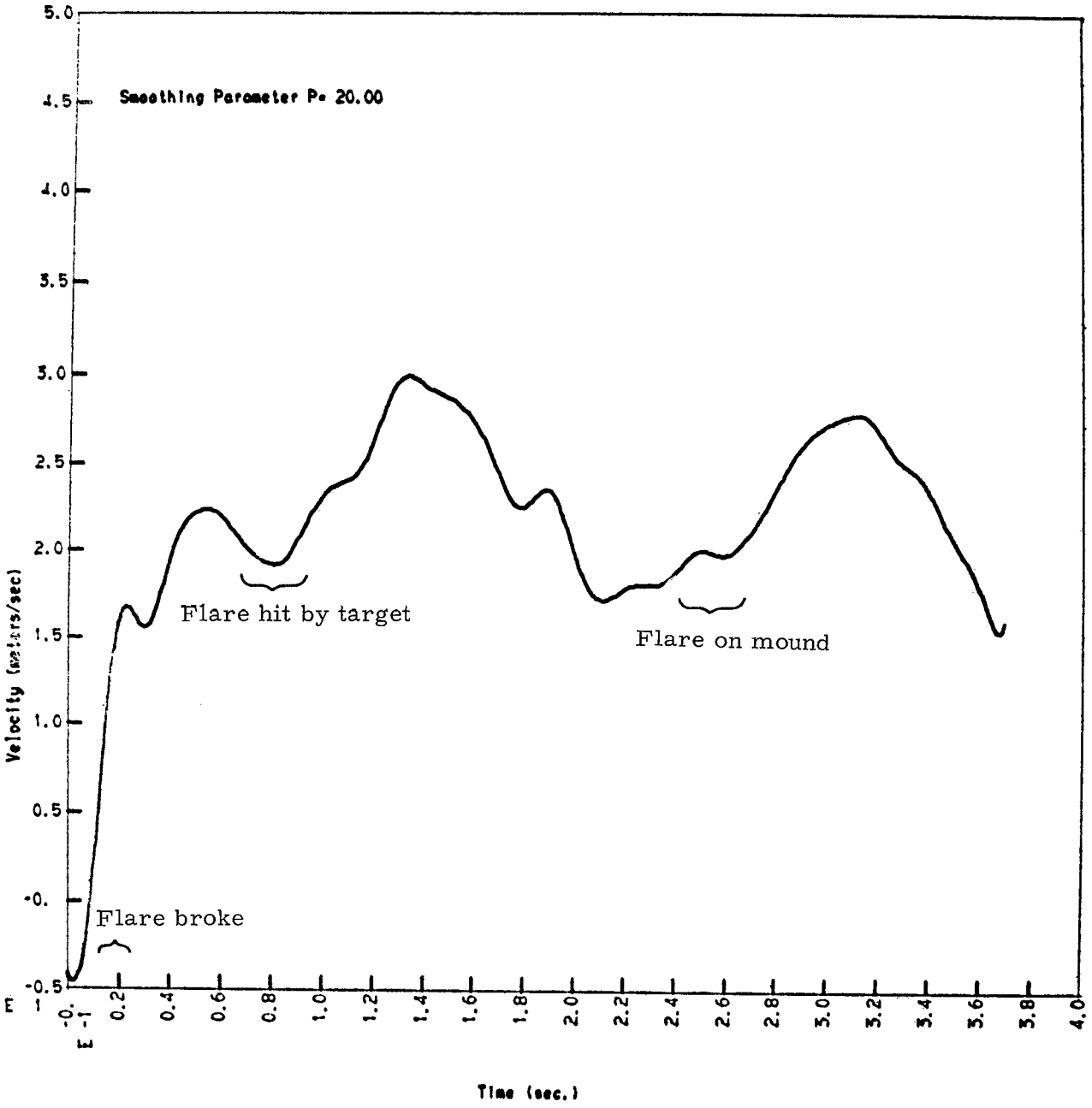

FIGURE D-28
Vertical Velocity Target 16

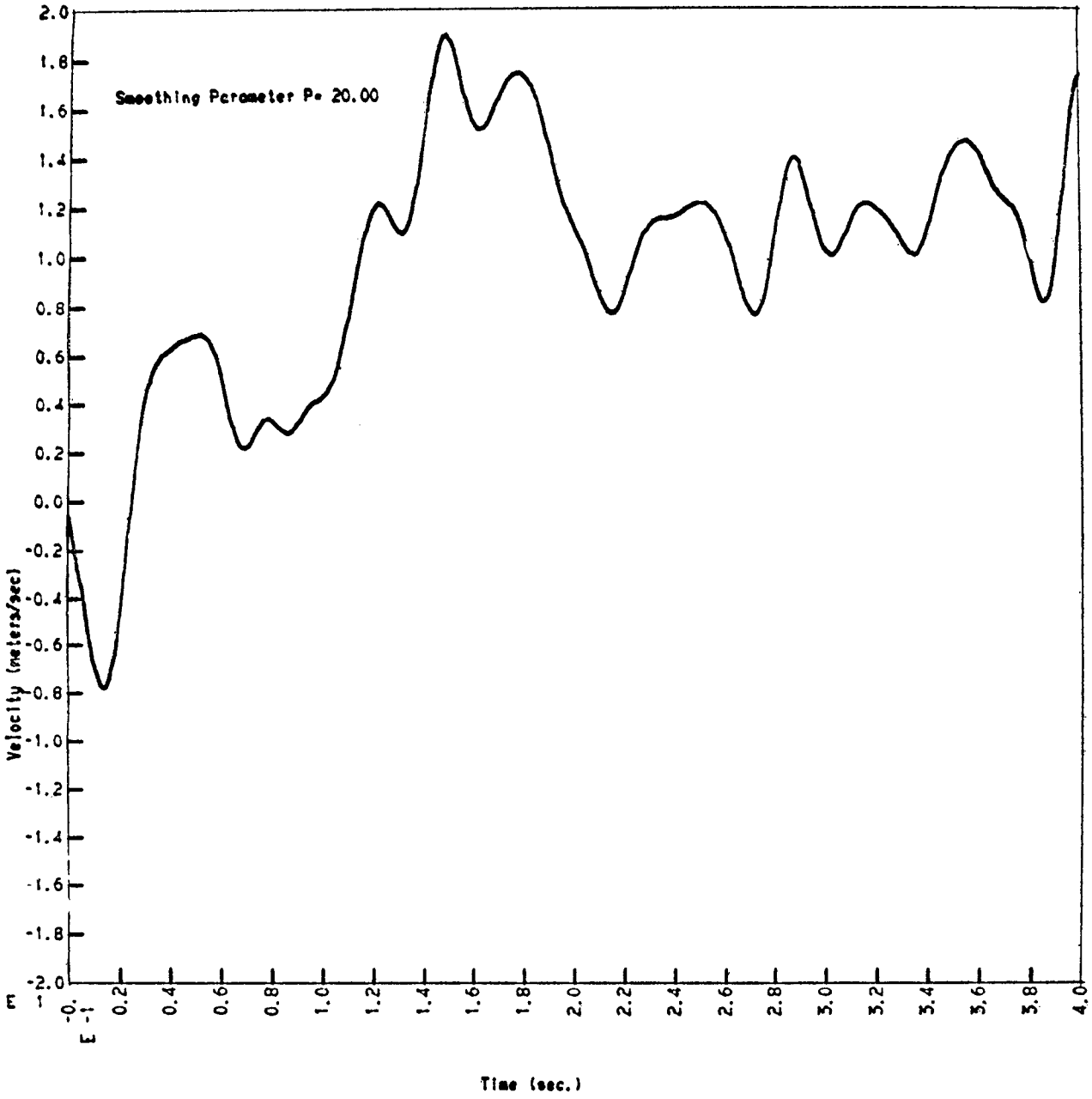

FIGURE D-29
Horizontal Velocity Target 17

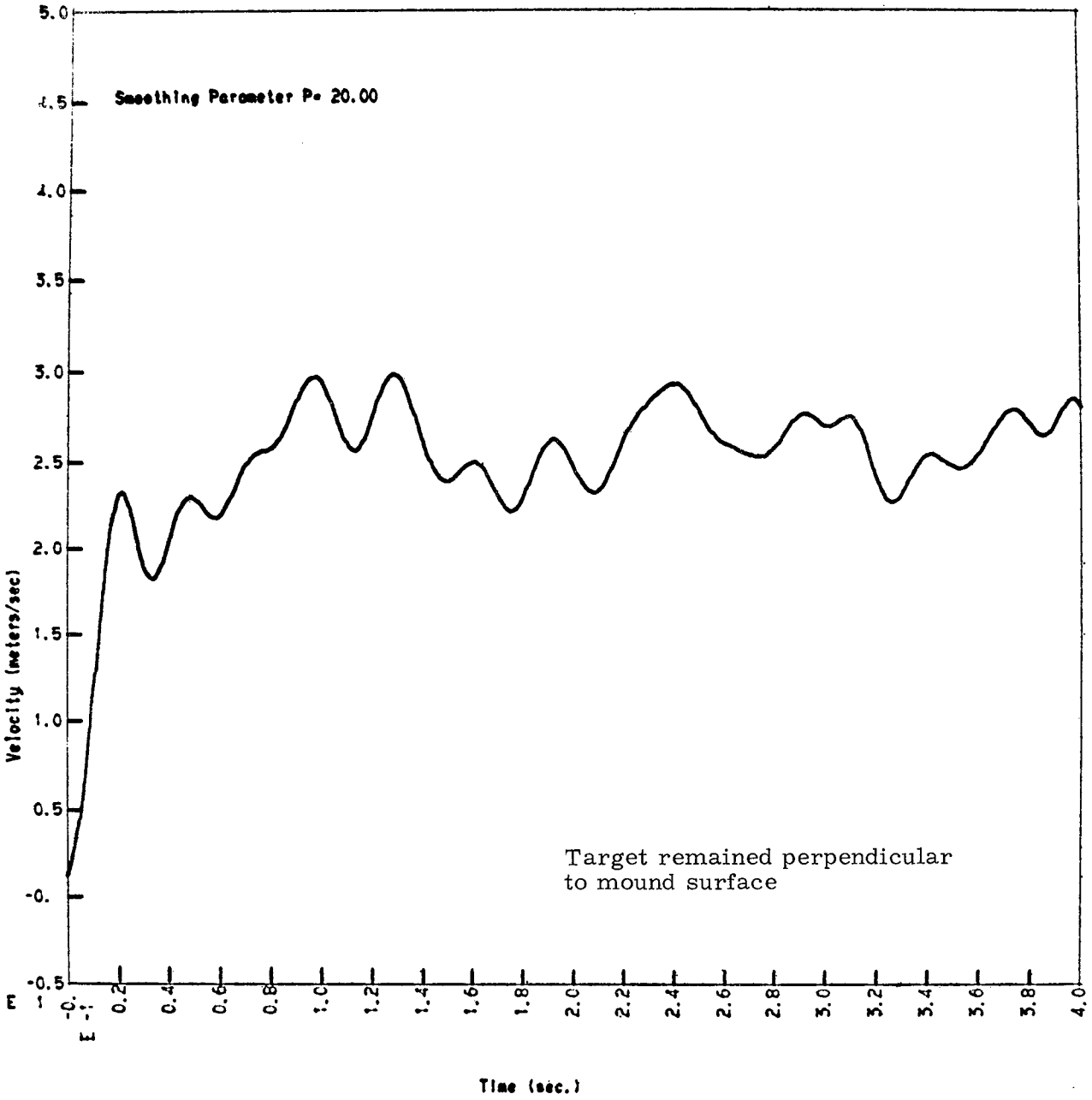

FIGURE D-30
Vertical Velocity Target 17

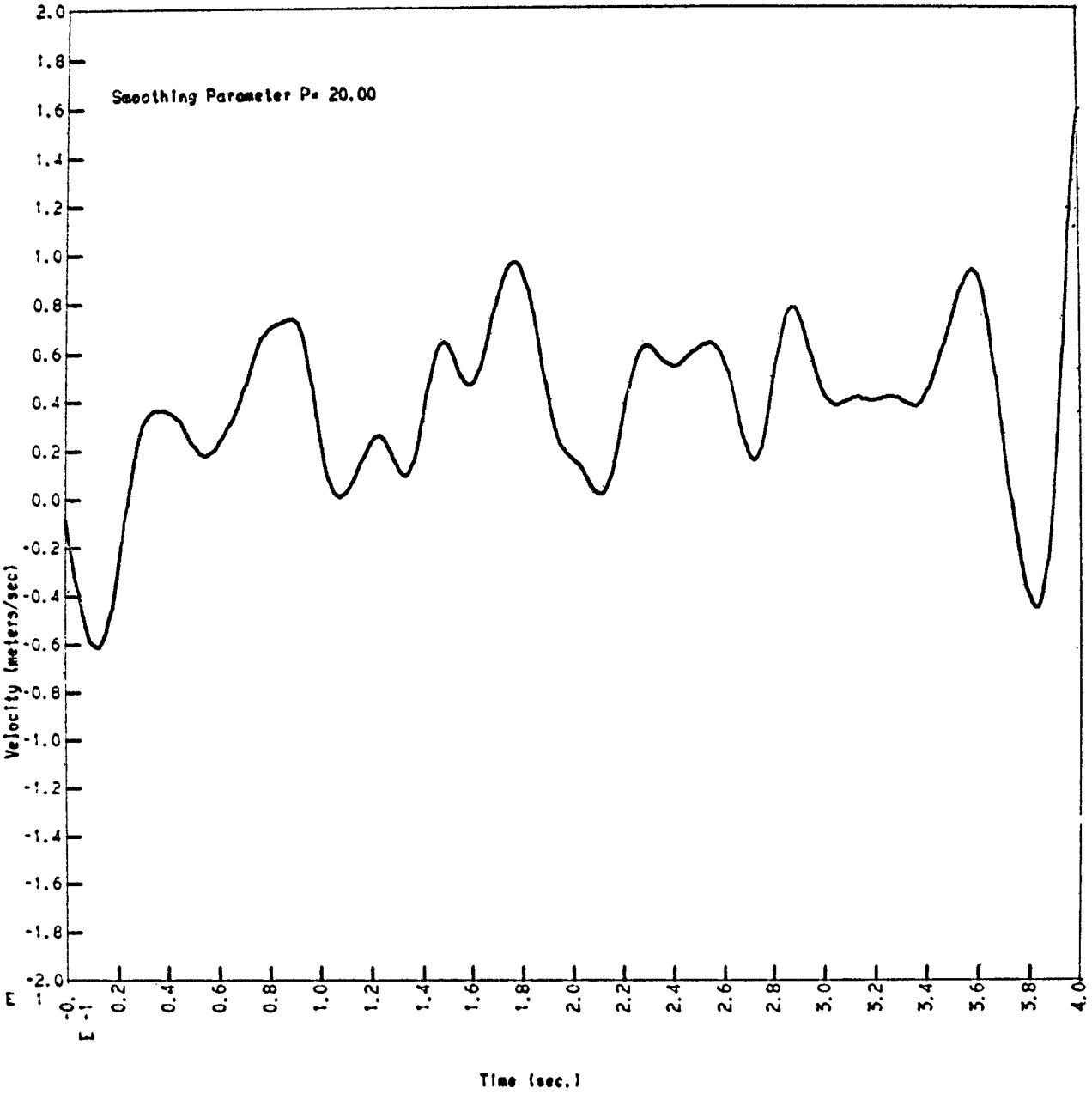

FIGURE D-31
Horizontal Velocity Target 19

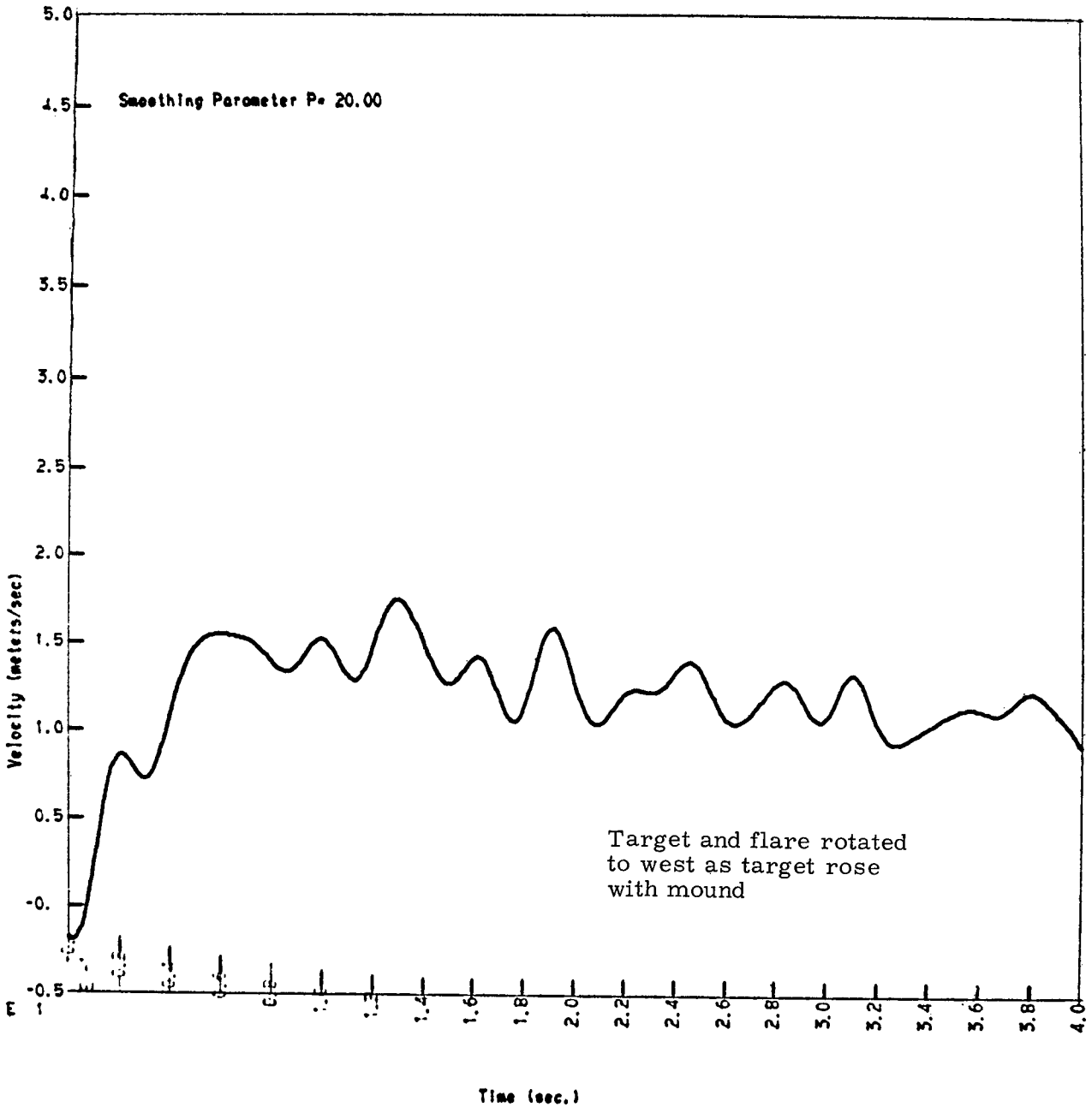

FIGURE D-32
Vertical Velocity Target 19

APPENDIX E

POSTSHOT TARGET LOCATIONS

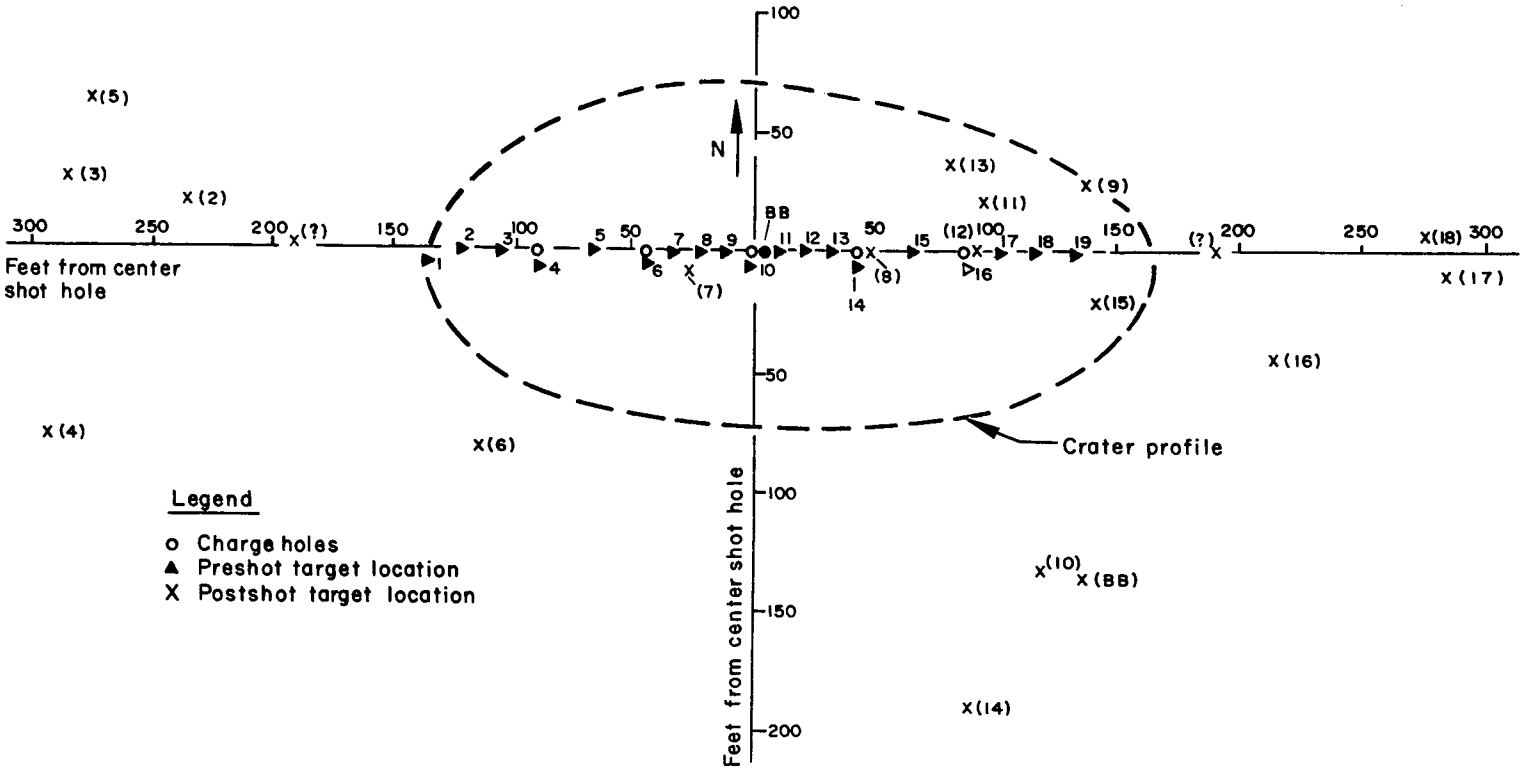

Fig. E-1 Postshot and preshot target locations for Dugout.

TABLE E-1 POSTSHOT LOCATIONS OF DUGOUT TARGETS. COORDINATES OF HOLE U-18i(GZ) ARE N853,290.00, E594,030.00

	Elevation	Coordinates (ref. C. B. 8/40-41, F. B. 537/29-30, F. B. 57/7-8)	
Accelerometer 6A	5385.4	N 852,993.10,	E 593,968.02
Accelerometer 7A	5385.9	N 853,012.10,	E 593,967.02
Accelerometer 8A	5386.3	N 853,155.05,	E 594,170.95
Accelerometer 9A	5387.0	N 853,153.05,	E 594,168.95
Bowling Ball	5386.8	N 853,154.05,	E 594,168.95
Target 7	5346.4	N 853,282.00,	E 594,003.01
Accel. 1/target ?	5354.2	N 853,290.00,	E 594,077.98
Target 13	5374.2	N 853,326.99,	E 594,113.97
Target 12	5359.8	N 853,290.00,	E 594,120.97
Target 11	5366.8	N 853,311.99,	E 594,127.97
Target 9	5381.8	N 853,320.99,	E 594,167.95
Target 15	5385.0	N 853,268.01,	E 594,174.95
Target 24	5384.1	N 853,565.90,	E 594,104.97
Target ?	5384.6	N 853,514.92,	E 594,041.00
Target 26	5382.5	N 853,639.88,	E 594,036.00
Target 25	5380.4	N 853,781.83,	E 594,055.99
Target 6/accel. 5	5395.0	N 853,207.03,	E 593,917.04
Target 10	5388.8	N 853,157.05,	E 594,152.96
Target 16	5385.2	N 853,246.02,	E 594,244.92
Target 17	5378.0	N 853,282.00,	E 594,318.90
Target 18	5379.2	N 853,296.00,	E 594,305.90
Target ?	5381.4	N 853,296.00,	E 594,269.92
Target 14	5390.2	N 853,100.07,	E 594,123.97
Target 23	5385.9	N 852,997.10,	E 594,007.01
T. S. 6	5387.8	N 853,298.00,	E 594,240.93
T. S. 5	5382.0	N 853.274.01,	E 594,318.80

TABLE E-1 (Continued)

	Elevation	Coordinates (ref. C. B. 8/42, F. B. 537/25)	
Target 4	5387.6	N 853,210.03,	E 593,739.09
T. S. 3	5388.1	N 853,213.03,	E 593,798.07
T. S. 4	5388.0	N 853,205.03,	E 593,799.07
Target 3	5389.1	N 853,317.99,	E 593,745.09
Accel./target 5	5388.6	N 853,350.98,	E 593,755.09
T. S. 1	5389.66	N 853,275.01,	E 593,827.06
Accel. ?/target ?	5389.0	N 853,309.99,	E 593,795.07
T. S. 2	5396.6	N 853,269.01,	E 593,829.06

DUGOUT TECHNICAL REPORTS

Report No.	Agency	Author	Title
PNE-600F	LRL	Nordyke, et al.	Technical Director's Summary Report – Project Dugout
PNE-601F	NCG	Spruill	Apparent Crater Studies
PNE-602F	WES	Strohm	Crater Explorations
PNE-603F*	LRL	Terhune	Surface Motion Measurements
PNE-604F	LRL	Rohrer	Cloud Development
PNE-605F	CGS	Mickey	Strong-Motion Seismic Measurements
PNE-607F	SC	Reed	Multiple Row Charge Blast Wave Observations at Long Range
PNE-608F	SC	Vortman	Close-in Air Blast From a Row Charge in Basalt
PNE-609F	WES	Ingram	Deep Underground Shock Measurements

*PNE-603F and PNE-606F incorporated under one document number per request of Milo Nordyke.

DISTRIBUTION LIST
(TID-4500, Category UC-35)

No. Copies	
8	ABERDEEN PROVING GROUND
1	AEROJET-GENERAL CORPORATION
	AIR FORCE CAMBRIDGE RESEARCH LABORATORIES
1	AIR FORCE INSTITUTE OF TECHNOLOGY
1	AIR FORCE WEAPONS LABORATORY
1	ALBUQUERQUE OPERATIONS OFFICE
1	ARGONNE NATIONAL LABORATORY
5	ARMY ENGINEER NUCLEAR CRATERING GROUP
1	ARMY ENGINEER RESEARCH AND DEVELOPMENT LABORATORIES
6	ARMY ENGINEER WATERWAYS EXPERIMENT STATION
1	ARMY MATERIEL COMMAND (NA)
1	ARMY MATERIEL COMMAND (RP)
	ARMY MISSILE COMMAND
1	ARMY NATICK LABORATORIES
1	ARMY PICATINNY ARSENAL
1	ARMY (SEVENTH) SUPPORT COMMAND
1	ATOMIC ENERGY COMMISSION, BETHESDA
25	AEC DIVISION OF PEACEFUL NUCLEAR EXPLOSIVES
1	AEC PATENT OFFICE
1	AEC SCIENTIFIC REPRESENTATIVE, ARGENTINA
1	AEC SCIENTIFIC REPRESENTATIVE, BELGIUM
1	AEC SCIENTIFIC REPRESENTATIVE, ENGLAND
1	AEC SCIENTIFIC REPRESENTATIVE, FRANCE
1	AEC SCIENTIFIC REPRESENTATIVE, JAPAN
3	ATOMIC ENERGY COMMISSION, WASHINGTON
1	ATOMIC POWER DEVELOPMENT ASSOCIATES, INC
2	ATOMICS INTERNATIONAL
2	BATTELLE MEMORIAL INSTITUTE
1	BATTELLE-NORTHWEST
12	BEERS (ROLAND F.), INC.
1	BEERS (ROLAND F.), INC., LAS VEGAS
1	BLUME (JOHN A.) AND ASSOCIATES
1	BROOKHAVEN NATIONAL LABORATORY
1	BUREAU OF MINES, BARTLESVILLE
1	BUREAU OF MINES, LARAMIE
1	BUREAU OF MINES, WASHINGTON
1	BUREAU OF NAVAL WEAPONS
1	BUREAU OF SHIPS (CODE 1500)
1	BUREAU OF YARDS AND DOCKS
1	DEFENSE ATOMIC SUPPORT AGENCY, LIVERMORE
1	DEFENSE ATOMIC SUPPORT AGENCY, SANDIA
1	DEFENSE ATOMIC SUPPORT AGENCY, WASHINGTON
1	DU PONT COMPANY, AIKEN
1	DU PONT COMPANY, WILMINGTON
1	EDGERTON, GERMESHAUSEN, AND GRIER, INC., LAS VEGAS
2	ENVIRONMENTAL SCIENCE SERVICES ADMINISTRATION, LAS VEGAS
1	ENVIRONMENTAL SCIENCE SERVICES ADMINISTRATION, WASHINGTON
1	FUNDAMENTAL METHODS ASSOCIATION
1	GENERAL ATOMIC DIVISION
1	GENERAL ELECTRIC COMPANY, CINCINNATI
1	GENERAL ELECTRIC COMPANY, SAN JOSE
3	HAZLETON NUCLEAR SCIENCE CORPORATION
2	HOLMES AND NARVER, INC.

No. Copies	
2	LOS ALAMOS SCIENTIFIC LABORATORY
1	LOVELACE FOUNDATION FOR MEDICAL EDUCATION AND RESEARCH
	MOUND LABORATORY
1	MUESER, RUTLEDGE, WENTWORTH AND JOHNSTON
1	NASA MANNED SPACECRAFT CENTER
2	NASA SCIENTIFIC AND TECHNICAL INFORMATION FACILITY
1	NATIONAL AGRICULTURAL LIBRARY
1	NATIONAL MILITARY COMMAND SYSTEM SUPPORT CENTER
1	NATIONAL REACTOR TESTING STATION (PPCO)
1	NAVAL RADIOLOGICAL DEFENSE LABORATORY
5	NEVADA OPERATIONS OFFICE
1	NEW YORK OPERATIONS OFFICE
1	NRA, INC.
1	OAK RIDGE OPERATIONS OFFICE
1	OFFICE OF NAVAL RESEARCH (CODE 422)
7	OFFICE OF THE CHIEF OF ENGINEERS
1	OHIO STATE UNIVERSITY
1	PHYSICS INTERNATIONAL COMPANY
1	PUBLIC HEALTH SERVICE
	PUBLIC HEALTH SERVICE, CINCINNATI
5	PUBLIC HEALTH SERVICE, LAS VEGAS
	PUBLIC HEALTH SERVICE, WINCHESTER
1	PURDUE UNIVERSITY
1	RADIOPTICS, INC.
1	RAND CORPORATION
1	RESEARCH ANALYSIS CORPORATION
2	REYNOLDS ELECTRICAL AND ENGINEERING COMPANY, INC.
5	SAN FRANCISCO OPERATIONS OFFICE
4	SANDIA CORPORATION, ALBUQUERQUE
1	SANDIA CORPORATION, LIVERMORE
1	SAVANNAH RIVER OPERATIONS OFFICE
1	SCHOOL OF AEROSPACE MEDICINE
1	SOUTHWEST RESEARCH INSTITUTE
1	TENNESSEE VALLEY AUTHORITY
1	UNION CARBIDE CORPORATION (ORGDP)
4	UNION CARBIDE CORPORATION (ORNL)
	UNION CARBIDE CORPORATION (ORNL-Y-12)
3	U. S. GEOLOGICAL SURVEY, DENVER
1	U. S. GEOLOGICAL SURVEY, FLAGSTAFF
2	U. S. GEOLOGICAL SURVEY, MENLO PARK
1	U. S. GEOLOGICAL SURVEY (PECORA)
1	U. S. GEOLOGICAL SURVEY, WASHINGTON
1	U. S. MISSION TO THE INTERNATIONAL ATOMIC ENERGY AGENCY
2	UNIVERSITY OF CALIFORNIA, BERKELEY
4	UNIVERSITY OF CALIFORNIA, LIVERMORE
1	UNIVERSITY OF CALIFORNIA, LOS ANGELES
1	UNIVERSITY OF MICHIGAN (YESIAC)
	UNIVERSITY OF PUERTO RICO
1	UNIVERSITY OF TENNESSEE (UTA)
1	WHITE SANDS MISSILE RANGE
63	DIVISION OF TECHNICAL INFORMATION EXTENSION
75	CLEARINGHOUSE FOR FEDERAL SCIENTIFIC AND TECHNICAL INFORMATION